

**KINETICS AND SOLVENT EFFECTS IN THE SYNTHESIS OF IONIC
LIQUIDS**

BY

Jay Schleicher

Submitted to the School of Engineering and the
Faculty of the Graduate School of the University of Kansas.
In partial fulfillment of the requirements for the degree of
Master of Science in Chemical Engineering

Chairperson: Professor Aaron Scurto

Committee members* _____*

Professor Bala Subramaniam

Professor Susan Stagg-Williams

Date defended: _____

The Thesis Committee for Jay Schleicher certifies
that this is the approved version of the following thesis:

**KINETICS AND SOLVENT EFFECTS IN THE SYNTHESIS OF IONIC
LIQUIDS**

Committee:

Chairperson* Professor Aaron Scurto

Professor Bala Subramaniam

Professor Susan Stagg-Williams

Date approved:_____

Dedicated To:
My Supportive and Encouraging
Wife: Misty Schleicher
and
My Parents: William and Barbara Schleicher

Acknowledgements:

I would like to pay special respects to my advisor, Professor Aaron Scurto, for his guidance and assistance during my time at the University of Kansas, and for assigning me a project which utilizes both, my chemistry background as well as my chemical engineering degree. Also, I would like to acknowledge the entire Chemical Engineering faculty and staff for all their assistance, and in particular Cyndi Hurst, Professor Colin “Chip” Howat, Professor Julie Howat, Professor Carl Locke, Professor Trung Van Nguyen, and Professor Marylee Southard for their extended interest in my success. I would like to thank Wei Ren, Azita Aghosseini, and Sylvia Nwosu for their assistance and camaraderie in the laboratory. I wish them great success in their future endeavors.

On a personal note, I would like to thank my wife, Misty Schleicher, for her moral support and the number of sacrifices she has endured throughout my degree, and for understanding the long hours I spent absent from home while working in the laboratory. I would not be where I am today if she was not by my side. I would also like to thank my parents, William and Barbara Schleicher, for the values they have instilled upon me, and for molding me into the individual I have become today. Under their guidance I have gained a strong work ethic, learned that persistence pays off, and that family always comes first. They have truly been an inspiration to me. I would also like to acknowledge all my friends and extended family for supporting and believing in my success. It is a great feeling to know I have so many people behind me who care and believe that I can succeed at everything I do.

Thank you,

Jay Schleicher

Abstract:

Ionic liquids (ILs) are being recognized as environmentally friendly (“green”) solvents. However, their synthesis is often conducted in the very solvents that they will reportedly replace. This research has investigated the kinetics and solvent effects involved in synthesizing ILs in organic solvents and using compressed carbon dioxide. The kinetics for producing ILs have been found to be highly dependent on solvent polarities, and varied by over an order of magnitude. These dramatic effects were correlated to various polarity parameters to predict the kinetic rates. A detailed study of solvent toxicity and environmental impact was conducted to explore greener synthesis methods. Compressed CO₂ was investigated as a potential benign alternative as the phase behavior and kinetics can be tuned for combined reaction and separation. Through understanding the kinetics, human/environmental impact, and phase equilibrium, ILs may be produced in a manner which may achieve their environmentally-benign potential.

Table of Contents:	
Acknowledgements.....	iii
Abstract.....	iv
Table of Contents.....	v
Table of Figures.....	vii
Table of Tables.....	ix
Table of Symbols.....	x
1. Introduction.....	1
1.1. IL Background.....	1
1.2. Problems with Ionic Liquid Production and Use	2
1.2.1. IL Synthesis /Analysis.....	3
1.2.2. IL Reaction Engineering and Process Intensification.....	4
1.3. Research Objectives.....	5
References.....	7
2. Experimental Methods.....	11
2.1. Kinetic Measurements.....	11
2.1.1. Ambient Pressure.....	12
2.1.1.1. Mixture Densities.....	12
2.1.2. High Pressure.....	14
2.1.3. NMR Analysis.....	16
2.2. Determining Kamlet Taft Parameters.....	22
2.2.1. Solvatochromic Probes.....	22
2.2.2. UV-Vis.....	25
2.3. Vapor-Liquid Equilibrium: Carbon Dioxide Studies.....	26
2.4. Materials.....	28
References.....	30
3. Solvent Effects on Kinetics of Ionic Liquid Synthesis.....	32
3.1. Introduction to Kinetic Theory and Analysis.....	32
3.1.1. Eyring Equation.....	33
3.1.2. Hughes and Ingold Rules.....	35
3.1.3. Literature overview.....	36
3.2. Experimental Results/Modeling.....	37
3.3. Kinetic Parameters.....	44
3.4. Steric, Electronic, and Concentration Effects on Kinetic Rate.....	46
3.4.1. Leaving Group Contribution.....	47
3.4.2. Chain Length Contribution.....	48
3.4.3. Steric Effects.....	49
3.4.4. Concentration Effects on Kinetic Constant.....	50
3.5. Summary of Results.....	51
References.....	53
4. Diffusion of Reactants and IL in Organic Compounds.....	56
4.1. Theory of NMR Diffusion.....	56
4.2. NMR Diffusion Procedure.....	59
4.3. Diffusion Results.....	63

4.4. Diffusion Controlled Kinetic Analysis.....	67
4.4.1. Analyzing Diffusion Controlled Kinetics; DMSO.....	67
4.5. Summary of Results.....	68
References.....	70
5. Reaction Engineering and Environmental Impact Analysis.....	72
5.1. Rowan Solvent Selection Table.....	73
5.2. GlaxoSmithKline's(GSK) Pharmaceutical Solvent Selection Table.....	75
5.3. Environmental Factor Analysis.....	79
5.4. Separations and Energy Analysis / Suggested Optimal Organic Solvents.....	80
5.5. Reaction Engineering Analysis.....	82
5.5.1. Adiabatic Temperature Rise.....	85
5.5.2. Non-Adiabatic Reactor.....	87
5.5.3. Reactor Sizing / Energy Cost for Adiabatic and Non-Adiabatic Process.....	88
5.6. Summary of Results.....	92
References.....	94
6. Ionic Liquid Synthesis and Phase Equilibrium in Carbon Dioxide.....	96
6.1. Phase Behavior.....	98
6.1.1. Six Types of Phase Behavior.....	98
6.1.2. Phase Behavior for 1-methylimidazole/CO ₂ ; 1-bromohexane/CO ₂	100
6.2. Phase Equilibrium.....	102
6.2.1. Mixture Critical Points.....	103
6.2.2. Phase Equilibrium Below Mixture Critical Point.....	103
6.3. Kinetics.....	105
6.4. Summary of Results.....	111
References.....	112
7. Conclusion/Future Work.....	115
7.1. Conclusion.....	115
7.2. Future Work.....	117
Appendix I: Data for Figures.....	119
Appendix II: Sigmaplot Regression Equation/Constraints.....	121
Appendix III: Procedure for NMR Diffusion.....	123
Appendix IV: Autoclave Schematic.....	129

Table of Figures:

Figure 1- 1 : Illustration of common cation/anion IL classification.....	2
Figure 1- 2 : Reaction between tripropylamine with methylbromide to form tripropylmethylammonium bromide.....	3
Figure 2- 1: Assembled and dismantled autoclaves.....	15
Figure 2- 2 : 1-methylimidazole ¹ H NMR in chloroform-d.....	18
Figure 2- 3 : 1-bromohexane ¹ H NMR in chloroform-d.....	18
Figure 2- 4 : 1-hexyl-3-methylimidazolium Bromide [HMIm][Br] ¹ H NMR in chloroform-d.....	19
Figure 2- 5 : 1-bromohexane ¹ H NMR in chloroform-d with peak integration.....	20
Figure 2- 6 : ¹ H NMR chemical shifts for reactants and product using ¹ H NMR in chloroform-d.....	21
Figure 2- 7 : Solvatochromic probes used in this study.....	23
Figure 2- 8 : Vapor Liquid apparatus.....	28
Figure 3- 1 : Reaction between triethylamine with bromohexane through a transition state.....	33
Figure 3- 2 : Gibbs Free Energy of transition.....	34
Figure 3- 3a-d : ln k against KT parameters and E _T (30) scale.....	41
Figure 3- 4 : LSER for the 10 solvents used in this study neglecting the polarizability correction term in the LSER regression for the rates of reactions at 40°C.....	42
Figure 3- 5 : LSER for the 10 solvents used in this study using the polarizability correction term in the LSER regression for the rates of reactions at 40°C.....	43
Figure 3- 6 : Methanol hydrogen bonding with 1-methylimidazole.....	45
Figure 3- 7 : 1-methylimidazole with alkylbromides of various alkyl lengths.....	48
Figure 4- 1 : Tanner and Stejskal pulse sequence.....	58
Figure 4- 2 : Bipolar Longitudinal Eddy Decay (BPP-LED) sequence.....	60
Figure 4- 3 : Typical Diffusion experiment: I/I ⁰ against % of total applied gradient.....	62
Figure 4- 4 : Diffusion coefficients for 1-methylimidazole and 1-bromohexane in acetonitrile at different mole fractions of solute at 25°C.....	67
Figure 5- 1 : Reaction between 1-methylimidazole and 1-bromohexane.....	80
Figure 5- 2 : Effect of acetone on the adiabatic temperature rise as determined by conversion.....	86
Figure 5- 3 : Mole fraction of acetone in the feed stream against the amount of heat removal for a non-adiabatic process.....	87
Figure 6- 1 : Reaction between 1-bromohexane and 1-methylimidazole forming [HMIm][Br].....	96
Figure 6- 2 : C _p for CO ₂ against pressure at 40°C.....	96
Figure 6- 3 : Six types of phase behavior for binary systems.....	99
Figure 6- 4 : Phase behavior for the binary mixture 1-methylimidazole/CO ₂	102
Figure 6- 5 : a.) Mole fraction of CO ₂ in the liquid phase versus Pressure data taken at 40°C for reactants and for the 1:1 mole ratio reactant mixture. b.) Mole fraction of CO ₂ in the liquid phase versus pressure data taken at 40°C for the product [HMIm][Br]	104

Figure 6- 6 : a) Volume expansion versus pressure data taken at 40°C for reactants and for the 1:1 mole ratio reactant mixture. b) Volume expansion versus pressure data taken at 40°C for the product [HMIm][Br]	104
Figure 6- 7 : Phase behavior at sub-critical conditions and above critical conditions for the reaction mixture.....	106
Figure 6- 8 : a.) Mole fraction of CO ₂ versus pressure data at 40°C b.) Volume expansion data versus the pressure at 40°C.....	107

Table of Tables:

Table 2- 1: Literature comparison of KT parameter.....	25
Table 3- 1: Hughes and Ingold's qualitative trends for nucleophilic substitution reactions.....	36
Table 3- 2 : Rates of reaction for initial 5 solvents at 40°C as well as KT parameters and $E_T(30)$ values.....	38
Table 3- 3 : Rates of reaction for the 10 solvents analyzed at three specified temperatures.....	40
Table 3- 4 : KT and $E_T(30)$ values for the 10 solvents used in this study.....	40
Table 3- 5 : Table of kinetic parameters.....	45
Table 3- 6 : Rates of reaction with different leaving groups.....	47
Table 3- 7 : Reaction between 1-methylimidazole and a number of branched bromoalkanes at 40°C in acetonitrile.....	49
Table 3- 8 : Concentration effects on the rate constant in acetonitrile.....	51
Table 3- 9 : KT parameters and $E_T(30)$ values for the reaction mixture.....	51
Table 4- 1 : Diffusion Rate of reactants and product in a number of solvents at a temperature of 25°C and $x_{\text{solute}}=0.05$	65
Table 4- 2 : Diffusion rate of 1-methylimidazole and 1-bromohexane in acetonitrile at different solute concentrations.....	65
Table 4- 3: Calculating the k_d in DMSO for the reaction between 1-methylimidazole and 1-bromohexane.....	68
Table 5- 1 : (RSST) 12 categories for solvent selection.....	73
Table 5- 2 : (GSK-SST) 9 categories for solvent selection.....	76
Table 5- 3 : Results from the (RSST) for determining the Pharmaceutical Index with a examples of the various factors.....	77
Table 5- 4 : (GSK-SST) results for solvent selection.....	78
Table 5- 5 : E-factor analysis for industry.....	79
Table 5- 6 : Boiling points, latent heats, sensible heats and total energy obtained for energy analysis.....	82
Table 5- 7 : Properties needed for calculating an adiabatic / non adiabatic process..	83
Table 5- 8 : Reactor Sizing and energy requirements for an adiabatic and non adiabatic process operating at 55°C with 90% conversion.....	91
Table 6- 1 : Table of C_p for organic solvents and CO ₂ at 40°C.....	97
Table 6- 2 : Experimentally acquired mixture critical points for reactants in CO ₂ taken at 40°C.....	103
Table 6- 3 : Overall kinetic rate constants taken at different pressures at a temperature of 40°C using a 1:1 mole ratio of 1-methylimidazole to 1-bromohexane.....	108
Table 6- 4 : KT parameters for CO ₂ , reactants, and product.....	109
Table 6- 5 : Comparison of rates of reactions for CO ₂ with those obtained in organic solvents.....	110

Table of Symbols:

$^{\circ}\text{C}$	degrees Celsius
^1H	Proton
$^1\text{H NMR}$	Proton Nuclear Magnetic Resonance
2^{nd}	Second Order
[Alk_MIm][X]	1-alkyl-3-methylimidazolium halide
B_0	External Magnetic Field
[BMIm][Br]	1-butyl-3-methylimidazolium Bromide
BPP-LED	Bipolar Longitudinal Eddy Decay
C_i	Component Concentration (moles/Liter)
C_i^o	Initial Component Concentration (moles/Liter)
C_p	Heat Capacity
CO_2	Carbon Dioxide
c	Speed of Light
cm	Centimeter
D	Diffusion Coefficient
DMSO	Dimethyl Sulfoxide
E_a	Activation Energy
FDA	United States Food and Drug Administration
$E_T(30)$	Scale of Polarity based on Solvatochromic Probe (Reichardt's Dye)
E-Factor	Environmental Factor
F_i^0	Initial Molar Flow Rate for Component (i) (Moles/Liter-sec)
GSK-SST	GlaxoSmithKline Pharmaceutical Solvent Selection Table
GRAS	Generally Regarded/Recognized as Safe
g	Gradient Field Strength
g^{max}	Maximum Field Gradient Strength
[HMIm][Br]	1-Hexyl-3-Methylimidazolium Bromide
H_i	Molar Enthalpy for Component (i)
HBA	Hydrogen Bond Acceptor
HBD	Hydrogen Bond Donor
HBr	Hydrogen Bromide
HCl	Hydrogen Chloride
HI	Hydrogen Iodide
h	Planck's Constant
I	NMR Peak Intensity
I^o	Reference Peak Intensity
I/v	(NMR Peak Intensity)/(protons giving rise to Peak)
ILs	Ionic Liquids
in.	Inch
KJ	Kilojoules
KT	Kamlet Taft
kK	kilokaysers ($1000\text{kK}=\text{cm}^{-1}$)

k^o	Frequency Factor (Arrhenius Equation)
k	Kinetic Rate Constant
k_B	Boltzmann's Constant
k_d	Diffusion Limiting Kinetic Rate Constant
LCEP	Lower Critical End Point
LLE	Liquid-Liquid Equilibrium
LSER	Linear Solvation Energy Relationship
$\ln k$	Natural Logarithm of the Kinetic Rate Constant
M	Molar (moles/Liter)
Mimid	1-Methylimidazole
m	Meter
m_i	Mass of Component (i)
min	Minute
mg	Milligram
mL	Milliliters
mol	Moles
mM	Millimolar (millimoles/Liter)
N_A	Avogadro's Number
NIST	National Institute of Standards and Technologies
NMR	Nuclear Magnetic Resonance
n_i^o	Initial Moles of Component (i)
n_i	Moles of Component (i)
\dot{n}_i	Molar Flow Rate for Component (i) (moles/second)
\dot{n}_{Tot}	Total Molar Flow Rate (i) (moles/second)
nm	Nanometer
PDE	Permitted Daily Exposure
PFG	Pulse Field Gradient
PF_6	Hexafluorophosphate
PT	Pressure-Temperature
ppm	Parts Per Million
Q	Total Heat
R	Ideal Gas Rate Constant
R^*	Reacting Distance (Chapter 4)
R_i	Hydrodynamic Radius for Component (i) (Chapter 4)
RSST	Rowan Solvent Selection Table
RTIL	Room Temperature Ionic Liquids
r_i	Kinetic Rate of Reaction
rf	Radio Frequency
S_N1	First-Order Nucleophilic Substitution Reaction
S_N2	Second-Order Nucleophilic Substitution Reaction
sec	Second
T	Temperature
TLV	Threshold Limiting Value

TMS	Tetramethylsilane
t	Time
UCEP	Upper Critical End Point
UV-Vis	Ultraviolet-Visible Spectrophotometer
V_f	Final Volume
V_i	Initial Volume
V	Reactor Volume
V^{mix}	Volume of Mixing
ν_o	Lamor Frequency
ν	Frequency
$\nu(i)_{max}$	Maximum Absorbance for Solvatochromic Probe (i)
VLE	Vapor-Liquid Equilibrium
VLLE	Vapor-Liquid-Liquid Equilibrium
VOC	Volatile Organic Compounds
X_i	Extent of Reaction / Conversion
x_i	Mole Fraction of Component (i)

Greek Symbols:

α	Kamlet Taft acidity parameter
β	Kamlet Taft basicity parameter
Δ	Diffusion Time
ΔE	Transition State Energy
ΔG^\ddagger	Gibbs Energy of Activation
ΔH^\ddagger	Enthalpy of Activation
ΔH^{rxn}	Heat of Reaction
ΔH^{vap}	Latent Heats of Vaporization
ΔS^\ddagger	Entropy of Activation
δ	Time duration for gradient pulse (Chapter 4)
δ	Polarizability Correction Term (Section 2.2.1)
δ_H	Chemical Shift for Proton (parts per million)
γ	Gyromagnetic Ratio
η	Viscosity
μL	Microliter
π	Pi (3.14)
π^*	Kamlet Taft dipolarity/polarizability parameter
ρ_i	Density of component (i)
τ	Dephasing and Rephrasing Term
ν_i	Transition State Energy for Component (i) (Hertz)
ν_0	Radio Frequency (Megahertz)
ω_0	Lamor Frequency (radians/second)

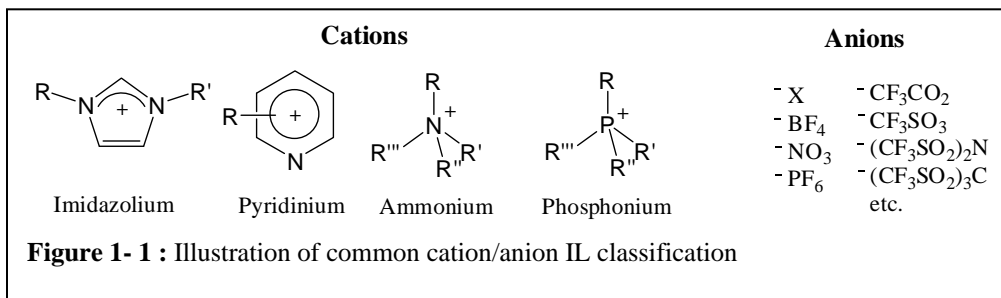
1. Introduction

Ionic liquids (IL) have been recognized in recent years as potentially being the next great class of environmentally-friendly solvents based on their lack of vapor-pressure as well as their molecularly “tunable” properties. ILs are being developed for a vast number of applications at an exponential rate. ILs have been known to have a long history in electrochemistry¹⁻³ and in recent years are playing a significant role in electrochemistry combined with nanomaterial technologies.^{4, 5} ILs have emerged as excellent solvents for enhancing activity, selectivity and catalysis stability in oligomerization and hydroformylation reactions⁶ as well as being used in biocatalysis for a wide range of chemical transformations.⁷⁻⁹ Recently, there has been a growing demand for imidazolium based ionic liquids and intermediates for N-heterocyclic carbene ligands for the creation of metal homogenous catalysts.¹⁰ They have also been used to dissolve and process cellulose and other carbohydrates,¹¹ as well as used for catalyst recovery.¹² In the field of analytical chemistry ILs have been found to be useful as stationary phases in chromatography and other separation and detection techniques.¹³⁻¹⁵ Related to separation techniques, ILs have also shown the ability to break a number of azeotropes.¹⁶⁻¹⁸ Furthermore, ILs are presently being investigated as desulfurization reagents in diesel fuel¹⁹ and extractants in the recovery of ethanol and butanol for biofuel applications.²⁰

1.1. IL Background

ILs have shown versatility in many fields of research and applications, so the question is what are ILs, and what makes ILs so unique? By definition ILs are organic salts which have a melting temperature below 100°C. ILs that melt below 25°C are called room temperature ILs (RTIL).²¹ Figure 1- 1 illustrates the most common classes of ILs. Depending on the functional *R* group or cation/anion pairing one can control the viscosity, solubility properties, melting point, density, acidity/basicity, polarizability, hydrogen bond donor/acceptor ability, chirality, etc., and it has been estimated that more than 10¹⁴ different cation and anion combinations exists.²² Also, since ILs have extremely low vapor pressures, worker and

environmental exposure is limited to only liquid contact, unlike volatile organic solvents where exposure is through the liquid or vapor. Preliminary toxicity studies have shown that, in general, ILs are low to moderate in toxicity.²³⁻²⁹ Moreover, the flammability of ionic liquids is very low, with high flash points resulting from the decomposition.³⁰ These attributes make ILs an attractive “greener” solvent replacement.



1.2. Problems with Ionic Liquid Production and Use

If ionic liquids are to be truly “green”, they must be made in a “green” manner. A large majority of IL synthesis are conducted in the very organic solvents which they are reportedly replacing. Ford *et al.*³¹ have demonstrated the synthesis of ammonium based ILs in petroleum ethers. Wilkes *et al.*³² use chloromethane and chloroethane to synthesize imidazolium based ILs. Bonhote *et al.*³³ produce imidazolium based ILs in 1,1,1-trichloroethane, and dichloromethane. Cammarate *et al.*³⁴ as well as Holbrey *et al.*³⁵ produced imidazolium based ILs in toluene. Selvan *et al.*³⁶ produced imidazolium based ILs in tetrahydrofuran. Neve *et al.*³⁷ produced pyridinium ILs in acetonitrile. Dzybuba and Bartsch³⁸ use dichloromethane to produce alkyaryl imidazolium ILs. MacFarlane *et al.*³⁹ use dichloromethane to process ammonium, imidazolium, and pyrrolidinium ILs. It has been estimated that nearly 20 millions tons of volatile organic solvents are released into the atmosphere each year resulting from industrial operations,⁴⁰ therefore, for ionic liquids to truly be a “green” solvent replacement they themselves must be synthesized in a corresponding benign manner. Another problem which needs to be addressed if ILs are to be utilized in an industrial application is the present cost of ILs. It is estimated that ILs range from \$1-\$10 dollars per gram,⁴⁰ which is ~2 orders of magnitude

greater than what is practical for large-scale use in industry.⁴⁰ The primary reason for the high cost of ILs results from **small batch scale operation** and **non-existent kinetic** and thermodynamic data for their synthesis. Typically, ILs are synthesized by recipe i.e. reflux overnight, or two nights, or for a week.^{31, 34, 41} For industrial production this is not practical, and/or sufficient for running a reactor, especially if the process were to be continuous.

1.2.1. IL Synthesis/Analysis

ILs are most commonly synthesized by a quaternization reaction of a substituted amine or phosphine followed by anion exchange if necessary as shown in Figure 1- 2. However, several alternative techniques have emerged and include halide-free production methods. Yoshizawa *et al.*⁴² have synthesized a number of zwitterionic type ILs, which contain both the anion and cation in a single molecule, by reacting imidazoles with 1,3-propanesultone. Bonhote *et al.*³³ use ethyl triflate and ethyl trifluoroacetates for the alkylation of 1-methylimidazole. Kunkel and Maas⁴³ have synthesized guanidinium ILs using tetraalkylureas and triflic anhydride. Ue *et al.*⁴⁴ use the alkylation of 1-ethylimidazole with dimethyl carbonate. Lectercq *et al.*⁴⁵ use a complex mechanism involving the reaction between tetrahydrofuran or 1,4-dioxane with triflic anhydride to form a diester which is then reacted with a N-substituted imidazole. Holbrey *et al.*³⁵ used an alkylation technique between dimethyl sulfate or diethyl sulfate with N-substituted imidazole to form imidazolium alkyl sulfate ILs.

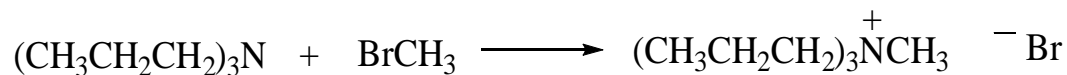


Figure 1- 2 : Reaction between tripropylamine with methylbromide to form tripropylmethylammonium bromide

Throughout the quaternization reaction two neutral reactants form oppositely charged ions through a polar transition state. Because the reaction proceeds through a polar transition state, the rate of reaction is influenced heavily by the polarity of the solvent. This was first demonstrated by Menshutkin over a century ago while

studying the S_N2 reaction between tertiary amines with primary haloalkanes using 23 solvents.⁴⁶⁻⁴⁸ Since this time, a large number of studies have been performed examining the solvent effects on the transition state in the formation of salts, and as Reichardt⁴⁸ states, “For many physical organic chemists, the Menshutkin reaction was a kind of “guinea pig”, which has been extensively used for the study of solvent effects on chemical reactivity.” There have been many attempts to relate rates of reaction for the Menshutkin type reaction using many physiochemical solvent properties: i.e. dielectric constants, solubility parameters, $E_T(30)$ values (scale based on solvent polarity) etc. However, in general no one parameter was able to explain and/or correlate rates of reaction over a wide range of solvent types. Thus, a more rigorous analysis was developed by Kamlet and Taft (KT),⁴⁹ which examined different characteristics of polarity for a given solvent, specifically: acidity, basicity, and dipolarity/polarizability of a given solvent using solvatochromic probes. Using these unique solvent contributions, KT developed a Linear Solvation Energy Relationship (LSER) method for regressing solvent characteristics over a wide range of solvent types, i.e. polar aprotic solvents, polar protic solvents, etc.

1.2.2. IL Reaction Engineering and Process Intensification

Few studies are found in the literature for reaction engineering or process intensification of the production of ionic liquids. Varma and Namboodiri⁵⁰ have shown that ILs can be synthesized quickly using microwave radiation; the reaction times are increased dramatically in high yield. By controlling the microwave power at different exposure time, Varma and Namboodiri⁵⁰ have determined rates of conversion using this method, with reported yield exceeding 94% within seconds compared to hours using conventional methods. However, they report no kinetic constants for either a general synthesis or by means of a microwave process. Since this study, a number of researches have also been focusing on synthesizing ILs in similar manners.^{51, 52} Another process intensification method for producing ILs involves using micro-reactors. Waterkamp *et. al.*⁵³ have demonstrated that continuous flow micro-reactors are advantageous in producing ILs, because micro-

reactors have the ability to dissipate heat much more efficiently than conventional batch operations based on the high surface area of the walls compared to the volume of the reaction mixture. Using the exothermic quaternization reaction between 1-methylimidazole with 1-bromobutane, they have shown that micro-reactors can be operated at higher temperatures compared to batch reactors without an adiabatic runaway reaction occurring. However, micro-reactors used without solvent have difficulty with the production of many ionic liquids or their intermediates, as solids salts or liquids with high viscosity cannot easily be forced through the microchannels. Leveque et. al.⁵⁴ have demonstrated that a one pot synthesis for the quaternization reaction in producing ILs followed by an anion exchanging method, which the halide anion resulting from the quaternization reaction is replaced with a bulkier anion such as hexafluorophosphate (PF_6), can be obtained using ultrasonic irradiation. However, yields obtained were only moderate and no correlation was made in determining rate constants.

1.3. Research Objectives

The current study will examine the quaternization reaction between 1-methylimidazole and a number of haloalkanes in the synthesis of 1-alkyl-3-methylimidazolium halides $[\text{Alk_MIm}][\text{X}]$ in a wide variety of organic solvents, and using compressed carbon dioxide (CO_2) as a novel solvent replacement. Primarily, the studies conducted will examine how solvents selection affects the kinetic rate constants by using a Linear Solvation Free Energy Relation (LSER) method with Kamlet-Taft (KT) parameters. The LSER method will give insight to specific solvent characteristics which hinder and benefit the quaternization reaction. The following is an outline of topics which will be covered. Chapter 2 consists of the experimental procedures and apparatus used for measuring the rates of reaction, phase equilibria and polarity scales. Chapter 3 is a thorough analysis of the solvent effects using organic solvents, and includes a number of studies to examine the implications of the leaving group, alkyl-chain length, and branching of the haloalkane on the rate of reaction. Chapter 4 is an overview of mass transport in these reaction systems.

Chapter 5 will examine the toxicity and environmental impact of solvent selection as well as solvent classifications for the sustainable production of ILs. Also, a qualitative reactor design analysis for the quaternization reaction will be conducted in an organic solvent. Chapter 6 outlines reactions conducted using compressed CO₂ at a given isotherm to evaluate how CO₂ affects the overall rate of reaction. Chapter 7 is a summary of the results obtained, and will outline future work.

References:

1. Sato, T.; Masuda, G.; Takagi, K., Electrochemical properties of novel ionic liquids for electric double layer capacitor applications. *Electrochim. Acta* **2004**, 49, (21), 3603-3611.
2. Xu, J. Q.; Yang, J.; Zhang, W. B., Study of ionic liquid electrolytes for secondary lithium batteries. *Acta. Chim. Sin.* **2005**, 63, (18), 1733-1738.
3. Yu, P.; Lin, Y. Q.; Xiand, L.; Su, L.; Zhang, J.; Mao, L. Q., Molecular films of water-miscible ionic liquids formed on glassy carbon electrodes: Characterization and electrochemical applications. *Langmuir* **2005**, 21, (20), 9000-9006.
4. Adedin, S. Z. E.; Polleth, M.; Meiss, S. A.; Janek, J.; Endres, F., Ionic liquids as green electrolytes for the electrodeposition of nanomaterials. *Green Chem.* **2007**, 9, 549-553.
5. Barisci, J. N.; Wallace, G. G.; MacFarlane, D. R.; Baughman, R. H., Investigation of ionic liquids as electrolytes for carbon nanotube electrodes. *Electrochem. Comm.* **2004**, 6, (1), 22-27.
6. Wasserscheid, P.; Keim, W., Ionic Liquids - new "solutions" for transition metal catalysis. *Angew. Chemie. Int. Ed.* **2000**, 39, (21), 3773-3789.
7. Liu, Q. B.; Zhang, Z. H.; J., F., Progress in biocatalytic reactions in ionic liquids. *Prog. Chem* **2005**, 17, (6), 1060-1066.
8. Reetz, M. T.; Wiesenhofer, W., Liquid poly(ethylene glycol) and supercritical carbon dioxide as a biphasic solvent for lipase-catalyzed esterification. *Chem. Commun.* **2004**, 23, 2750-2751.
9. Sheldon, R. A.; Lu, R. M.; Sorgedragar, M. J.; Rantwijk, F. v.; Seddon, K. R., Biocatalysis in ionic liquids. *Green Chem.* **2002**, 4, (2), 147-151.
10. Rouhi, A. M., Olefin Metathesis gets Nobel Nod. *Chem & Eng News* **2005**, 83, (41), 8.
11. Murugesan, S.; Linhardt, R. J., Ionic liquids in carbohydrate chemistry - current trends and future direction. *Curr. Org. Synth.* **2005**, 2, (4), 437-451.
12. Zhang, X.; Fan, X.; Niu, H.; Wang, J., An ionic liquid as a recyclable medium for the green preparation of a,a'-bis (substituted benzylidene)cycloalkanones catalyzed by FeCl₃*6H₂O. *Green Chem.* **2003**, 5, 267-269.
13. Gross, G. M.; Reid, V. R.; Synovec, R. E., Recent advances in instrumentation for gas chromatography. *Curr. Anal. Chem.* **2005**, 1, (2), 135-147.
14. Koel, M., Ionic Liquids in Chemical Analysis. *Crit. Rev. Anal. Chem.* **2005**, 35, (3), 177-192.
15. Pandey, S., Analytical applications of room-temperature ionic liquids: A review of recent efforts. *Anal. Chim. Acta.* **2006**, 556, (1), 38-45.
16. Jork, C.; Seiler, M.; Beste, Y.-A.; Arlt, W., Influence of Ionic Liquids on the Phase Behavior of Aqueous Azeotropic Systems. *J. Chem. Eng. Data* **2004**, 49, 852-857.
17. Seiler, M.; Jork, C.; Kavarnou, A.; Arlt, W.; Hirsch, R., Separation of azeotropic mixtures using hyperbranched polymers or ionic liquids. *AIChE J* **2004**, 50, (10), 2439-2454.

18. Zhao, H., Innovative Applications of Ionic Liquids as "Green" Engineering Liquids. *Chem. Eng. Comm.* **2006**, 193, 1660-1677.
19. Bosmann, A.; Datsevich, L.; Jess, A.; Lauter, A.; Schmitz, C.; Wasserscheid, P., Deep desulfurization of diesel fuel by extraction with ionic liquids. *Chem. Commun.* **2001**, 2494-2495.
20. Fadeev, A. G.; Meagher, M. M., Opportunities for ionic liquids in recovery of biofuels. *Chem. Commun.* **2001**, 295-296.
21. Lancaster, L., Organic reactivity in ionic liquids: some mechanistic insights into nucleophilic substitution reactions. *J. Chem. Res.* **2005**, (7), 413-417.
22. Holbrey, J. D.; Seddon, K. R., Ionic Liquids. *Chem. Proc.* **1999**, 1, (4), 223-236.
23. Bernot, R.; Brueske, M.; Evans-White, M.; Lamberti, G., Acute and chronic toxicity of imidazolium-based ionic liquids on *Daphnia magna*. *Environ. Toxicol. Chem.* **2005**, 24, (1), 87-92.
24. Garcia, M.; Gathergood, N.; Scammells, P., Biodegradable ionic liquids: Part II. Effect of the anion and toxicology. *Green. Chem.* **2005**, 7, (1), 9-14.
25. Gathergood, N.; Garcia, M.; Scammells, P., Biodegradable ionic liquid: Part I. Concepts preliminary targets and evaluation. *Green. Chem.* **2004**, 6, (2), 166-175.
26. Jastorff, B.; Stormann, R.; Ranke, J.; Molter, K.; Stock, F.; Oberheitmann, B.; Hoffmann, W.; Hoffmann, J.; Nuchter, M.; Ondruschka, B.; Filser, J., How hazardous are ionic liquids? Structure-activity relationships and biological testing as important elements for sustainability evaluation. *Green Chem.* **2003**, 5, (2), 136-142.
27. Pretti, C.; Chiappe, C.; Pieraccini, D.; Gregori, M.; Abramo, F.; Monni, G.; Intorre, L., Acute toxicology of ionic liquids to the zebrafish (*Danio rerio*). *Green Chem.* **2006**, 8, 238-240.
28. Stepnoski, P.; Skladanowski, A.; Ludwiczak, A.; Laczynska, E., Evaluating the cytotoxicity of ionic liquids using human cell line HeLa. *Hum. Exp. Toxicol.* **2004**, 23, (11), 513-517.
29. Wasserscheid, P.; Hal, R. v.; Bosmann, A., 1-n-butyl-3-methylimidazolium ([bmim]) octylsulfate: an even 'greener' ionic liquid. *Green Chem.* **2002**, 4, 400-404.
30. Fox, D. M.; Awad, W. H.; Gilman, J. W.; Maupin, P. H.; DeLong, H. C.; Trulove, P. C., Flammability, thermal stability, and phase change characteristics of several trialkylimidazolium salts. *Green Chem.* **2003**, 5, 724-727.
31. Ford, W. T.; Hauri, R. J.; Hart, D. J., Synthesis and Properties of Molten Tetraalkylammonium Tetraalkylborides. *J. Org. Chem.* **1973**, 38, (22), 3916-3918.
32. Wilkes, J. S.; Levisky, J. A.; Wilson, R. A.; Hussey, C. L., Dialkylimidazolium Chloroaluminate Melts: A New Class of Room-Temperature Ionic Liquids for Electrochemistry, Spectroscopy, and Synthesis. *Inorg. Chem.* **1982**, 21, (3), 1263-1264.
33. Bonhote, P.; Dias, A.-P.; Papageorgiou, N.; Kalyanasundaram, K.; Gratzel, M., Hydrophobic, High Conductive Ambient-Temperature Molten Salts. *Inorg. Chem.* **1996**, 35, 1168-1178.

34. Cammarata, L.; Kazarian, S. G.; Salter, P. A.; Welton, T., Molecular states of water in room temperature ionic liquids. *Phys. Chem. Chem. Phys.* **2001**, 3, (23), 5192-5200.
35. Holbrey, J. D.; Reichert, W. M.; Swatloski, R. P.; Broker, G. A.; Pitner, W. R.; Seddon, K. R.; Rogers, R. D., Efficient, halide free synthesis of new, low cost ionic liquids: 1,3-dialkylimidazolium salts containing methyl- and ethyl-sulfate anions. *Green Chem.* **2002**, 4, (407-413).
36. Selvan, M. S.; McKinley, M. D.; Dubois, R. H.; Atwood, J. L., Liquid-Liquid Equilibria for Toluene + Heptane + 1-Ethyl-3-methylimidazolium Triiodide and Toluene + Heptane + 1-Butyl-3-methylimidazolium Triiodide. *J. Chem. Eng. Data* **2000**, 45, 841-845.
37. Neve, F.; Francescangeli, O.; Crispini, A.; Charmant, J., A2[MX4] Copper (II) Pyridinium Salts. From Ionic Liquids to Layered Solid to Liquid Crystals. *Chem. Mater.* **2001**, 13, 2032-2041.
38. Dzyuba, S. V.; Bartsch, R. A., Influence of structural variations in 1-alkyl(aralkyl)-3-methylimidazolium hexaphosphates and bis(trifluoromethylsulfonyl)imides on physical properties of the ionic liquids. *PhysChemPhys* **2002**, 3, (2), 161-167.
39. MacFarlane, D. R.; Golding, J.; Forsyth, S.; Forsyth, M.; Deacon, G. B., Low viscosity ionic liquids based on organic salts of the dicyanamide anion. *Chem. Comm.* **2001**, 1430-1431.
40. Brennecke, J. F.; Maginn, E. J., Ionic Liquids: Innovative Fluids for Chemical Processing. *AIChE J.* **2001**, 47, (11), 2384-2389.
41. Kilaru, P.; Baker, G. A.; Scovazzo, P., Density and Surface Measurements of Imidazolium-, Quaternary Phosphonium-, and Ammonium-Based Room-Temperature Ionic Liquids: Data and Correlations. *J. Chem. Eng. Data* **Web published 2007**.
42. Yoshizawa, M.; Hirao, M.; Ito-Akita, K.; Ohno, H., Ion conduction in zwitterionic-type molten salts and their polymers. *J. Mater. Chem.* **2001**, 11, 1057-1062.
43. Kunkel, H.; Maas, G., Hexaalkylguanidinium Trifluoromethanesulfonates - A General Synthesis from Tetraalkylureas and Triflic Anhydride, and Properties as Ionic Liquids. *Eur. J. Org. Chem.* **2007**, 22, 3746-3757.
44. Ue, M.; Takeda, M.; Takahashi, T.; Takehara, M., Ionic Liquids with Low Melting Points and Their Application to Double-Layer Capacitor Electrolytes. *Electrochem. Solid-State Lett.* **2002**, 5, (6), A119-A121.
45. Leclercq, L.; Suisse, I.; Nowogrocki, G.; Agbossou-Niedercorn, F., Halide-free highly-pure imidazolium triflate ionic liquids: Preparation and use in palladium-catalysis allylic alkylation. *Green Chem.* **2007**, 9, 1097-1103.
46. Menshutkin, N., *Z. Phys. Chem* **1890**, 5, 589.
47. Menshutkin, N., **1890**, 6, 41.
48. Reichardt, C., *Solvent and Solvent Effects in Organic Chemistry*. 3 ed.; Wiley-VCH: Weinheim, Germany, 2003; p 629.
49. Kamlet, M. J.; Abboud, J. M.; Abraham, M. H.; Taft, R. W., Linear Solvation Energy Relationship. 23. A Comprehensive Collection of the Solvatochromic

Parameters, π^* , α , β , and Some Methods for Simplifying Solvatochromic Equation. *J. Org. Chem.* **1983**, (48), 2877-2887.

50. Varma, R. S.; Namboodiri, V. V., An expeditious solvent-free route to ionic liquids using microwaves. *Chem. Comm.* **2001**, 7, 643-644.

51. Deetlefs, M.; Seddon, K. R., Improved preparations of ionic liquids using microwave radiation. *Green Chem.* **2003**, 5, 181-186.

52. Gmeiner, G.; Reichel, C.; Lendl, B.; Gaertner, P., Microwave-Assisted Synthesis of Camphor-Derived Chiral Imidazolium Ionic Liquids and Their Application in Diastereoselective Diels-Alder Reaction. *Synthesis* **2007**, (9), 1333-1338.

53. Waterkamp, D. A.; Heiland, M.; Schluter, M.; Sauvageau, J. C.; Beyersdorff, T.; Thoming, J., Synthesis of ionic liquids in micro-reactors-a process intensification study. *Green Chem.* **2007**, 9, 1084-1090.

54. Leveque, J.-M.; Cravotto, G.; Boffa, L.; Bonrath, W.; Draye, M., One-pot and Solventless Synthesis of Ionic Liquids under Ultrasonic Irradiation. *Synlett* **2007**, (13), 2065-2068.

2. Experimental Methods

2.1. Kinetic Measurements

The reaction between 1-methylimidazole and 1-bromohexane forming the ionic liquid 1-hexyl-3-methylimidazolium bromide [HMIm][Br] is a special class of reactions known as the Menshutkin reaction. The rate of reaction for Menshutkin reactions are highly depend on the solvent, and can vary by more than an order of magnitude. This study will examine how different solvent characteristics affect the kinetic rate constant using traditional organic solvents, generally regarded as safe (GRAS) solvents, and dense phase carbon dioxide (CO₂) as a solvent media. Solvent properties will be investigated using Kamlet Taft (KT) parameters which are based on solvent's acidity (α), basicity (β), and dipolarity/polarizability (π^*). Using a linear solvation energy relationship (LSER) the rate constants will be correlated to α , β , and π^* for each solvent in determining which solvent properties are needed to sustain a high rate of reaction. All kinetic experiments (organic solvents and CO₂) were conducted using a sampling technique and the rates of reactions were analyzed using nuclear magnetic resonance (NMR) spectroscopy. NMR has been used to measure concentrations and conversions in a wide range of reaction types.^{1, 2} The kinetic rate constants were determined from the expression for the disappearance of reactants (appearance of IL) using Equation 2- 1:

$$r_{IL} = -r_{Mimid} = -r_{AlkylHalide} = -\left(\frac{\partial C_{Mimid}}{\partial t}\right) = k[C_{Mimid}][C_{AlkylHalide}] \quad \text{Equation 2- 1}$$

where r is the reaction rate based on component i , k the kinetic constant, C_i are the concentrations for each component, t is time, $Mimid$ is subscripted for 1-methylimidazole, $AlkylHalide$ is subscripted for the alkylhalide involved in the reaction, and IL is subscripted for the product, ionic liquid. The kinetics were assumed and confirmed as being bimolecular. Kinetic constants were determined by regressing all experimental data in SigmaPlot 2000 version 6.00 using Equation 2- 2 for equal molar addition of starting materials,

$$C_{Mimid} = \left[kt + \frac{1}{C_{Mimid}^o} \right]^{-1} \quad \text{Equation 2- 2}$$

and Equation 2- 3 for different mole ratio of reactants.

$$C_{Mimid} = \frac{C_{AlkylHalide}}{M \exp(C_{Mimid}^o (M - 1)kt)} \quad \text{where } M = \frac{C_{AlkylHalide}^o}{C_{Mimid}^o} \quad \text{Equation 2- 3}$$

where C_i^o are the initial concentrations for reactants.

2.1.1. Ambient Pressure

Reactants and solvent were weighed in 20 mL scintillation vials containing a magnetic stir bar using a Mettler Toledo XS205 Dual Range balance which has an uncertainty of ± 0.01 mg. After weighing, a light flow of argon is blown into the vial before being sealed and placed in a preheated reactor block (product number CG-1991-03 purchased from Chemglass) which holds 16 standard 20 mL scintillation vials. An IKA RCT basic stirring hotplate equipped with an ETS-D4 fuzzy logic temperature controller was used to control the temperature to within $\pm 1^\circ\text{C}$. The accuracy of the hotplates was verified using an Omega thermocouple (type T) which has a temperature accuracy of $\pm 0.5^\circ\text{C}$. At timed intervals a small sample, approximately 100 μL , was drawn from each vial and placed in a Nuclear Magnetic Resonance (NMR) tube containing deuterated chloroform. A proton NMR was conducted on each sample using a Bruker 400 MHz Ultrashield NMR supplied with Topspin version 1.3 software to determine the percent conversion. The time between the sample extraction and the NMR acquisition was typically less than five minutes. From the resultant kinetic rates, this lag is insignificant to the accuracy of the conversion versus time data. See Section 2.1.3 for further NMR spectrum analysis.

2.1.1.1. Mixture Densities

Mixture densities at various compositions and temperatures are important for calculating conversion between mole fraction, mass fraction and molarity. Since all weight measurements were conducted at ambient conditions, the corresponding volume for each reaction mixture and temperature had to be calculated to account for any volume expansion. By carefully measuring the volume, the mixture density

could be obtained allowing for concentrations to be calculated accurately. Mixture volumes were calculated using a 10 mL volumetric flask which has an uncertainty of ± 0.05 mL and a 500 μ L syringe with an uncertainty of ± 2 μ L. The mole ratios used for each reaction were scaled down to an estimated volume of 10 mL using Equation 2- 4.

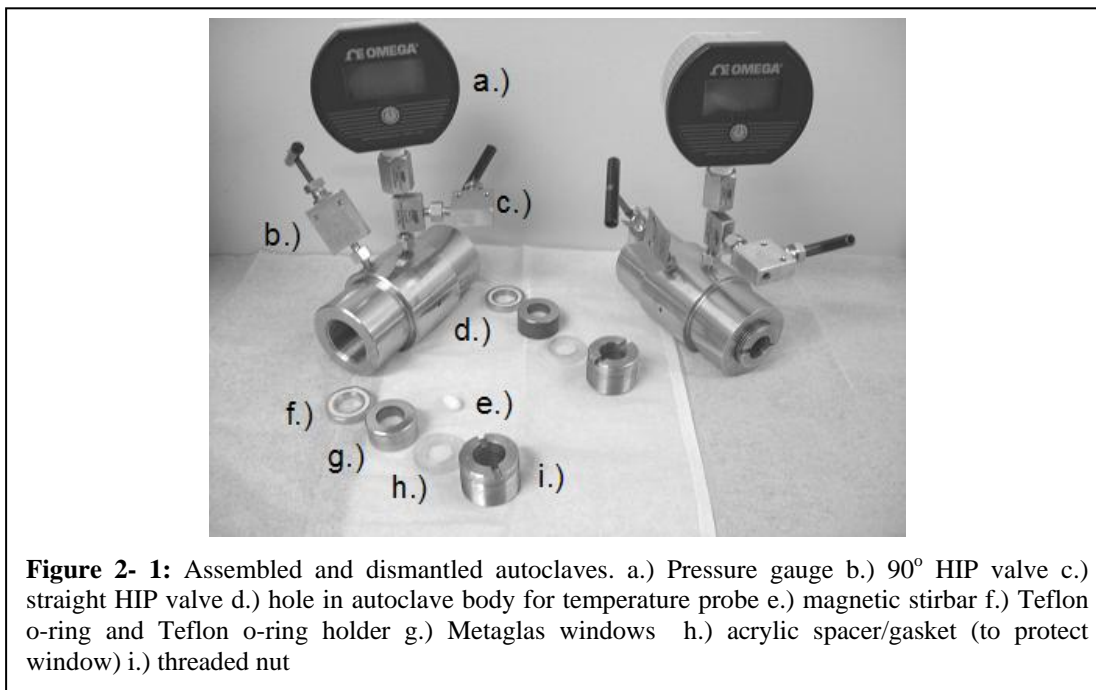
$$V_{mix} = \sum \frac{m_i}{\rho_i} \quad \text{Equation 2- 4}$$

where V_{mix} is the mixture volume (10 mL), m_i is the mass for each component, and ρ_i is the density of each component taken at 25°C. Each component was weighed into a 10 mL volumetric flask using the Mettler Toledo XS205 Dual Range balance. The volumetric flasks were then sealed and thoroughly mixed before being submerged in a stirring water bath at the specified temperature of the reaction. The temperature of the water bath was maintained using the IKA RCT basic hotplates and the temperature of the bath was verified using the Omega (type T) thermocouple. The volumetric flasks were submerged for a minimum of fifteen minutes prior to being removed to allow the temperature to equilibrate throughout the volumetric flask. Once the volumetric flasks were removed from the water bath the liquid level was quickly marked on the side of the volumetric flask. Once the volumetric flask cooled to ambient conditions the mixture was removed from the flask and the volumetric flask was washed thoroughly. Acetonitrile was then added to the volumetric flask to the 10 mL mark. The 500 μ L syringe containing acetonitrile was then added to the volumetric flask to the marked volume height drawn on the volumetric flask. By adding the amount of acetonitrile added to the volumetric flask using the micro syringe the total volume of the mixture was determined and recorded. By dividing the total mass placed in the volumetric flask (from reactants and solvent) by the total volume occupied by the liquid in the flask a mixture density was determined for each solvent at each temperature specified. The mixture density calculations were repeated a total of three times for each solvent and temperature, and the average density was used for the kinetic calculations. To verify that the mixture density did not change

significantly as the reaction proceeds, the density of the mixture before and after the reaction were experimentally measured. Results in methanol are used for illustration. Initially the reactants, 1-methylimidazole and 1-bromohexane, were added to a 10 mL volumetric flask along with methanol using the mole ratios for reactants and solvent used in determining the rate constants in chapter 3, section 3.2. The solution was then mixed thoroughly and the density of the mixture was calculated. In a second 10 mL volumetric flask the product, 1-hexyl-3-methylimidazolium bromide and methanol were added at the same ratio as the first volumetric flask (assuming 100% conversion). The volumetric flask was then mixed thoroughly and the mixture density was calculated. Comparing the two mixture densities, it was concluded that less than a 1% change in the mixture density occurred between the initial reactants and the results obtained at 100% conversion.

2.1.2. High Pressure

Dense phase carbon dioxide (CO₂) is being investigated as a possible solvent replacement for two main reasons. Since CO₂ is in a gaseous form at atmospheric conditions the separation process needed to remove the CO₂ after the reaction is eliminated by depressurizing the system. The other benefit to using CO₂ as a solvent media is the fact the CO₂ is typically considered a benign solvent with minimal health risk.⁸ All reactions conducted using dense phase CO₂ were performed using autoclave reactors manufactured in the Chemical Engineering department's machine shop at the University of Kansas (See Appendix for the autoclave blueprints). The design is similar to Leitner and coworkers.⁹ It is equipped with two HIP valves, a magnetic stir bar, two view windows, and an Omega digital pressure gauge, model number DPG5500B, which is accurate to within $\pm 0.25\%$ of full scale. Pictures of the autoclave are given in Figure 2- 1.



The autoclave was initially preheated to the desired temperature using an IKA RET basic C hotplate fitted with an IKA ETS-D4 fuzzy logic controller, which has an accuracy of $\pm 1^\circ\text{C}$. While the autoclave was preheating, a Teledyne ISCO Model 100DM syringe pump controlled by a Teledyne ISCO D-Series pump controller was attached to the autoclave through a 1/16 inch (in.) high pressure line. Once preheated, the reactants were added to the autoclave using two 2.5 mL micro syringes. The weight of reactants was determined by weighing each syringe containing the reactants before and after addition to the autoclave with the Mettler Toledo XS205 dual range balance. Once reactants were added to the autoclave, a timer was started and the autoclave was purged twice using carbon dioxide to remove all oxygen from the autoclave. The autoclave was then pressurized while the mixture was continuously stirred.

At specified times the temperature, pressure, time, and any visual notes were recorded before submerging the autoclave in an ice bath to quench the reaction. The carbon dioxide was evacuated slowly into a 25 mL volumetric flask containing a convenient organic solvent, which has minimal or no NMR peak overlap with

reactants and product using a 1/16 in. line connected to one of the HIP valves on the autoclave. The collection solvent was to trap any of the reactants in the vapor phase. Mass balances could not be confirmed unless the venting vapor was collected. The venting process took about 30 minutes to complete. Once the pressure reached ambient conditions, the autoclave was removed from the ice bath and one of the sides was opened. The liquid mixture in the autoclave was dissolved with solvent and extracted from the autoclave. The extracted solvent mixture was added the mixture collected from the venting vapor and mixed thoroughly. A small sample was then taken from the solution, 100 μ L, and added to an NMR tube containing deuterated chloroform. A proton NMR was then conducted using the Bruker 400 NMR to determine the conversion. This procedure was repeated a total of three times to calculate a standard deviation at each time point and operating pressure and temperature. A detailed analysis for determining conversion is given in section 2.1.3.

2.1.3. NMR Analysis

For a detailed analysis of the physics of NMR spectroscopy, the reader is referred to Gunther.¹⁰ NMR spectroscopy is a tool which exploits the magnetic properties of atomic nuclei containing non-zero magnetic moments within a magnetic field. Atoms such as ^1H , ^{19}F , ^{31}P , and the isotope ^{13}C are just a few, and the most commonly used atoms analyzed with NMR spectroscopy. In this study, standard proton NMR (^1H NMR) spectroscopy was used for calculating the rates of reactions by integrating specified reactants and product chemical shifts. The following figures: Figure 2- 2, Figure 2- 3, and Figure 2- 4 are spectral representations for reactants and product peaks, respectively, with the corresponding chemical shifts in deuterated chloroform (chloroform-d) using a tetramethylsilane (TMS) standard.

The proton labeling for the ^1H NMR spectrums given in Figure 2- 2, Figure 2- 3, and Figure 2- 4 were determined by the chemical shifts, proton integration, and by the observed splitting patterns, i.e. singlet, doublet, triplet, etc. The same analysis can be made using other atomic nuclei containing non-zero magnetic moments, however, for discussion, ^1H NMR will be analyzed more thoroughly. Chemical shifts are

represented by a change in transition state energy brought on using a high-frequency radio transmitter in a magnetic field, Equation 2- 5, and typically are on the order of magnitude of Hertz (Hz).

$$\Delta E = h\nu \quad \text{Equation 2- 5}$$

where ΔE is the change in transition state energy, h is Planck's constant, and ν is the frequency brought about by an electromagnetic field. Depending on the chemical environment which the protons reside a number of different transition state are observed, which are separated spectrally using chemical shifts. However, the degree of energy separation between the transition states have been shown to be highly field dependent, as given by the Lamor frequency (Equation 2- 6).

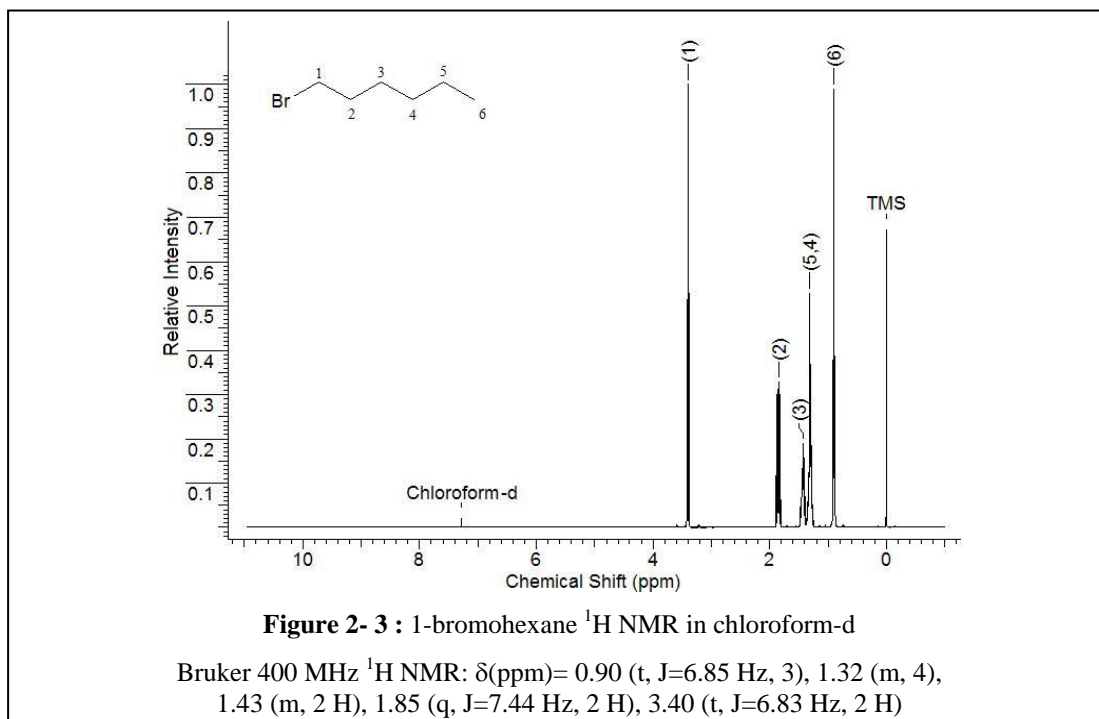
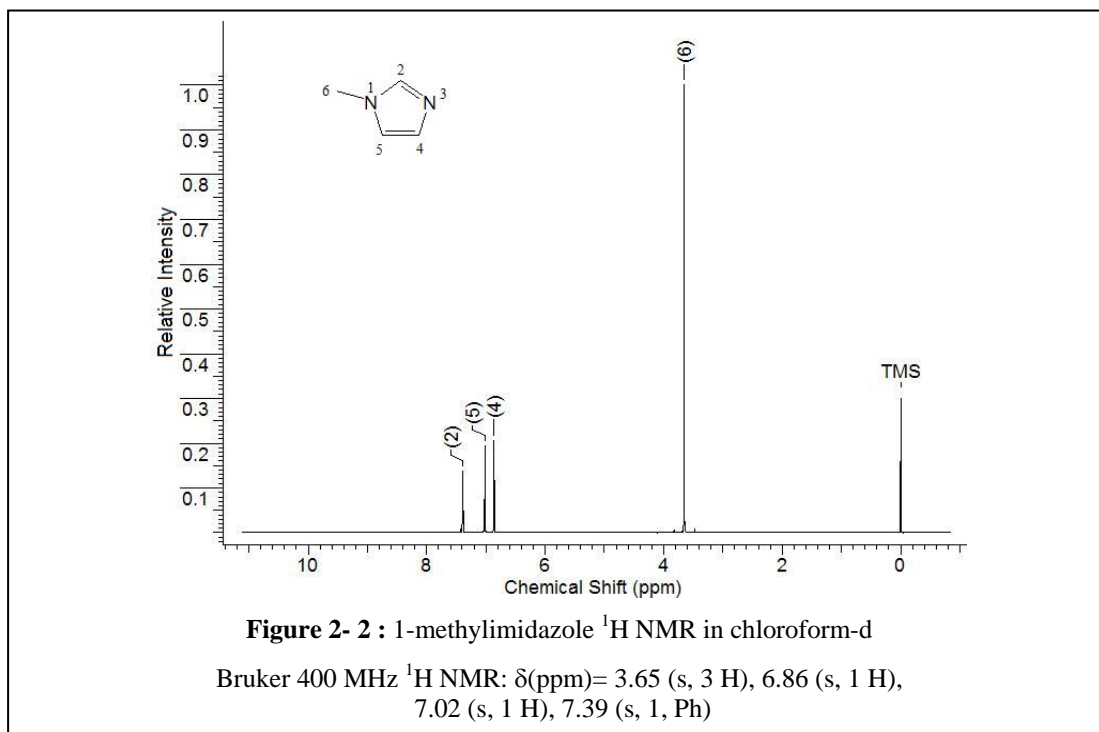
$$\nu_0 = \frac{\gamma B_0}{2\pi} \quad \text{where } \nu_0 = \frac{\omega_0}{2\pi} \quad \text{Equation 2- 6}$$

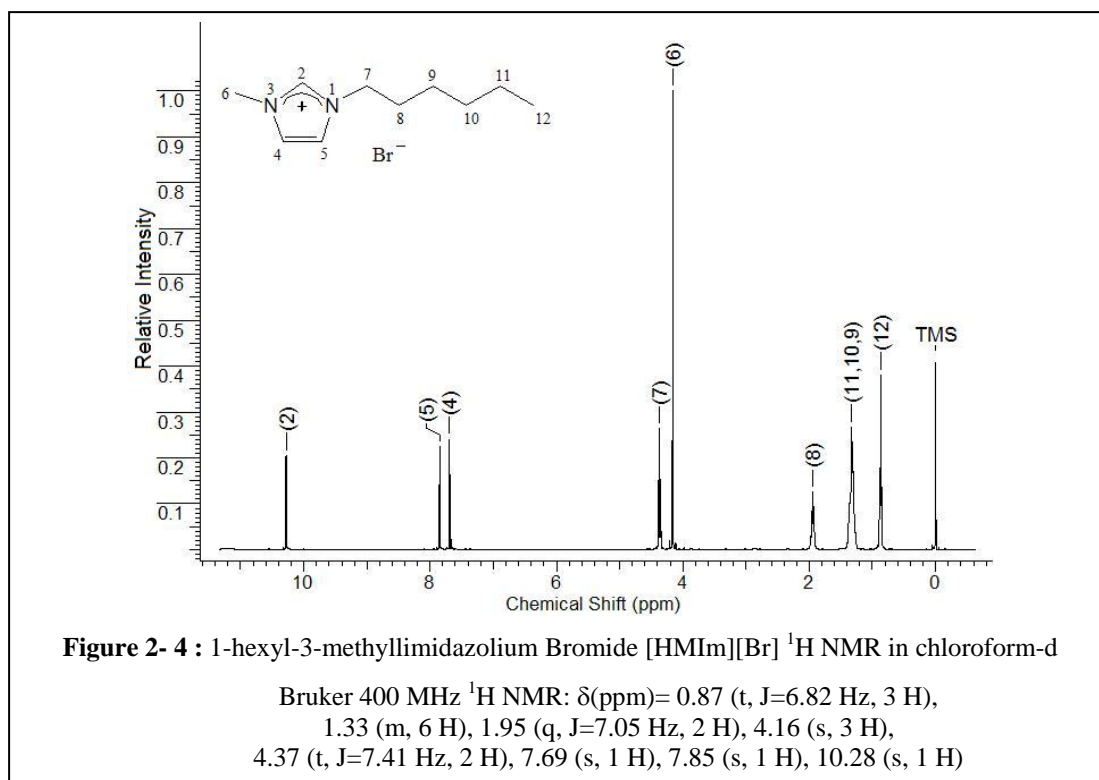
where B_0 is the external magnetic field's strength, γ is the gyromagnetic ratio equivalent to $2.675 \times 10^8 \text{ T}^{-1}\text{sec}^{-1}$ for protons¹⁰, ν_0 is the Lamor frequency (degrees/sec), and ω_0 is the Lamor frequency in (radians/sec). Thus, the transition state energy, chemical shift, resulting from a NMR with an external magnetic field of 1.4 Tesla would be different than using a NMR with an external magnetic field of 2.8 Tesla for the same protons. To rectify the discrepancies between different magnetic field strengths, a unitless quantity for chemical shift has been developed based on the external magnetic field using a reference compound as standard, typically TMS for ¹H NMR, which is given by Equation 2- 7.

$$\delta_H = \frac{\nu_{\text{substance}} - \nu_{\text{reference}}}{\nu_0} \quad \text{Equation 2- 7}$$

where δ_H is the chemical shift for a proton, $\nu_{\text{substance}}$ is the transition state energy for a particular proton, $\nu_{\text{reference}}$ is the reference transition state energy, typically (TMS), and ν_0 is the radio frequency. Since the transition state energies are given in Hertz (Hz) and the radio frequency are in units of Megahertz, chemical shifts are typically represented as parts per million (ppm). A large number of chemical shifts have been

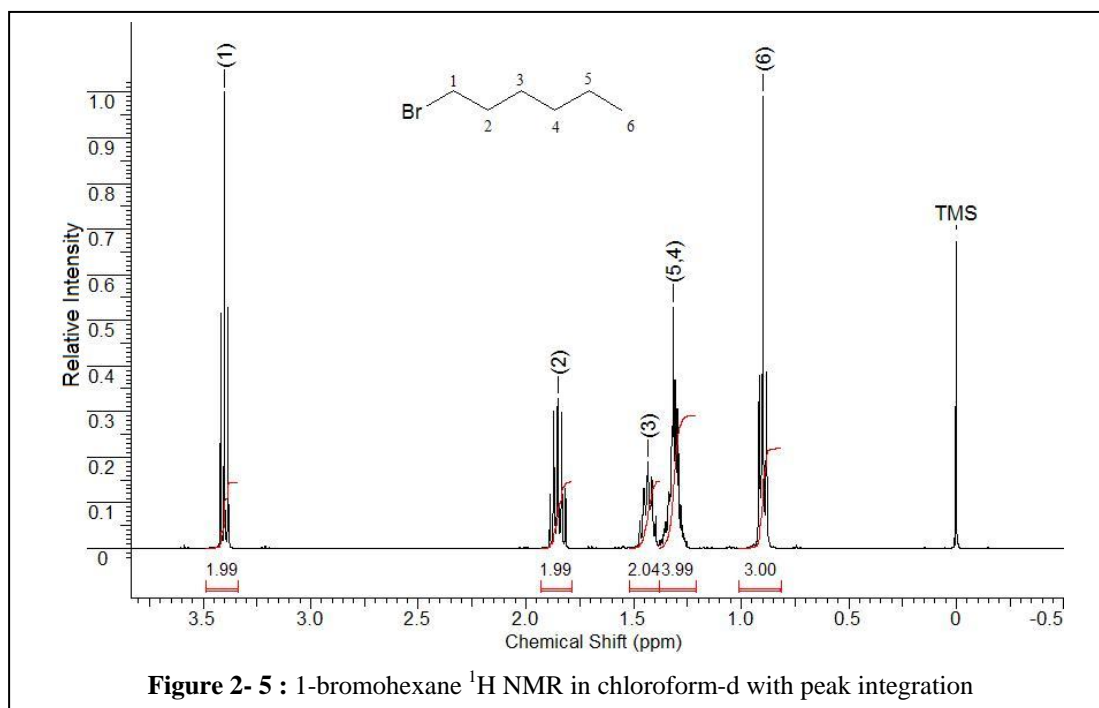
tabulated for protons based on the functional groups they are attached and are given in Gunther.¹⁰



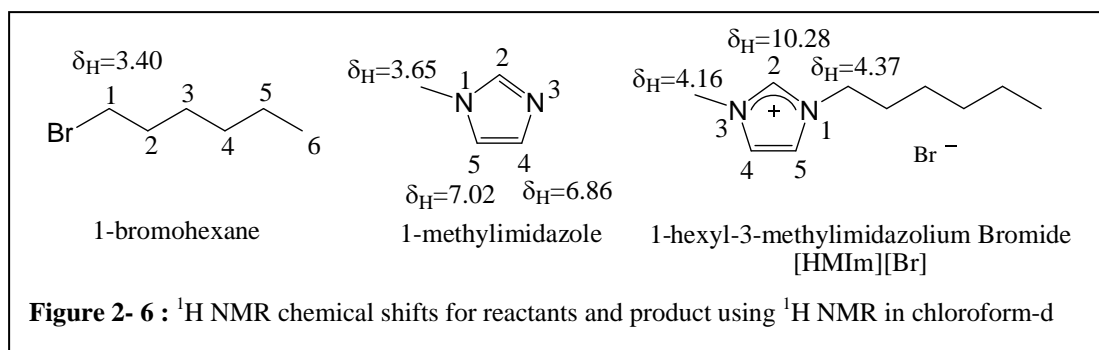


Besides chemical shift, integration and splitting patterns observe in NMR spectrums give insight into structure as well as assigning proton peaks (proton resonance signals). Integrations are calculated using a built-in electronic integrating software supplied with the spectrometer. In general, integration is a quantitative measurement of number of protons giving rise to a peak and is calculated using the area under a given peak, stated by Gunther.¹⁰ This will be examined shortly with 1-bromohexane. Splitting occurs by the magnetic interactions between individual protons; see Gunther.¹⁰ However, the general rule for determining splitting patterns is to count the number of proton(s) neighboring the protons analyzed at a given chemical shift and adding one. This is illustrated examining 1-bromohexane, Figure 2- 5. First looking at the chemical shift for 1-bromohexane it is seen that the chemical shift for the protons decreases the further away the protons are from the electronegative atom which is as expected from the proton chemical shift table given in Gunther.¹⁰ Examination of the integrations, after normalizing the area under the curves, (1) shows an integration of 2, representative of the 2 protons giving rise to the

signal, (2) gives rise to 2 protons as well, etc. Because the electronegative effects from the bromide atom are less the further away the protons are, (3), (4), and (5) have very similar chemical shifts with (4) and (5) overlapping. However, if you count the number of protons representative for (4) and (5), it is seen that the integration is fairly accurate. Examining the splitting pattern starting with (1), the number of neighboring protons is 2 resulting from the protons at (2), therefore, the splitting pattern should be the number of protons plus one to give a triplet for (1). Examining the protons at (2) shows four neighboring hydrogens from (1) and (3), thus, four hydrogens plus one result in a quintet for (2). The same analysis can be made for the remaining protons.



The analysis used for the pure 1-bromohexane can also be extended to mixtures. Conversion for the quaternization reaction between 1-methylimidazole and haloalkanes was conducted using a number of distinguishable chemical shift differences between the reactants and product. Figure 2- 6 is a compilation of chemical shifts for the quaternization reaction between 1-methylimidazole and 1-bromohexane used to analyze conversion.



The primary chemical shifts examined were $\delta_H=3.65$ on 1-methylimidazole and $\delta_H=3.40$ on 1-bromohexane and the corresponding chemical shifts $\delta_H=4.16$ and $\delta_H=3.40$. When solvent overlap was a concern such as methanol with chemical shifts at $\delta_H=3.31$ and $\delta_H=4.87$, the chemical shift for 1-methylimidazole at $\delta_H=7.02$ and $\delta_H=6.86$ were used with the products chemical shift $\delta_H=10.28$.

As previously shown examining 1-bromohexane, integration is a powerful quantitative tool for determining the amount of hydrogens present at a given NMR signal. Therefore, special consideration was made when integrating two peaks resulting from a different number of protons. For example, when a 1:1 mole ratio of 1-methylimidazole and 1-bromohexane are mixed the integrations at $\delta_H=3.65$ for 1-methylimidazole is 1.5 times greater than that of $\delta_H=3.40$ for 1-bromohexane, because there are three protons giving rise to the 1-methylimidazole peak, while only 2 protons are present for 1-bromohexane. To eliminate the confusion and possible error in analysis, all integrations for reactants and products were divided by the number of protons giving rise to each NMR signal. Conversion was calculated by examining the integration of reactant to product using Equation 2- 8.

$$X_a = \frac{\left[\frac{I}{v} \right]_{product}}{\left[\frac{I}{v} \right]_{product} + \left[\frac{I}{v} \right]_{reactant}} \quad \text{Equation 2- 8}$$

where X_a is conversion, $I/v_{product}$ corresponding to the integrated product peak divided by the number of hydrogens giving rise to the product peak and $I/v_{reactant}$

corresponding to the reactant peak divided by the number of hydrogens giving rise to the peak.

The NMR method was validated using two known concentrations of reactants and product resulting in a 25% and 75% conversion in acetonitrile. Reactants, solvent, and product were weighed using the Mettler Toledo XS205 Dual Range balance. The mixture was then thoroughly mixed, and a 100 μL sample was drawn and placed in an NMR tube containing chloroform-d. The mixture was then analyzed using the Bruker 400 MHz NMR using the peak integrations for reactant and product, which were then placed in Equation 2- 8. Comparing the result obtained numerically, with the calculations performed by integration showed less than a $\pm 0.4\%$ difference for both the 25% conversion 75% conversion calibration.

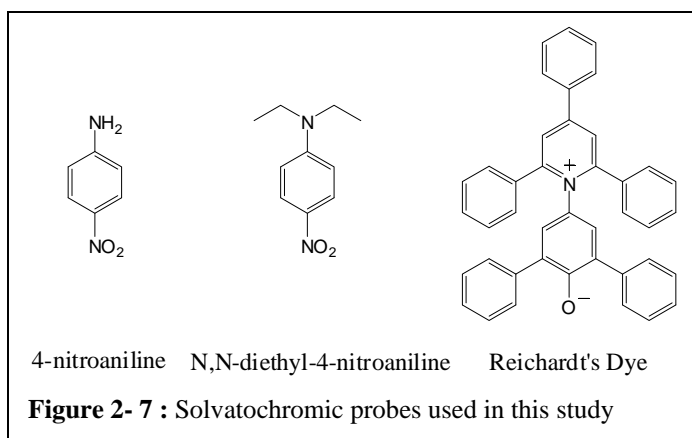
2.2. Determining Kamlet Taft Parameters

2.2.1. Solvatochromic Probes

Solvatochromic probes are specialized dyes used to examine particular solvent properties using an Ultraviolet-Visible (UV-Vis) spectrophotometer. Depending on the molecular interactions between the solvatochromic probe and the solvent molecules a shift in the solvatochromic probes' absorbing wavelength is observed in different solvents. The shift in wavelength can be either bathochromic, (also called red shift) in which the wavelength of maximum absorption increases with increased solvent polarity, or hypsochromic (blue shift) in which the wavelength decreases with increased solvent polarity. The direction of the shift with polarity is probe specific; some probes will have a red shift with increasing polarity while others can have a blue shift with increasing polarity. One particular solvatochromic probe (dye) which has been used extensively for measuring polarity for a wide range of pure and mixed solvents is Reichardt's solvatochromic pyridinium N-phenolate betaine dye (Reichardt's Dye), and the polarity scale associated with this dye is known as the $E_{\text{T}}(30)$ scale of polarity.¹¹ Kamlet, Taft, *et. al.*^{4, 5, 12, 13} have also examined solvent polarities using solvatochromic probes, however, they concluded that there are really many different measures of solvent "polarity" and used three different scales to

classify solvents, which have been termed Kamlet Taft (KT) parameters. KT parameters are a collection of polarity scales which uses solvatochromic probes (dyes) to examine different polarity properties, *viz.* acidity (α), basicity (β), and dipolarity/polarizability (π^*) for a given solvent.^{4-6, 13-16} Kamlet, Taft, *et. al.*⁴ define (α as a measure of a given solvent's acidity, or ability to donate a proton to a solvent-to-solute hydrogen bond, also referred to the hydrogen bonding donor ability (HBD) of the solvent. β is a measure of the solvent's basicity or ability to accept a proton in a solute-to-solvent interaction, also referred to the hydrogen bonding accepting (HBA) strength of the solvent. π^* is a measure of the solvent's ability to stabilize a charge or a dipole by the solvent's dielectric effects).⁴ A large number of α 's, β 's, and π^* 's have been tabulated for many common solvents using a variety of solvatochromic probe sets.^{4, 11}

There are many different solvatochromic probes that can be used to determine the KT parameters. Different sets of dyes produce slightly different quantitative results and thus comparison with other



studies should be made only with similar dye sets. In the following study, a solvatochromic comparison method will be used with the solvatochromic probes N,N-diethyl-4-nitroaniline (Dye 1), 4-nitroaniline (Dye 2), and Reichardt's dye (Dye 3), as shown in Figure 2- 7, in calculating α , β , and π^* parameters for pure solvents and for reaction mixtures. π^* for each solvent was calculated using N,N-diethyl-4-nitroaniline which is a solvatochromic dye which is only affected by π^* and has no α or β influence⁴:

$$\pi^* = \left[\frac{27.52kK - \nu(1)_{Max}}{3.18kK} \right] \quad \text{Equation 2- 9}$$

where π^* is the dipolarity/polarizability parameter, kK is kilokaysers ($1000kK = \text{cm}^{-1}$),¹⁷ $\nu(1)_{Max}$ is the maximum absorbing wavelength for Dye 1 (cm^{-1}). Equation 2- 9 uses cyclohexane ($\pi^*=0.00$) and dimethyl sulfoxide ($\pi^*=1.00$) as references. β was calculated using probes 4-nitroaniline and N,N-diethyl-4-nitroaniline. Examining these probes closer, it is seen that both solvatochromic probes are capable of acting as a hydrogen bond acceptor (HBA) in a hydrogen bonding donor (HBD) solvent through the nitro group, however only 4-nitroaniline can act as a HBD in HBA solvents.¹³ By graphing both dyes' wavelengths in non hydrogen bonding solvents a linear regression can be made, as given in Equation 2- 10.¹³

$$\nu(2)_{Max} = 1.035\nu(1)_{Max} + 2.64kK \quad \text{Equation 2- 10}$$

where $\nu(2)_{Max}$ and $\nu(1)_{Max}$ are the maximum absorbing wavelength for Dye 1 and Dye 2 (cm^{-1}). Since, 4-nitroaniline is the only dye out of the two, which can act as a HBD in HBA solvents. The degree of HBA for a given solvent can be evaluated by subtracting the calculated value determined in Equation 2- 10 for 4-nitroaniline with the experimentally observed wavelength for 4-nitroaniline. As reference, hexamethylphosphoramide ($\beta=1$) is used in calculating all β values, given by Equation 2- 11.¹³

$$\beta = \left[\frac{1.035\nu(1)_{Max} - \nu(2)_{Max} + 2.64kK}{2.80kK} \right] \quad \text{Equation 2- 11}$$

The α was calculated using the solvatochromic probe pairing N,N-diethyl-4-nitroaniline/Reichardt's Dye. In HBD solvents, Reichardt's dye has shown hypsochromic shifts resulting from both, the HBD ability as well as the dipolarity/polarizability. By calculating the π^* parameter in Equation 2- 9, α can be calculated using Equation 2- 12.⁴

$$\alpha = \left[\frac{\nu(3)_{Max} - 10.60kK - 5.12kK(\pi^* - 0.23\delta)}{5.78kK} \right] \quad \text{Equation 2- 12}$$

where $\nu(3)_{Max}$ is the maximum absorbing wavelength for Dye 3 (cm^{-1}), π^* is the dipolarity/polarizability, and δ is the "polarizability correction term" and is equal to 0

for non chlorinated solvents aliphatic solvents, 0.5 for polychlorinated aliphatics, and 1.0 for aromatic solvents.⁴ A detailed analysis of how the solvatochromic probes are used is given in section 2.2.2.

The kinetic rate constants can be quantified using KT parameters by using a Linear Solvation Energy Relationship (LSER) method¹¹, see Equation 2- 13

$$\ln k = \ln k^o + A\alpha + B\beta + C(\pi^* - D\delta) \quad \text{Equation 2- 13}$$

The regressed coefficients, *A*, *B*, *C*, and *D*, indicate the magnitude and direction (positive or negative) the polarity parameter contributes to the kinetic rate, and were determined by regressing rate constants with KT parameters using SigmaPlot 2000 version 6.00. In addition, Reichardt's dye, see Figure 2- 7, can be utilized to determine polarity based on the $E_T(30)$ scale and is given by Equation 2- 14.¹¹

$$E_T(30) = hc\nu(3)_{Max} N_A \quad \text{Equation 2- 14}$$

where $E_T(30)$ is a scale of polarity with units of kcal/mol, *h* is Planck's constant, *c* is the speed of light, $\nu(3)_{Max}$ is the maximum absorbance for Reichardt's dye, and N_A is Avogadro's number. To validate the experimentally calculated KT parameters, a few solvents were compared against literature reported KT parameters, which are displayed in Table 2- 1.

Table 2- 1: Literature comparison of KT parameter.

Solvent	α	β	π^*
Acetonitrile ³⁻⁶	(0.19-0.35) 0.230	(0.31-0.40) 0.376	(0.75-0.80) 0.787
Acetone ^{3, 4, 6, 7}	(0.08-0.202) 0.110	(0.48-0.54) 0.523	(0.62-0.66) 0.704
Dichloromethane ^{3, 4, 6}	(0.01-0.04) 0.04	(-0.01-0.00) -0.02	(0.79-0.82) 0.79

() literature obtained KT values

As seen in Table 2- 1, the values obtained experimentally for α , β , and π^* are very close to reported values.

2.2.2. UV-Vis

The solvatochromic probe studies for solvents and reaction mixtures were performed using a Varian Cary 300 Bio UV-Visible Spectrophotometer with a Dual Cell Peltier Accessory Temperature Controller, which was supplied with Cary

WinUV software version 3.00(182). A one centimeter path length cuvette was used for all studies. Before beginning any experiments, the UV-Vis spectrophotometer was allowed to warm up for at least one hour and a validation on the instrument performance was verified prior to taking any scans. Once preheated, 3 mL of the solvent was added to the cuvette and a background spectrum was taken for the solvent. Three mg of the solvatochromic probe was then added to a 20 mL vial containing 3 mL of solvent. The vial was then mixed and 50 μ L was drawn from the vial and placed in the cuvette containing the 3 mL of solvent. The cuvette was mixed and placed in the UV-Vis spectrophotometer. A quick scan was made from 800-200 nanometers (nm) at a rate of 600 nm/min to narrow the region where the solvatochromic probe had a maximum absorbance. Once the scan was complete, the maximum absorbance for each probe were noted along with the corresponding wavelength. For the 4-nitroaniline and N,N-diethyl-4-nitroaniline solvatochromic probes, the maximum absorbances were between 300-420 nm. The Reichardt's dye solvatochromic probe contained many absorbances in the ultraviolet and visible region. The wavelength of interest for the Reichardt's dye is in the visible region and varied between 800-550 nm. Once the maximum absorbance was determined, the sweep width was narrowed to 150 nm around the maximum absorbing wavelength of interest for each solvatochromic probe and the scan rate was decreased to 200 nm/min. If the maximum absorbance for the probe was greater than one or less than 0.6, the cuvette was diluted or concentrated accordingly. A scan was taken and the wavelength at the maximum absorbance was recorded for calculating the KT parameters. The cuvette was then cleaned thoroughly using acetone and dried using compressed air before the next set of solvent runs. Each set of data was replicated three times to obtain a standard deviation.

2.3. Vapor-Liquid Equilibrium: Carbon Dioxide Studies

Vapor-Liquid volume expansion and phase compositions were conducted using a static vapor-liquid equilibrium method as described in detail by Ren and Scurto¹⁸ and an overview will be given here. A schematic of the apparatus is

illustrated in Figure 2- 8. A modified view cell was used containing a magnetic stir bar, which only moves up and down in the cell. The view cell's temperature was maintained using a water bath equipped with a Haake DC30 heater which is precise to $\pm 0.01^{\circ}\text{C}$. Pressure for the view cell was monitored using a Heise (model DXD) pressure transducer which has an uncertainty to $\pm 0.02\%$ full range. A Teledyne ISCO (model 100DM) syringe pump controlled by a Teledyne ISCO D-Series pump controller supplied the Coleman Instrument grade (99.99%) carbon dioxide to the view cell and the line temperature from the pump to the view cell was controlled using two Staco Energy voltage regulators (model 3PN1010B) and the line temperatures were monitored using three Measure Computing (type T) thermocouples, (model number USB-TC), which are accurate to within $\pm 0.5^{\circ}\text{C}$. A Fisher Scientific ISOTemp 3016 heater was used to heat the pump to 60°C , and the temperature of the pump was monitored using an Ertco-Eutechnics thermometer, (model number 4400), which has an uncertainty of $\pm 0.02^{\circ}\text{C}$. The volume of the pump, the temperature of the thermocouples, and the pressure reading from the pressure transducer are all monitored using Labview 8.20 software. (See reference for Ren and Scurto¹⁸ for more details of the apparatus .)

Prior to running vapor-liquid equilibrium experiments, the instrumentation and water bath are allowed to thermally equilibrate for a minimum of thirty minutes. A syringe is used to transfer the sample to the view cell through a 1/16 in. HIP port on top of the view cell, and was weighed before and after the addition using an AND (model HM-202) balance with an uncertainty of ± 0.01 mg. The view cell was then vented twice to remove atmosphere from the cell and the volume of the pump was recorded using the Labview software along with the height of the liquid layer after the venting process. The view cell was then pressurized to a specified pressure and the sample was continuously mixed while monitoring the change in pressure using the Labview software. Equilibrium was assumed when the pressure decrease did not exceed ± 0.01 bar/ 5 min after mixing the liquid and vapor-liquid interface one hundred times. The equilibrium temperature, water bath temperature, cell's pressure,

height of liquid, and the volume of the pump were then recorded along with the line and pump temperatures before being pressurized to a higher pressure. The same procedure was followed for each pressure point and typically was done in ten to fifteen bar increments.

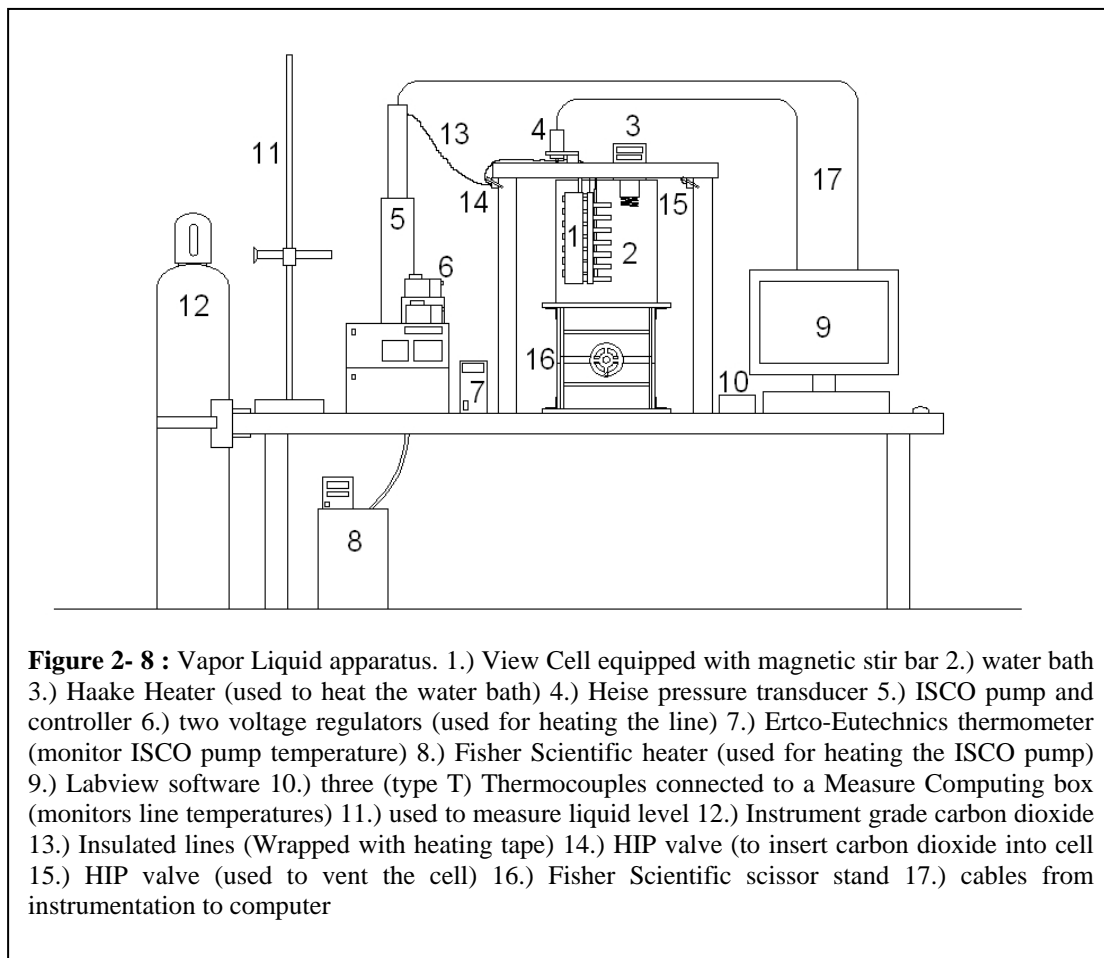


Figure 2- 8 : Vapor Liquid apparatus. 1.) View Cell equipped with magnetic stir bar 2.) water bath 3.) Haake Heater (used to heat the water bath) 4.) Heise pressure transducer 5.) ISCO pump and controller 6.) two voltage regulators (used for heating the line) 7.) Ertco-Eutechnics thermometer (monitor ISCO pump temperature) 8.) Fisher Scientific heater (used for heating the ISCO pump) 9.) Labview software 10.) three (type T) Thermocouples connected to a Measure Computing box (monitors line temperatures) 11.) used to measure liquid level 12.) Instrument grade carbon dioxide 13.) Insulated lines (Wrapped with heating tape) 14.) HIP valve (to insert carbon dioxide into cell 15.) HIP valve (used to vent the cell) 16.) Fisher Scientific scissor stand 17.) cables from instrumentation to computer

2.4. Materials

Reagents: 1-methylimidazole (>99%), 1-chlorohexane (95%), 1-iodohexane (>98%), 1-bromopropane (99%) were obtained from Acros Organics, while 1-bromohexane (>99%), 1-bromopentane (99%), 2-bromopentane (95%), 1-bromo-3-methylbutane (96%), 2-bromo-2-methylbutane (95%), and 1-bromodecane (98%) were obtained from Sigma Aldrich.

Solvents: acetonitrile (>99.9%), acetone (>99.9%), methanol (>99.9%), chlorobenzene (99.9%), dichloromethane (99.8%), dimethyl sulfoxide (>99%), cyclopentanone (>99%), ethyl lactate (>98%), 2-butanone (>99.7%), and cyclohexane (>99.9%) were all obtained from Sigma Aldrich, while ethyl formate (>98%) was purchased from Acros Organics.

Solvatochromic probes: 4-nitroaniline (>99%) was purchased from Sigma Aldrich, N,N-diethyl-4-nitroaniline (97%) was purchased from Oakwood Products Inc., and Reichardt's Dye (>90%) was received from Fluka.

All starting materials were distilled and kept under argon gas prior to use. All the solvents except for ethyl formate, cyclohexane, ethyl lactate, and 2-butanone were dried using 3 Angstrom or 4 Angstrom Molecular sieve. The solvatochromic probes Reichardt's Dye, 4-nitroaniline, and N,N-diethyl-4-nitroaniline were used as received from the vendor.

References:

1. Shtarov, A. B.; Krusic, P. J.; Smart, B. E.; Dolbier, W. R., Bimolecular Kinetic Studies with High-Temperature Gas-Phase ^{19}F NMR: Cycloaddition Reactions of Fluoroolefins. *J. Am. Chem. Soc.* **2001**, 123, 9956-9962.
2. Stahl, I.; von-Kiedrowski, G., "Kinetic NMR Titration": Including Chemical Shift Information in the Kinetic Analysis of Supramolecular Reaction Systems such as Organic Replicators. *J. Am. Chem. Soc.* **2006**, 128, 14014-14015.
3. Crowhurst, L.; Mawdsley, P.; Perez-Arlandis, J.; Salter, P.; Walton*, T., Solvent-Solute Interactions in Ionic Liquids. *J. Phys. Chem.* **2003**, (5), 2790-2794.
4. Kamlet, M. J.; Abboud, J. M.; Abraham, M. H.; Taft, R. W., Linear Solvation Energy Relationship. 23. A Comprehensive Collection of the Solvatochromic Parameters, π^* , α , β , and Some Methods for Simplifying Solvatochromic Equation. *J. Org. Chem.* **1983**, (48), 2877-2887.
5. Kamlet, M. J.; Taft, R. W., The Solvatochromic Comparison Method. 2. The α -scale of Solvent Hydrogen-Bond Donor (HBD) Acidities. *J. Amer. Chem. Soc.* **1976**, (98:10), 2886-94.
6. Migron, Y.; Marcus*, Y., Polarity and Hydrogen-bonding Ability of Some Binary Aqueous-Organic Mixtures. *J. Chem. Soc., Faraday Trans.* **1991**, 87, 1339-1343.
7. Kamlet, M. J.; Abboud, J. L.; Taft, R. W., The Solvatochromic Comparison Method. 6. The π^* Scale of Solvent Polarity. *J. Amer. Chem. Soc.* **1977**, 99, (18), 6027-6037.
8. Poliakov, M.; Fitzpatrick, J. M.; Farren, T. R.; Anastas, P. T., Green Chemistry: Science and Politics of Change. *Science* **2002**, 297, 807-810.
9. Solinas, M.; Pfaltz, A.; Cozzi, P. G.; Leitner, W., Enantioselective Hydrogenation of Imines in Ionic Liquid/Carbon Dioxide Media. *J. Am. Chem. Soc.* **2004**, 126, (49), 16142-16147.
10. Gunther, H., *NMR Spectroscopy: Basic principles, concepts, and applications in chemistry*. 2 ed.; John Wiley & Sons: 1995; p 1-581.
11. Reichardt, C., *Solvent and Solvent Effects in Organic Chemistry*. 3 ed.; Wiley-VCH: Weinheim, Germany, 2003; p 629.
12. Kamlet, M. J.; Hall, T. N.; Boykin, J.; Taft, R. W., Linear Solvation Energy Relationship. 6. Additions to the Correlations with the π^* Scale of Solvent Polarity. *J. Org. Chem.* **1979**, 44, (15), 2599-2604.
13. Kamlet, M. J.; Taft, R. W., The Solvatochromic Comparison Method. I. The β -scale of Solvent Hydrogen-Bond Acceptor (HBA) Basicities. *J. Amer. Chem. Soc.* **1976**, (98:2), 377-383.
14. Lu, J.; Liotta, C.; Eckert, C., Spectroscopically Probing Microscopic Solvent Properties of Room-Temperature Ionic Liquids with the Addition of Carbon Dioxide. *J. Phys. Chem.* **2003**, (107), 3995-4000.
15. Muldoon, M. J.; Gordon*, C. M.; Dunkin, I. R., Investigations of Solvent-Solute Interactions in Room Temperature Ionic Liquids using Solvatochromic Dyes. *RSC* **2001**, (2), 433-435.

16. Oehlke, A.; Hofmann, K.; Spange*, S., New Aspects on Polarity of 1-alkyl-3-methylimidazolium Salts as Measured by Solvatochromic Probes. *New J. Chem.* **2006**, (30), 533-536.
17. Yokoyama, T.; Taft, R. W.; Kamlet, M. J., The Solvatochromic Comparison Method. 3. Hydrogen Bonding by Some 2-Nitroaniline Derivatives. *J. Am. Chem. Soc.* **1976**, 98, (11), 3233-3237.
18. Ren, W.; Scurto, A., High-Pressure Phase Equilibria with Compressed Gases. *Rev. Sci. Instrum.* **2007**, in press.

3. Solvent Effects on Kinetics of Ionic Liquid Synthesis

It has long been observed that rates of reactions for a number of organic reactions are heavily influenced by the solvent media. This was first demonstrated systematically by Nikolai Menshutkin over a century ago while studying the second-order nucleophilic substitution (S_N2) quaternization reaction between tertiary amines with primary haloalkanes using 23 solvents.²⁻⁴ For his work with tertiary amines with primary haloalkanes, the reaction has been named after him. Since his discovery, there have been thousands of papers published which examine solvent effects on a wide range of chemical reactions.

3.1. Introduction to Kinetic Theory and Analysis

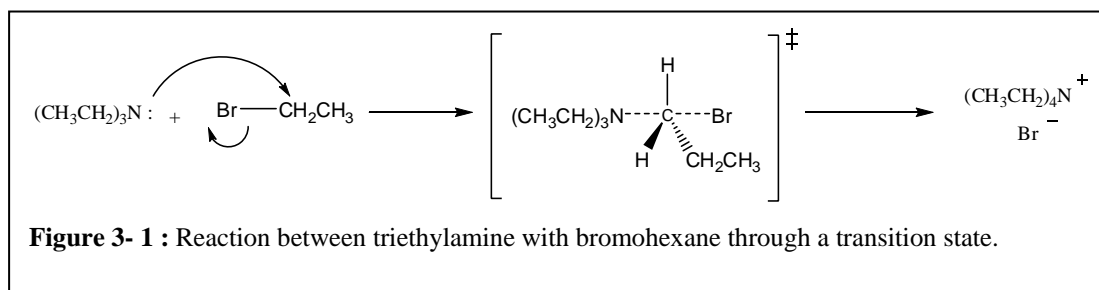
The Arrhenius equation is a well established kinetic equation which relates the kinetic rate constant to temperature effects. First discovered by Svante Arrhenius in 1889,⁶ the Arrhenius equation is based on a simple collision model, which states; when two molecules collide they have to overcome a certain degree of energy (Activation Energy) for the reaction to proceed. If the energy of a system does not match or exceed the activation energy (E_a) the molecules cannot overcome the energy hump and will not result in product. It was also rationalized that the temperature at which the reaction proceeds affects the activation energy needed for a system. At higher temperatures, the molecules in a solution have higher kinetic energy, thus they are colliding much faster which lowers the overall activation energy of the system. Combining the temperature affects with the theory of an activation energy Arrhenius devised his well known Arrhenius equation as given in Equation 3- 1.

$$k = k_o \exp\left(\frac{-E_a}{RT}\right) \quad \text{Equation 3- 1}$$

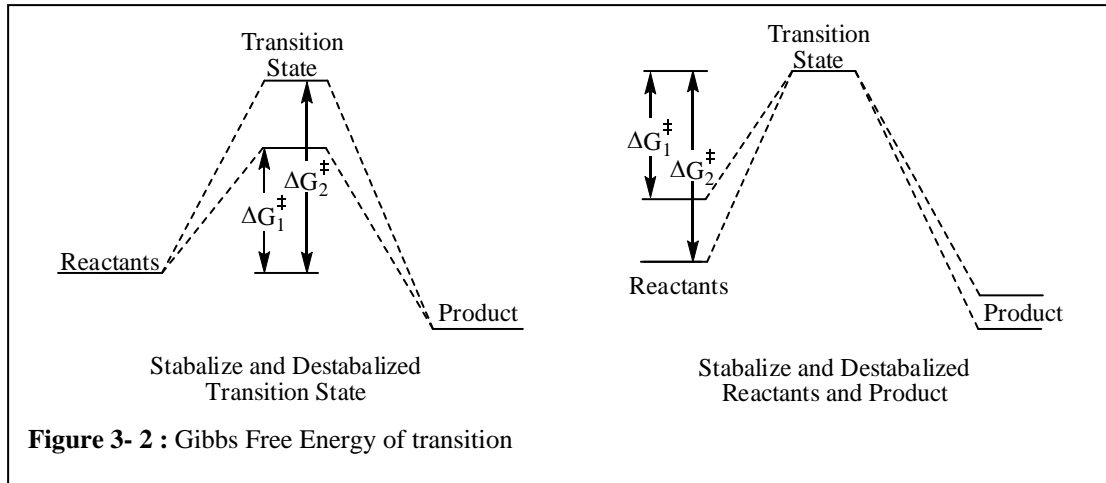
where E_a is the activation energy, R is the gas constant, T is temperature, and k_o is the frequency factor, which is a measure of the frequency of collisions between the reactant molecules.

3.1.1. Eyring Equation

Then, in 1935, Henry Eyring published his findings for explaining kinetic theory based on an activated complex theory or “transition state theory”, which is now used extensively for examining solvent effects.⁵⁻⁸ (For the general background work leading up to the activated complex theory I refer the reader to Eyring⁶). A visual representation of the transition state theory is given in Figure 3- 1 using Menshutkin’s well known reaction between tertiary amines with haloalkanes.



Unlike the Arrhenius equation, the Eyring equation is theoretically determined based on a transition state model; thus can be applied to solution mixtures as well as gases. For reactions to proceed, the reactants first need to pass through a higher energy state known as a transition state, where the activated complex resides, before products can be formed. Depending on the solvent used in a chemical reaction the Gibbs energy of activation (ΔG^\ddagger) can be altered significantly through enthalpic and entropic effects. Two main ways that solvents can affect the ΔG^\ddagger are by: stabilizing /destabilizing the energy of reactants through solvation of reactants, or by stabilizing and destabilizing the activated complex during the transition state through solvation as shown in Figure 3- 2 (adapted from Reichardt⁵).



The Eyring's equation originates from the transition state energy needed to overcome during an activation complex as shown by Equation 3- 2.^{5, 6}

$$\Delta G^\ddagger = \Delta H^\ddagger - T\Delta S^\ddagger = -RT \ln K^\ddagger \quad \text{Equation 3- 2}$$

where ΔG^\ddagger is the Gibbs free energy of activation, ΔH^\ddagger is the Enthalpy of activation, ΔS^\ddagger is the Entropy of activation, T is temperature, R is the gas constant, and K^\ddagger is the thermodynamic equilibrium constant for the activated complex. From statistical mechanics, there exists a relationship between the rate constant and K^\ddagger as given in Equation 3- 3.^{5, 6}

$$k = \frac{k_B T}{h} K^\ddagger \quad \text{Equation 3- 3}$$

where k_B is the Boltzmann's constant, k is the rate constant, and h is Planck's constant. Placing Equation 3- 3 into Equation 3- 2 the ΔH^\ddagger and ΔS^\ddagger can be expressed in terms of the rate constant k by Equation 3- 4.^{5, 6}

$$k = \frac{k_B T}{h} \exp\left(\frac{-\Delta H^\ddagger}{RT}\right) \exp\left(\frac{\Delta S^\ddagger}{R}\right) \quad \text{Equation 3- 4}$$

By rearranging Equation 3- 4, as shown in Equation 3- 5, one can graph the $\ln(k/T)$ against $(-1/T)$ and a linear line should exist with a slope $(\Delta H^\ddagger/R)$ and a y-intercept being the remainder of the right hand side of Equation 3- 5.

$$\ln\left(\frac{k}{T}\right) = -\frac{\Delta H^\ddagger}{RT} + \ln\left(\frac{k_B}{h}\right) + \frac{\Delta S^\ddagger}{R} \quad \text{Equation 3- 5}$$

3.1.2. Hughes and Ingold Rules

Using the transition state theory and a qualitative solvation model Hughes, Ingold *et al.*^{5, 9-11} have examined a number of organic substitution and elimination reactions using a simple qualitative solvation model to determine differences in rates of reaction based on the charge difference between the reactants and activated complex: neutral, positive, or negative. They have shown for a chemical reaction having a greater charge density in the activated complex, during the transition state, compared to the initial reactants an increase in solvent polarity will result in an increase in reactivity.^{5, 9-11} If however, the charge density is greater in the initial reactants compared to the activated complex in the transition state an increase in solvent polarity will decrease the rate of reaction.^{5, 9-11} Finally, a charge density similar for initial reactants and for the activated complex; solvent polarity does not play a role and the change in the rates of reaction are negligible.^{5, 9-11} The results from Hughes, Ingold *et al.* analysis for first-ordered nucleophilic substitution (S_N1) reactions as well as second-ordered nucleophilic substitution (S_N2) reactions are displayed in Table 3- 1, which has been adapted from Reichardt.⁵ The quaternization reaction between tertiary amines and haloalkanes, the Menshutkin reaction, is represented by reaction type 3 in Table 3- 1(adapted from Reichardt⁵).

Table 3- 1: Hughes and Ingold's qualitative trends for nucleophilic substitution reactions

Reaction Type	Reaction Mechanism	Reactants	Transition State	Charge separation during transition	Increased solvent polarity effects on rate of reaction
1	S _N 1	R-X	R ^{δ+} · X ^{δ-}	Separation-unlike charges	Increase rate of reaction
2	S _N 1	R-X ⁺	R ^{δ+} · X ^{δ+}	Dispersion-like charges	Decrease rate of reaction
3	S _N 2	R-X + Y	X ^{δ-} · R · Y ^{δ+}	Separation-unlike charges	Increase rate of reaction
4	S _N 2	R-X + Y ⁻	X ^{δ-} · R · Y ^{δ-}	Dispersion-like charges	Decrease rate of reaction
5	S _N 2	R-X ⁺ + Y	X ^{δ+} · R · Y ^{δ+}	Dispersion-like charges	Decrease rate of reaction
6	S _N 2	R-X ⁺ + Y ⁻	X ^{δ+} · R · Y ^{δ-}	Dispersion-of charges	Decrease rate of reaction

3.1.3. Literature overview

Many attempts have been made to correlate rates of reaction or ΔG^\ddagger with solvent physical characteristics: dipole moments, dielectric constants, solvent polarity, solubility parameters, etc.¹²⁻¹⁸ Out of all the correlations examined it was determined that only a moderate to fair correlation exists using individual solvent properties, and in most instances only similar solvent types were examined in the correlation i.e. only polar protic solvents or polar aprotic solvent with rates of reactions. For studies which examined rates of reactions in both polar protic and polar aprotic solvents, it was determined that no *single* correlation exists which could account for different solvent types. Thus, multiple solvent properties must be included to correlate rates of reaction to solvent effects. One such method, devised by Kamlet and Taft, is a solvatochromic comparison method (See section 2.2). Within the solvatochromic comparison method, a number of solvatochromic probes (dyes) are examined with the use of an Ultraviolet Visible (UV-Vis) spectrophotometer. Depending on the solute-solvent interactions between the solvatochromic probes and the solvent, a bathochromic shift in the wavelength, the wavelength for the maximum absorption increases with increased solvent polarity, or the wavelength can shift

hypsochromically, the wavelength decreases with increased solvent polarity. By accounting for different solute-solvent interactions different solvatochromic probes can give insight to a solvent's acidity (α), basicity (β), and dipolar/polarizability (π^*), which are often referred to as Kamlet Taft (KT) parameters. By combining the KT parameters with a Linear Solvation Energy Relationship (LSER) valuable insight can be obtained for the desired solvent properties as related to the rate of reaction in a number of solvents.

3.2. Experimental Results/Modeling

Initially, this study focused on 5 traditional solvents, used at the laboratory- and industrial-scale, for the reaction of 1-methylimidazole with 1-bromohexane to form the ionic liquid [HMIm][Br]. The initial solvents (acetonitrile, methanol, dichloromethane, and chlorobenzene) have a wide range of polarity and different levels of toxicity and environmental impact factors which will be discussed in chapter 6. For each reaction, the mole ratio of reactants to solvent was maintained at 1:1:20 to avoid any effect of the reactant and/or product on the polarity and reaction rate. Each reaction was conducted at three different temperatures: 25°C, 40°C, and 60°C yielding insight to the transition state and activation parameters. For the chlorobenzene system, the mixture split into two phases (IL-rich and reactant/solvent-rich) after approximately ~6% conversion; despite the possibility of different reaction rates in each phase, only the overall kinetic rate is reported for this preliminary analysis. All rates of reaction were regressed assuming 2nd order kinetics using SigmaPlot (see section 2.1) and are present in Table 3- 2 at 40°C along with the Kamlet Taft (KT) parameters and $E_T(30)$ values determined experimentally using three independent measurements taken at 25°C. It is seen in Table 3- 2 that the rate of reaction is the greatest in acetonitrile and is more than one order of magnitude higher than that of methanol.

Table 3- 2 : Rate constants for initial 5 solvents at 40°C as well as KT parameters and $E_T(30)$ values

Solvent	$k \times 10^6$ ($M^{-1} \text{ sec}^{-1}$) 40°C	Kamlet Taft Parameters			$E_T(30)$ (kcal mol^{-1})
		α	β	π^*	
Acetonitrile	21.56 ± 0.21	0.23	0.38	0.79	45.62
Acetone	12.67 ± 0.06	0.11	0.52	0.72	42.58
Dichloromethane	8.47 ± 0.11	0.04	-0.02	0.79	40.88
Chlorobenzene ^a	3.64 ± 0.11	0.05	0.08	0.62	36.91
Methanol	2.03 ± 0.08	0.91	0.63	0.70	55.53

All rates of reaction at 40°C were conducted at a 1:1:20 mole ratio (1-methylimidazole:1-bromohexane:solvent) for the initial 5 solvents selected. The errors in the experimentally determined KT parameters were less than or equal to 0.01 and the errors resulting from the $E_T(30)$ values are less than or equal to 0.04 between three experimentally determined measurements a.) Phase split from one phase to two phases.

By regressing the natural logarithm of k ($\ln k$) against the LSER coefficients based on the KT parameters (acidity α , basicity β , polarizability correction factor δ , and dipolarity/polarizability π^*), a correlation was found which fits Equation 3- 6 with a $R^2=1.0$.

$$\ln k = -62.08 - 3.79\alpha + 20.89\beta + 56.36(\pi^* + 0.23\delta) \quad \text{Equation 3- 6}$$

From the regression, it is seen that the π^* parameter (dipolarity/polarizability) has the largest positive effect on the rate constants, followed by the β parameter (basicity). The α parameter (acidity) has a negative effect on the rate of reaction. Thus, to optimize the rate, a solvent with large β and π^* with a small α should be chosen.

The general effects of polarity on the synthesis of ionic liquids as determined from the solvent subset can then be used to aid the choice of other solvents that enhance the reaction rate, but with lower toxicity and environmental impact. In a superficial toxicity /environmental analysis, the FDA industrial guidelines list may be used;¹⁹⁻²² a detailed analysis is found in Chapter 6. The FDA solvent guidelines classify solvents into 4 categories: Class 1, 2, 3, and Generally Regarded as Safe (GRAS) solvent. Under these guidelines any Class 1 solvent shall not be used in the production of pharmaceuticals as they are known or suspected human carcinogen; the list includes: Benzene, carbon tetrachloride, 1,2-dichloroethane, etc.^{19, 20} Class 2

solvents should be limited in the production of pharmaceuticals and have been deemed toxic; however, the toxicity resulting from exposure is reversible.^{19, 20} The amount of solvent acceptable under the classification of Class 2 is based on the inherent toxicity for a given solvent which is determined by the FDA's permitted daily exposure (PDE) limitations.^{19, 20} Class 3 solvents are accepted in the production of pharmaceuticals and have low toxicity.^{19, 20} PDE requirements for Class 3 solvents must be less or equivalent to 50mg/day.^{19, 20} GRAS solvents are preferred solvents which are accepted in the production of pharmaceuticals and have been deemed safe as food additives.^{21, 22} These guidelines are obviously based upon toxicity to humans, and in particular, ingestion or injection and do not necessarily address environmental issues.

A detailed analysis on solvent toxicity and environmental impact will be covered in chapter 6. The KT parameters were determined in several solvents from the list of Class 3 and GRAS solvents. Five additional solvents were chosen with guidance from Equation 3- 6 and reported KT values from Kamlet, Taft *et. al.*¹: ethyl formate, ethyl lactate (also a bio-renewable solvent^{23, 24}), dimethyl sulfoxide, 2-butanone, and cyclopentanone.

The results for all of the solvents studied are presented in Table 3- 3 along with the solvent-free reaction (neat) at specified temperatures of 25°C, 40°C, and 60°C. The experimentally measured KT parameters and $E_T(30)$ are represented in Table 3- 4; the majority of the new solvents did not have a complete set of KT parameters and $E_T(30)$ values in the literature based on a consistent set of solvatochromic probes and were thus measured here.

Table 3- 3 : Rates of reaction for the 10 solvents analyzed at three specified temperatures

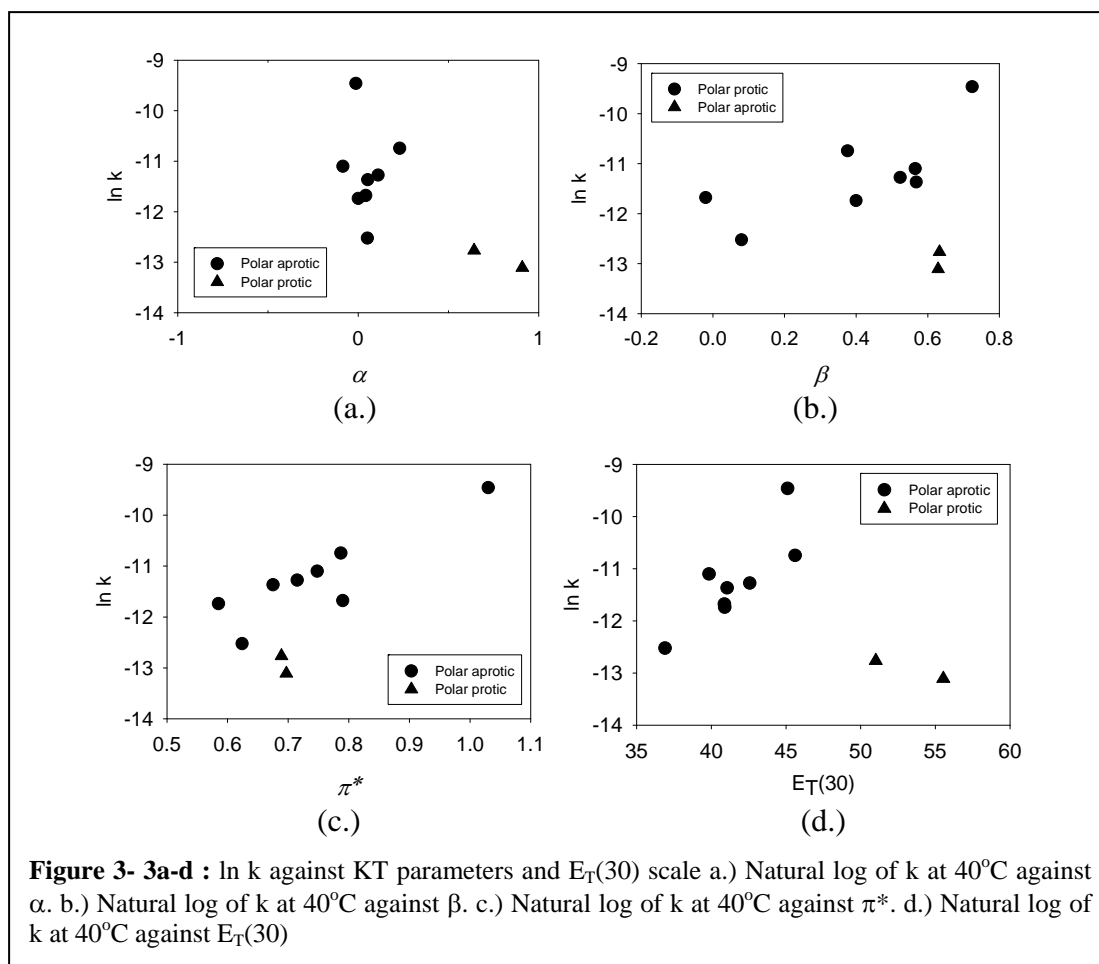
Solvent	$k \times 10^6 \text{ (M}^{-1} \text{ sec}^{-1}\text{)}$	$k \times 10^6 \text{ (M}^{-1} \text{ sec}^{-1}\text{)}$	$k \times 10^6 \text{ (M}^{-1} \text{ sec}^{-1}\text{)}$
	25°C	40°C	60°C
Dimethyl Sulfoxide	22.22 ± 0.11	77.89 ± 1.72	322.31 ± 3.53 ^b
Acetonitrile	6.03 ± 0.14	21.56 ± 0.21	110.64 ± 1.42
Neat ^{a,d}	4.53 ± 0.04	17.63 ± 0.06	106.34 ± 13.2
Cyclopentanone	3.75 ± 0.03	15.11 ± 0.11	76.11 ± 1.72
Acetone	3.69 ± 0.17	12.67 ± 0.06	63.67 ± 0.61
2-butanone	2.69 ± 0.03	11.56 ± 0.08	53.75 ± 0.28
Dichloromethane	2.28 ± 0.11	8.47 ± 0.11	N/A ^c
Ethyl Formate	1.61 ± 0.03	7.97 ± 0.14	N/A ^c
Chlorobenzene ^a	1.11 ± 0.06	3.64 ± 0.11	24.64 ± 1.39
Ethyl Lactate	0.53 ± 0.03	2.86 ± 0.06	20.28 ± 0.28
Methanol	0.42 ± 0.03	2.03 ± 0.08	17.14 ± 0.11

All rates of reaction were conducted at a 1:1:20 mole ratio (1-methylimidazole:1-bromohexane:solvent) unless otherwise stated for the 10 solvents selected. a.) Phase split occurred during reaction. b.) Reaction conducted at 1:1:80 mole ratio 1-methylimidazole:1-bromohexane:dimethyl sulfoxide due to exothermicity of reaction. c.) above the normal boiling point of the solvent. d.) Reaction conducted solvent free (Neat)

Table 3- 4 : Experimentally determined K_T and $E_T(30)$ values for the 10 solvents used in this study.

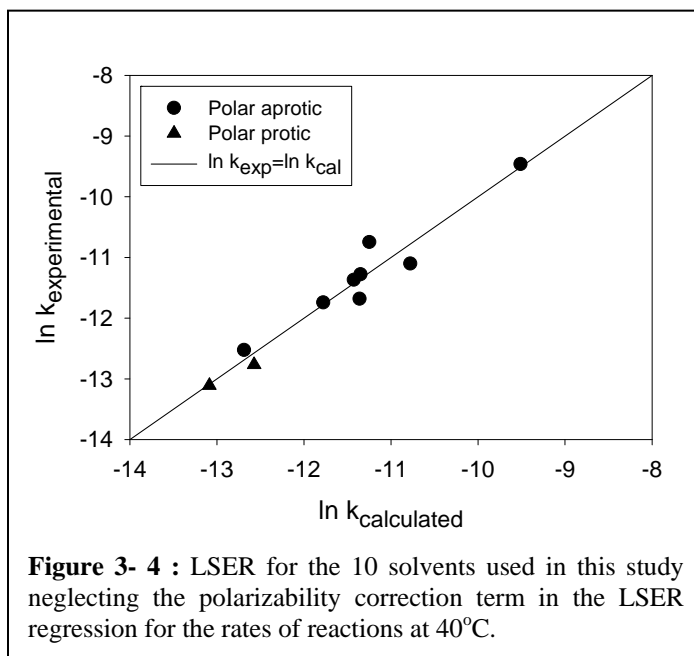
Solvent	Kamlet Taft Parameters			$E_T(30)$
	α	β	π^*	(kcal mol ⁻¹)
Dimethyl Sulfoxide	-0.01	0.72	1.03	45.11
Acetonitrile	0.23	0.38	0.79	45.6
Cyclopentanone	-0.09	0.57	0.75	39.6
Acetone	0.11	0.52	0.72	42.6
2-butanone	0.05	0.57	0.68	41.1
Dichloromethane	0.04	-0.02	0.79	40.9
Ethyl Formate	0.00 ^a	0.40	0.59	40.9 ^a
Chlorobenzene ^a	0.05	0.08	0.62	36.9
Ethyl Lactate	0.64	0.63	0.69	51.0
Methanol	0.91	0.63	0.70	55.5

The errors in the experimentally determined K_T parameters were less than or equal to 0.01 and the error resulting from the $E_T(30)$ values are less than or equal to 0.04 between three independent measurements a.) Value taken from Literature, Ref.¹ Could not be experimentally determined due to solubility issues with the solvatochromic probes.



Using a one parameter approach, the $\ln k$ for each solvent was regressed against each of the different polarity types: α , β , π^* , and $E_T(30)$ values given in Table 3- 4 to ascertain if rates of reaction can be predicted using only a single solvent polarity parameter. The results for this analysis are given in Figure 3- 3a-d. From Figure 3- 3a-d it is seen that a large scatter is present when examining each individual parameter against the natural logarithm of the rates of reaction. Therefore, a single parameter approach is not efficient in understanding how the solvent is affecting the rates of reaction. This trend was also seen in similar systems by Abraham et al.²⁵ who worked with a trimethylamine/p-nitrobenzyl chloride system, and a similar conclusion was obtained by Skrzypczak and Neta²⁶ studying the reaction of 1,2-dimethylimidazole and benzylbromide.

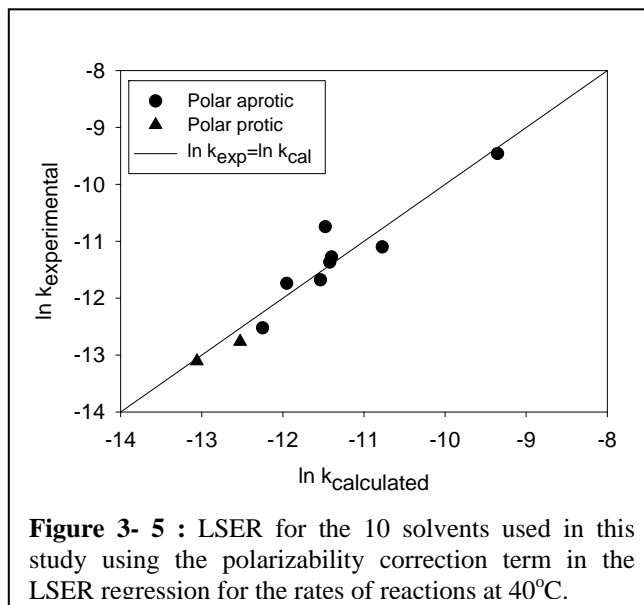
Thus, all of the KT parameters must be combined into a LSER regression to quantitatively correlate the reaction rates. Initially, the LSER method was conducted using all 10 solvents in Table 3- 3, while neglecting the polarizability correction term, δ (See section 2.2.1). The results for this analysis are given in Figure 3- 4 and Equation 3- 7 with an $R^2=0.91$.



$$\ln k = -15.30 - 2.12\alpha + 1.19\beta + 5.91\pi^* \quad \text{Equation 3- 7}$$

As expected, when using a multiparameter analysis, the LSER method estimates quantitatively the rates of reaction for both polar aprotic solvents as well as polar protic solvents using the solvent parameters α , β , and π^* . Taking the LSER regression one step further, we can add the polarizability correction term, which only affects solvents containing multiple chlorine atoms and aromatic solvents in the LSER regression. The results are presented in Figure 3- 5 and Equation 3- 8. It is seen that the LSER regression is slightly better with the addition of the polarizability correction term, however, to a great extent does not contribute significantly to the regression. If however, more chlorinated or aromatic solvents were used in the analysis, the contribution in using the correction term might play a more significant role in the LSER regression. Now that a LSER regression has been obtained for the

formation of [HMIm][Br] a number of rate of reaction for it's production can be easily predicted solely based on the KT values for a wide range of solvents using either Equation 3- 7 with an $R^2=0.91$, or Equation 3- 8 with an $R^2=0.95$. The benefit of using the LSER regression is that quick solvent screening and selection can be achieved using easily attainable KT parameters without the expense of long trial and error rates of reaction calculations.



$$\ln k = -14.72 - 2.07\alpha + 0.07\beta + 4.99(\pi^* - 0.20\delta) \quad \text{Equation 3- 8}$$

One last study investigated using the LSER regression is to examine how the LSER regressions for the rates of reaction are affected by temperature. A LSER regression was performed at each temperature specified in Table 3- 3. For each LSER regression all 10 solvents were used with the exception of 60°C; in which only 8 of the solvents were used in the regression as two solvents (Ethyl Formate and Dichloromethane) were above their boiling point at 60°C. Equation 3- 9 (at 25°C with a $R^2=0.92$), Equation 3- 10 (at 40°C with a $R^2=0.95$), and Equation 3- 11 (60°C with a $R^2=0.99$) are the results from the LSER regression, and include the polarizability correction factor.

$$\ln k = -16.58 - 2.27\alpha + 0.03\beta + 5.65(\pi^* - 0.13\delta) \quad \text{Equation 3- 9}$$

$$\ln k = -14.72 - 2.07\alpha + 0.07\beta + 4.99(\pi^* - 0.20\delta) \quad \text{Equation 3- 10}$$

$$\ln k = -12.78 - 1.23\alpha + 2.06\beta + 6.00(\pi^* - 0.23\delta) \quad \text{Equation 3- 11}$$

Examining the α parameter, which is a measure of the hydrogen bonding abilities for solvents, it is seen that the coefficient decreases with increased temperature. This is expected since at higher temperatures hydrogen bonds are weaker due to higher kinetic energy which results in less solvent to solute hydrogen bonding. Since hydrogen bonds are more easily broken at high temperatures the negative influence resulting from hydrogen bonding, as determined by the LSER regression, decreases the influence on α as seen by the coefficients. It should be noted that the regression at 60°C is only based on 8 of the 10 solvents unlike the regression made at 25°C and 40°C and may contain a small bias. Thus, examining only the regressions at 25°C and 40°C it may be concluded that the decrease in coefficients are a result of diminishing chemical forces between the solvent and solute molecules due to the increased kinetic energies resulting in the higher temperature reactions.

3.3. Kinetic Parameters

Using the Hughes Ingold rule, reaction type 3 in Table 3- 1, the rates of reactions should increase with solvent polarity. Thus, examining the $E_T(30)$ values for polarity given in Table 3- 4 it would seem that the polar protic solvents should have the highest rates of reaction out of all the solvents examined. However, examining the rate constants for the polar protic solvents in Table 3- 3, which contain the highest polarities, produce the slowest rates of reaction. This seems to be counter intuitive of the Hughes-Ingold rule, with the rates of reaction being the slowest in the polar protic solvents. One possible explanation for why the rates of reaction are significantly slower in polar protic solvents compared to the polar aprotic solvents may reside in hydrogen bond formation which exist in polar protic solvents between the lone pair of electrons on the imidazole ring with the solvent as shown in Figure 3- 6. Before the reaction can proceed, the hydrogen bonding between the imidazole ring and the solvent has to be broken before nucleophilic attack on the 1-bromohexane. Next, examining only the rates of reaction between the polar aprotic solvents and neglecting the polar protic solvents, it is seen that the Hughes-Ingold rule

qualitatively applies to the reaction between 1-methylimidazole and 1-bromohexane with the more polar of the aprotic solvents having higher rates of reactions.

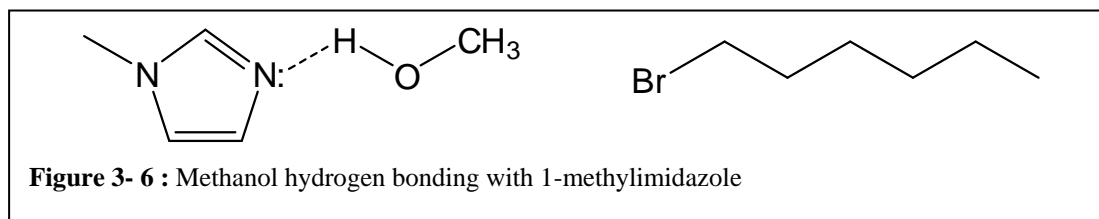


Table 3- 5 is a list of the rate constants and the activation parameters using the Arrhenius equation as well as the Eyring Equation for the reaction between 1-methylimidazole with 1-bromohexane taken from the results obtained in Table 3- 3.

Table 3- 5 : Table of kinetic parameters

Solvent	k_o ($M^{-1}sec^{-1}$)	E_a (KJ/mol)	ΔH^\ddagger (KJ/mol)	ΔS^\ddagger (J/mol)
Dimethyl Sulfoxide	2.51×10^6	63.05	60.43	-131.19
Acetonitrile	6.51×10^6	68.73	66.11	-123.26
Cyclopentanone	1.04×10^7	71.00	68.38	-119.37
Acetone	2.20×10^6	67.26	64.64	-132.30
2-butanone	6.25×10^6	70.50	67.88	-123.60
Dichloromethane ^a	1.85×10^6	67.98	65.44	-133.45
Ethyl Formate ^a	5.07×10^8	82.75	80.21	-86.78
Chlorobenzene	7.51×10^6	73.43	70.81	-122.07
Ethyl Lactate	6.36×10^8	86.05	83.43	-85.18
Methanol	9.87×10^8	87.85	85.24	-81.52

a.) Values in the table were only calculated using the rates of reaction at two specified temperatures, 25°C and 40°C, because of boiling point limitations.

The E_a from the Arrhenius equation and the ΔH^\ddagger from the Eyring equation in Table 3- 5 are related to each other by the following expression.

$$E_a = \Delta H^\ddagger + RT \quad \text{Equation 3- 12}$$

where, E_a is the activation energy, ΔH^\ddagger is the enthalpy of activation, R is the gas constant, and T is the temperature. Haberfield *et. al.*²⁷ suggest from their analysis for the Menshutkin reaction between pyridine and a number of benzyl halides in dimethylformamide and methanol, that the trends seen for ΔH^\ddagger may result from two possible occurrences. First, the solvation of the nucleophile in the polar aprotic solvents compared to that of polar protic solvents may result in the destabilization of

the reactants in the polar aprotic solvents, thus the energy difference between the activated complex (transition state energy) and the reactants energy is minimized.²⁷ This is analogous to the Gibbs energy of activation difference as displayed in Figure 3- 2. The second possible explanation for the reduced ΔH^\ddagger in the polar aprotic solvents may result from the stabilization of the activated complex in the polar aprotic solvents analogous to the Gibbs free energy of activation given in Figure 3- 2.²⁷ Or a combination of both effects may be resulting in the lowering of the ΔH^\ddagger for the polar aprotic solvents.²⁷ When examining the ΔS^\ddagger it is seen for all the polar aprotic solvents, the relative energy are quite similar. However, when comparing the polar aprotic solvents ΔS^\ddagger with that of polar protic solvents, excluding dichloromethane and ethyl formate since only two temperatures were used in the determination of ΔS^\ddagger , there is a distinct difference in ΔS^\ddagger with the polar aprotic solvents being 20 J/mol lower than the polar protic solvents. The entropy difference between the polar aprotic solvents and polar protic solvents can be explained by hydrogen bonding. In a polar protic solvent, the solvent can hydrogen bond with the lone pair of electrons on the imidazole ring. Thus, examining the entropy in terms of the reactant state, there will be more order for the polar protic solvents compared to the polar aprotic solvents where hydrogen bonding does not occur. This will lower the entropy for the reactants making the ΔS^\ddagger much less than that for the polar aprotic solvents resulting in the 1-methylimidazole and solvent being more random in solution for the polar aprotic solvents.

3.4. Steric, Electronic, and Concentration Effects on Kinetic Rate

Several studies were conducted in determining the mechanism by which the quaternization reaction between 1-methylimidazole and a number of haloalkanes proceeds. It has been very well established in literature that Menshutkin reactions take place via a S_N2 type mechanism.²⁸⁻³³ However, Giernoth³⁴ has asserted that the reaction between 1-methylimidazole and 1-chlorobutane takes place through an S_N1 type reaction as observed in *in situ* IR spectroscopy. The following studies were performed to validate the S_N2 mechanism and to determine how certain perturbations;

i.e., leaving group, chain length, and branching affects the kinetic rate constants using 1-methylimidazole and a number of haloalkane.

3.4.1. Leaving Group Contribution

It is widely known that the leaving group abilities highly affects rates of reaction when operating under a second-order nucleophilic substitution (S_N2) reaction.³⁵ In the following investigation a number of halo-hexanes were examined at 40°C in acetonitrile and is shown in Table 3- 6. The general rule for good leaving groups is that they must be weak conjugate bases for strong acids. This is especially true for halogen leaving groups. Out of the three halogen leaving groups analyzed is seen that reactivity decreases in the following order: Iodide(I) > Bromide(Br) > Chloride(Cl); and that the relative rates of reaction are over an order of magnitude different switching from Cl to Br, and the rate of reaction is nearly 4 times fast switching from Br to I. This trend is as expected since the conjugate acids are in the order of strength HI > HBr > HCl based on their respective negative logarithm of the acid dissociation constant (pK_a) values.³⁵

Table 3- 6 : Rates of reaction with different leaving groups			
Solvent	$k \times 10^6 M^{-1}sec^{-1}$ 1-chlorohexane	$k \times 10^6 M^{-1}sec^{-1}$ 1-bromohexane	$k \times 10^6 M^{-1}sec^{-1}$ 1-iodohexane
Acetonitrile	0.179 ± 0.001	21.56 ± 0.21	79.25 ± 0.77

Concentration: 0.76mol/liter (1:1:~20 mole ratio, 1-methylimidazole:haloalkane) in acetonitrile at 40°C.

Hence, 1-iodohexane at first inspection would seem to be the best choice, on the basis of the high rate of reaction. However, in an industrial process, the cost of raw materials is a concern to maximize the profit margin expected for the product. Using a number of vendors: Acros Organics, Alfa Aesar, Sigma Aldrich, and Pfaltz and Bauer Chemicals a quick analysis was used to compare the different prices for each haloalkane assuming that a purity of 98% or better was acceptable for all the reactants in Table 3- 6 for an industrial application. All prices which were obtained from the vendors were based on the highest amount which was supplied at a reduced price. However, the quantities examined were not on an industrial scale and are

subject to further reduction in price based on bulk consumption. The average price (2007) for 1-chlorohexane using the vendors specified amounts was approximately \$0.20/mL, 1-bromohexane was \$0.06/mL, and for 1-iodohexane the average cost was \$0.57/mL. Thus, it is seen that 1-bromohexane has the lowest cost out of the three haloalkanes with 1-chlorohexane being over three times the unit price, and 1-iodohexane being almost 10 times the unit price compared to 1-bromohexane. Between the two fastest haloalkanes used in the study it is seen that the rate of reaction using 1-iodohexane is nearly 4 times faster than that seen for 1-bromohexane. However, when comparing the unit cost between the two, 1-bromohexane and 1-iodohexane, it can be concluded that the unit price for 1-iodohexane is nearly 10 folds that of 1-bromohexane. Thus, based on this quick cost analysis of the haloalkanes, and examining the rates of reactions it can be concluded that there has to be a balance between the cost and the rates of reactions to optimize the profit margin in an industrial application.

3.4.2. Chain Length Contribution

The effect of n-alkyl chain length on the kinetic rate was probed using alkyl bromides and is shown in Figure 3- 7. In the figure the x axis is the number of carbons attached to the halide, or in other words C2 is 1-bromoethane, C6 is 1-bromohexane and so forth. As a S_N2 type reaction occurs through a backside attack, the molecule is inverted, thus any obstruction caused by the addition of

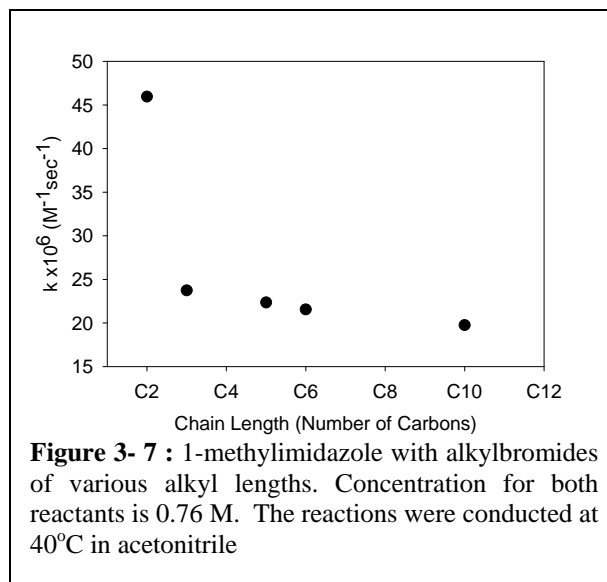


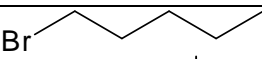
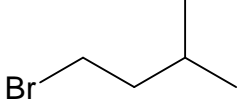
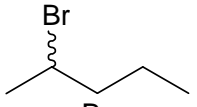
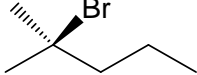
Figure 3- 7 : 1-methylimidazole with alkylbromides of various alkyl lengths. Concentration for both reactants is 0.76 M. The reactions were conducted at 40°C in acetonitrile

carbons and hydrogens (extension of chain length) will hinder the rate of reaction.³⁵ This is clearly seen when comparing the reaction rate with 1-bromoethane compared to 1-bromopropane. However, incremental increases in methylene units results in

only marginal decrease in the reaction rate as the additional length, and hence additional conformers, is spatially distant from the transition state and leaving group.

3.4.3. Steric Effects

The steric effect of the alkyl halides and 1-methylimidazole on the kinetic rate was conducted using 5-carbon alkyl bromides. The results are depicted in Table 3- 7. As shown, the location of the branching plays a significant role in the rates of reaction observed. The kinetic rate with 2-bromopentane is over an order of magnitude lower than with 1-bromopentane. As the point of branching (steric hindrance) is located further from the alpha carbon with the halide (e.g. 1-bromo-3-methylbutane), the kinetic rate increases. If this were an S_N1 type reaction, as suggested for the production of 1-butyl-3-methylimidazolium chloride from *in situ* IR spectroscopy by Giernoth³⁴, the branching would stabilize the carbocation and increase the kinetic rate; thus 2-bromo-2-methylbutane being a tertiary carbon would have the fastest rate of reaction if this reaction followed a S_N1 type reaction because the tertiary carbon near the bromide atom would stabilize the carbocation formation. However, these observations are completely consistent with a traditional S_N2 mechanism.³⁵

bromoalkane	Structure	$k \times 10^6 \text{ M}^{-1}\text{sec}^{-1}$
1-bromopentane		22.35 ± 0.40
1-bromo-3-methylbutane		14.73 ± 0.02
2-bromopentane		1.13 ± 0.05
2-bromo-2-methylbutane		< 0.001

Concentration of 0.76 mol/liter for both reactants.

3.4.4. Concentration Effects on Kinetic Constant

The kinetic constant with many reactions is independent of the initial concentrations as the reaction rate is proportional to the reactant concentrations in: $r=k[A][B]$ given from Equation 2-1 in chapter 2. If this equation is correct, then the kinetic constant, k , will be invariable regardless of the initial concentration. Table 3-8 illustrates the results of the reaction of 1-bromohexane with 1-methylimidazole at different initial concentrations. Examining the data it is seen that the reaction rate is slightly lower when excess 1-bromohexane is used and the largest rate occurs when 1-methylimidazole is in excess. Thus, it may be concluded that the reaction mechanism is not truly 1st order with respect to each individual concentrations for each component and is more complex. Another possible explanation for the change in rate constant may reside in a change in polarity of the mixture when an excess of either starting material is used. The KT parameters, now of the mixture, α , β , and π^* , are given in Table 3-9, and were experimentally determined based on the initial conditions (no conversion). As seen from the KT parameters for the mixture, the polarity might be playing a role in determining rates of reaction. Examining the table it is seen that at higher concentration of 1-bromohexane there is a larger value of α , and a lower value for β and π^* . The opposite is true for excess amount of 1-methylimidazole. When examining the LSER regression, it was determined that there needs to be a minimal value for α , and large values for both β and π^* . Thus, as seen by Table 3-9, the trend seen for the rate constants in Table 3-8 are the expected trends observed based on the mixture polarities. However, further research has to be conducted to resolve if the change in rates of reaction are consistent with solvent polarity change, or if the reaction mechanism is more complex than originally assumed.

Table 3- 8 : Concentration effects on the rate constant in acetonitrile

Mole Ratio ^a	1-methylimidazole Conc. (M)	1-bromohexane Concentration (M)	k (M ⁻¹ sec ⁻¹) T=40°C
1 : 2 : 17.2	0.77	1.54	19.56 ± 0.17
1 : 1 : 20.0	0.76	0.76	21.56 ± 0.21
2 : 1 : 18.4	1.54	0.77	24.94 ± 0.16

a) Mole ratio (X:Y:Z) corresponds to (1-methylimidazole:1-bromohexane:acetonitrile)

Table 3- 9 : KT parameters and E_T(30) values for the reaction mixture

Mole Ratio ^a	k (M ⁻¹ sec ⁻¹)	Kamlet Taft Parameters		
	T=40°C	α	β	π*
1 : 2 : 17.2	19.56 ± 0.17	0.21 ± 0.06	0.46 ± 0.02	0.78 ± 0.04
1 : 1 : 20.0	21.56 ± 0.21	0.18 ± 0.01	0.48 ± 0.02	0.79 ± 0.01
2 : 1 : 18.4	24.94 ± 0.16	0.18 ± 0.01	0.53 ± 0.01	0.81 ± 0.01

a) Mole ratio (X:Y:Z) corresponds to (1-methylimidazole:1-bromohexane:acetonitrile)

3.5. Summary of Results

To conclude, it is seen that the quaternization reaction between 1-methylimidazole and 1-bromohexane is highly dependent on the solvent media. The rates of reaction can be altered by more than an order of magnitude based on the solvent selection. Polar aprotic solvents were desired over polar protic solvents with DMSO having the largest rate of reaction out of the 10 solvents. Using Kamlet-Taft parameters and the E_T(30) scale, it was demonstrated that the kinetic rate constants could only be quantitatively correlated with multiple polarity scales. Thus, the multiparameter approach using the KT parameters α , β , π^* , in a LSER regression could satisfactorily correlate the solvent effects on the kinetics. It was demonstrated through LSER regression, that optimal solvents have little acidity (α) and large basicity (β) and dipolarity/polarizability (π^*). The regressed LSER expression is useful to screen a number of solvents quickly without the need for experimentation. The choice of leaving group on the haloalkane can significantly alter the kinetic rate constant by more than an order of magnitude, with iodo-alkanes being the fastest and chloro-alkanes being the slowest. However, a compromise must be made between the unit cost and the desired rate of reaction in choosing an appropriate haloalkane. The

rates of reactions only slightly decreased with longer bromo-alkane reactions as 1-bromoethane was much faster than the remaining alkyl chain lengths studied. Bromopentanes isomers yield dramatically different kinetic rates based upon the degree of steric hindrance at the point of attack of the nucleophilic 1-methylimidazole. These results confirm that the reaction follows a S_N2 type mechanism as opposed to a S_N1 type reaction reported by Giernoth.³⁴ Examining the rates of reaction using different mole ratios of the starting material it was shown the rate constant altered depending on the composition. The polarity parameters of these mixtures indicated that the change in kinetics was most probably due to the change in mixture polarity.

References:

1. Kamlet, M. J.; Abboud, J. M.; Abraham, M. H.; Taft, R. W., Linear Solvation Energy Relationship. 23. A Comprehensive Collection of the Solvatochromic Parameters, π^* , α , β , and Some Methods for Simplifying Solvatochromic Equation. *J. Org. Chem.* **1983**, (48), 2877-2887.
2. Fradera, X.; Amat, L.; Torrent, M.; Mestres, J.; Constans, P.; Besalu, E.; Marti, J.; Simon, S.; Lobato, M.; Oliva, J. M.; Luis, J. M.; Andres, J. L.; Sola, M.; Carbo, R.; Duran, M., Analysis of the change on the potential energy surface of Menshutkin reactions induced by external perturbations. *J. Mol. Struct. (Theochem)* **1996**, 371, 171-183.
3. Menshutkin, N., *Z. Physik. Chem.* **1890**, 5, 589.
4. Menshutkin, N., *Z. Physik. Chem.* **1890**, 6, 41.
5. Reichardt, C., *Solvent and Solvent Effects in Organic Chemistry*. 3 ed.; Wiley-VCH: Weinheim, Germany, 2003; p 629.
6. Eyring, H., The activated complex and the absolute rate of chemical reactions. *Chem. Rev.* **1935**, 17, (1), 65-77.
7. Eyring, H., The Activated Complex in Chemical Reactions. *J. Chem. Phys.* **1935**, 3, 107-115.
8. Wynne-Jones, W. F. K.; Eyring, H., The Absolute Rate of Reactions in Condensed Phases. *J. Chem. Phys.* **1935**, 3, 492-502.
9. Hughes, E. D., Mechanism and kinetics of substitution at a saturated carbon atom. *Trans. Faraday Soc.* **1941**, 37, 603-637.
10. Hughes, E. D.; Dhar, M. L.; Ingold, C. K.; Mandour, A. M. M.; Maw, G. A.; Woolf, L. I., Mechanism of elimination reactions. XVI. Constitutional influence in elimination. General discussion. *J. Chem. Soc.* **1948**, 2093-2119.
11. Hughes, E. D.; Ingold, C. K., Mechanism of substitution at a saturated carbon atom. IV. Discussion of constitutional and solvent effects on the mechanism, kinetics, velocity and orientation of substitution. *J. Chem. Soc.* **1935**, 244-255.
12. Abraham, M. H., Substitution at Saturated Carbon. Part VIII. Solvent Effects on the Free Energy of Trimethylamine, the Nitrobenzyl Chlorides, and the Trimethylamine-Nitrobenzyl Chloride Transition State. *J. Chem. Soc.* **1971**, 2, 299-308.
13. Kosower, E. M., The Effect of Solvent on Spectra III. The Use of Z-values in Connection with Kinetic Data. *J. Amer. Chem. Soc.* **1958**, 80, 3267-3270.
14. Stefani, A. P., Solvent Effects in Electroneutral Reactions I. Combination and Disproportionation of Ethyl Radicals in Solution. *J. Amer. Chem. Soc.* **1968**, 90, (7), 1694-1700.
15. Wong, K. F.; Eckert, C. A., Solvent Design for Chemical Reactions. *Ind. Eng. Chem. Des. Dev.* **1969**, 8, (4), 568-573.
16. Tommila, E., Relation between the reaction velocity and dielectric constant of the medium. *Acta Chem. Scand.* **1959**, 13, 622-623.
17. Auriel, M.; Hoffmann, E. d., Quantitative Study of Solvent Effects on Menshutkin Reaction between 1,4-Diazabicyclo[2.2.2]octane and (2-

- chloroethyl)benzene, (2-Bromoethyl)benzene, and (2-Iodoethyl)benzene. *J. Amer. Chem. Soc.* **1975**, 97, (26), 7433-7437.
18. Stearn, A. E.; Eyring, H., The Deduction of Reaction Mechanisms from the Theory of Absolute Rates. *J. Chem Phys.* **1937**, 5, 113-123.
19. U.S.FDA, Guidance for Industry Q3C Impurities: Residual Solvents. <http://www.fda.gov/cber/gdlns/q3cresolvent.pdf> **1997**.
20. U.S.FDA, Guidance for Industry Q3C Tables and List. <http://www.fda.gov/cber/gdlns/ichq3ctablist.pdf> **2003**.
21. U.S.FDA, FDA/Center for Food Safety & Applied Nutrition: Food Additive List. In CFSAN/Office of Food Additive Safety: <http://www.cfsan.fda.gov/~dms/opa-appa.html#ftnE>: 2006.
22. U.S.FDA, EAFUS: A Food Additive Database. <http://vm.cfsan.fda.gov/~dms/eafus.html> **2007**.
23. McLaren, J., Future Renewable Resource Needs: Will Genomics Help? *J. Chem. Technol. Biotechnol.* **2000**, (75), 927-932.
24. Wilke, D., Chemicals from Biotechnology: molecular plant genetics will challenge the chemical and the fermentation industry. *Appl. Microbiol. Biotechnol.* **1999**, (52), 135-145.
25. Abraham, M. H., Solvent Effects on Transition States and Reaction Rates. *Prog. Phys. Org. Chem.* **1974**, 11, 1-87.
26. Skrzypczak, A.; Neta, P., Rate Constants for Reaction of 1,2-dimethylimidazole with Benzyl Bromide in Ionic Liquids and Organic Solvents. *Int. J. Chem. Kinet.* **2004**, 36, (4), 253-258.
27. Haberfield, P.; Nudelman, A.; Bloom, A.; Bloom, R.; Ginsberg, H., Enthalpies of Transfer of Transition States in the Menshutkin Reaction from a Polar Protic to a Dipolar Aprotic Solvent. *J. Org. Chem.* **1971**, 36, (13), 1792-1795.
28. Arnett, E. M.; Reich, R., Electronic Effects on the Menshutkin Reaction. A Complete Kinetic and Thermodynamic Dissection of Alkyl Transfer to 3- and 4-Substituted Pyridines. *J. Am. Chem. Soc.* **1980**, 102, 5892-5902.
29. Halls, M. D.; Schlegel, H. B., Chemistry Inside Carbon Nanotubes: The Menshutkin SN2 Reaction. *J. Phys. Chem. B* **2002**, 106, 1921-1925.
30. Maran, U.; Pakkanen, T. A.; Karelson, M., Semiempirical Study of the Solvent Effect on the Menshutkin Reaction. *J. Chem. Soc. Perkin. Trans. 2* **1994**, (12), 2445-2452.
31. Persson, J.; Berg, U.; Matsson, O., Steric Effects in SN2 Reactions. Primary Carbon Kinetic Isotope Effects in Menshutkin Reactions. *J. Org. Chem* **1995**, 60, 5037-5040.
32. Shaik, S.; Ioffe, A.; Reddy, A. C.; Pross, A., Is the Avoided Crossing State a Good Approximation for the Transition State of a Chemical Reaction? An Analysis of Menshutkin and Ionic SN2 Reactions. *J. Am. Chem. Soc.* **1994**, 116, 262-273.
33. Bowman, D. C., Teaching Solvent Effects on SN2 Reactions by the Introduction of Ionic Liquids. *Chem. Educator* **2006**, 11, 64-66.
34. Giernoth, R., In Situ IR Spectroscopy in Ionic Liquids: Toward the Detection of Reactive Intermediates in Transition Metal Catalysis. In *Ionic Liquids IIIA*:

Fundamentals, Progress, Challenges, and Opportunities, Rogers, R. D.; Seddon, K. R., Eds. American Chemical Society: 2005; Vol. ACS symposium Series 901, pp 79-88.

35. Vollhardt, K. P. C.; Schore, N. E., *Organic Chemistry Structure and Function 3rd Edition*. W. H. Freeman and Company: 1998.

4. Diffusion of Reactants and IL in Organic Compounds

Determining the conditions where reaction become diffusion controlled is an important consideration for reactor engineering. If reactions are carried out in a diffusion-limited regime, the residence time needed for the desired conversion may be significantly longer than anticipated, resulting in a lower desired conversion. The following analysis will examine the diffusion rates for both reactants, 1-methylimidazole and 1-bromohexane, as well as the product [HMIm][Br] in a number of solvents. The diffusion coefficients are measured using proton Nuclear Magnetic Resonance (^1H NMR) which has been used in the literature to determine diffusion coefficients.²⁻⁶ The following chapter will describe the theory behind NMR diffusion followed by the experimental procedure used in determining the diffusion coefficient. At the end of the chapter the results obtained for the diffusion coefficients are then used in calculating a diffusion limiting kinetic rate constant for comparison to the rate constant obtained in section 3.2 for DMSO.

4.1. Theory of NMR Diffusion

A detailed review of diffusion measurements using the NMR method is given by Price.^{7, 8} The following is an overview of the two publications by Price.^{7, 8} The theory behind NMR diffusion and the effects of a static magnetic field on nuclear spins originates from the Lamor equation and is given by Equation 4- 1.⁷

$$\omega_0 = \gamma B_0 \quad \text{Equation 4- 1}$$

where ω_0 is the Lamor frequency, γ is the gyromagnetic ratio, which is dependent on the nucleus examined, and B_0 is the strength of the static magnetic field. Typically, B_0 is oriented in the z-direction, length wise for a NMR tube, and is spatially homogeneous throughout the static magnetic field, thus making ω constant throughout the sample.⁷ When a spatially dependent magnetic field gradient is applied parallel to the B_0 , then ω becomes spatially dependent and can be expressed as Equation 4- 2.⁷

$$\omega_{\text{eff}}(n, r) = n(\omega_0 + \gamma(g \cdot r)) \quad \text{Equation 4- 2}$$

where g is defined as the gradient field which is parallel to B_0 and can be expressed by Equation 4- 3:⁷

$$g = \nabla B_0 = \frac{\partial B_z}{\partial x} i + \frac{\partial B_z}{\partial y} j + \frac{\partial B_z}{\partial z} k \quad \text{Equation 4- 3}$$

where i , j , and k are unit vectors in different directions.⁷ Since NMR tubes by their very nature are long narrow diameter tubes it is common to measure diffusion gradients along the z -direction, where z is the length of the NMR tube. Therefore, the magnitude of g in Equation 4- 2 and Equation 4- 3 is only a function of the position in the z -axis and can be expressed by Equation 4- 4.⁷

$$g = g_z = g \cdot k \quad \text{Equation 4- 4}$$

Therefore, for a single quantum change in the z -direction Equation 4- 2 can be expressed as Equation 4- 5.⁷

$$\phi(t) = \gamma B_0 t + \gamma \int_0^t g(t') z(t') dt' \quad \text{Equation 4- 5}$$

where the left hand side is the total phase shift resulting from the static field as well as the applied field.⁷ The first term on the right hand side in Equation 4- 5 is the static field contribution and the second term is the applied gradient; both contributions result in a phase shift.⁷ As seen the second term in Equation 4- 5 is affected by the gyromagnetic ratio, the strength and time duration of the gradient, and the displacement of the molecules in the z -direction. Typically, the applied gradient is constant throughout the diffusion experiment and can be pulled outside of the integral.⁷ It is important at this point to note that the first term in Equation 4- 5 is assumed constant throughout the diffusion experiment and is associated with only the external magnetic field, while the second term is used to dephasing and rephasing different nuclear spins.⁷ The equation derived for determining diffusion rates with the NMR method is given by Price⁷ and is represented by Equation 4- 6 for a bipolar longitudinal eddy decay (BPP-LED) sequence used in this study.

$$I = I^o \exp^{-(g\delta\gamma)^2 D(\Delta-\delta/3-\tau/2)} \quad \text{Equation 4- 6}$$

where I is the observed intensity, I^o the reference intensity of the signal, g is a percentage of the total applied gradient, δ the time duration for the gradient pulse, γ the gyromagnetic ratio of the nucleus, D is the diffusion coefficient, Δ the diffusion time, and τ the correction time for the dephasing and rephasing between the dipolar gradients. The value of g is represented by the percentage of the maximum current provided by the gradient amplifier, and is typically 10 amperes at 100% of the field strength.⁹ It is also assumed that the gradient strength is linearly proportional to the gradient amplification throughout the entire range.⁹

To qualitatively explain how NMR diffusion works we will examine the modified Hahn spin-echo pulse sequence known as a Stejskal and Tanner sequence, which was used by Price⁸ as a simple explanation for diffusion using the NMR method. A visual representation of the Stejskal and Tanner sequence is given in Figure 4- 1 which has been adapted from Tanner and Stejskal.¹⁰ The principles behind the Stejskal and Tanner sequence, also known as a Pulse Field Gradient (PFG) sequence, are very similar to that of the bipolar longitudinal eddy decay (BPP-LED) sequence^{8,11} selected for this analysis; Figure 4- 2 adapted from Wu *et. al.*¹¹

Looking at the PFG sequence it is seen that a $\pi/2$ radio frequency (rf) pulse is initially applied to a sample, which rotates the overall magnetization from the z-axis to

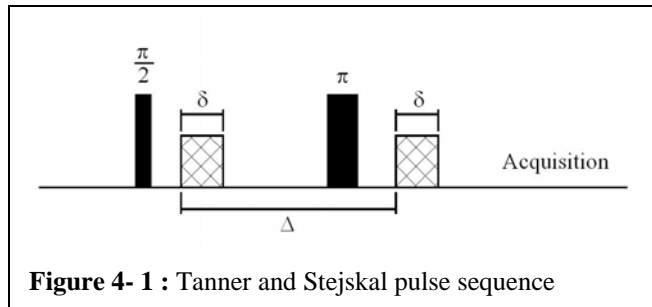


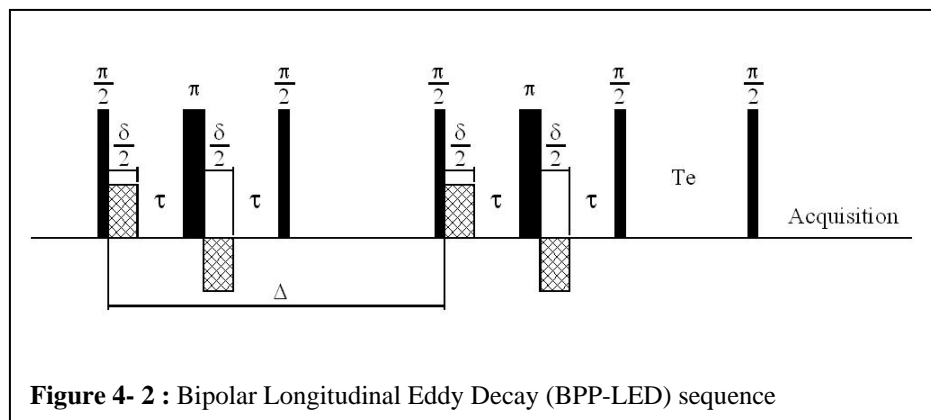
Figure 4- 1 : Tanner and Stejskal pulse sequence

the x-y plane.⁸ During the first τ period, occurring from the rf pulse at $\pi/2$ to π , a gradient pulse is applied for some duration of time, δ , at a given gradient strength, g which labels the position of each nucleus spin in the z-direction.^{8,10} At the end of the first τ a second π rf pulse is applied which inverts the sign of the initial rf pulse, which can be seen as flipping the nucleus' spins 180° , and is followed with a gradient pulse of equal magnitude as the first gradient pulse.¹⁰ The gradient pulses are produced by a small gradient coil placed near the center of the sample. When a

gradient pulse is applied, a magnetic field gradient is produced along the z-axis. Depending on the location of the nucleus in the z-direction, the rotation of the nucleus' spins are affected differently, with a large change in spin occurring near the gradient coil. If there is no diffusion in the z-direction it is seen that the total gradient pulses would cancel. However, if the molecules diffused in the positive or negative z-direction the molecules would experience a difference in field strength between the first and second gradient pulses, thereby the signal would not totally cancel, and depending on how far the molecule moved in the z-direction affects the amount of signal observed. Moreover, special consideration must be given to a phenomena known as eddy currents. If eddy currents are present and not accounted for after the first gradient pulse there would be an additional magnetic field present at the time the second pulses.⁸ This would result in the two gradient pulses not canceling in the pulse sequence even if diffusion in the z-direction did not occur.⁸

4.2. NMR diffusion procedure

In order to verify that the kinetic rate constants are in the kinetically controlled regime, the diffusivities in the reaction mixture were measured using a NMR technique. NMR is an instrument which measures the translational diffusion rate for homogeneous solution, and can determine diffusion coefficients as low as 10^{-17} m²/sec.⁷ Diffusion was determined using a Bruker 400 MHz Ultrashield NMR using a standard z-gradient BBO probe supplied with Topspin version 1.3 software. All diffusion experiments were conducted in standard 5 millimeter NMR tubes and the pulse sequence selected for calculating the diffusion coefficients was a bipolar longitudinal eddy decay BPP-LED sequence adapted from Wu *et. al.*¹¹ (Figure 4- 2). The BPP-LED sequence was selected over the PFG sequence, on the basis that the BPP-LED sequence affectively reduces and dissipates eddy currents better than the PFG sequence using two gradient pulses of opposite signs within the sequence.⁸

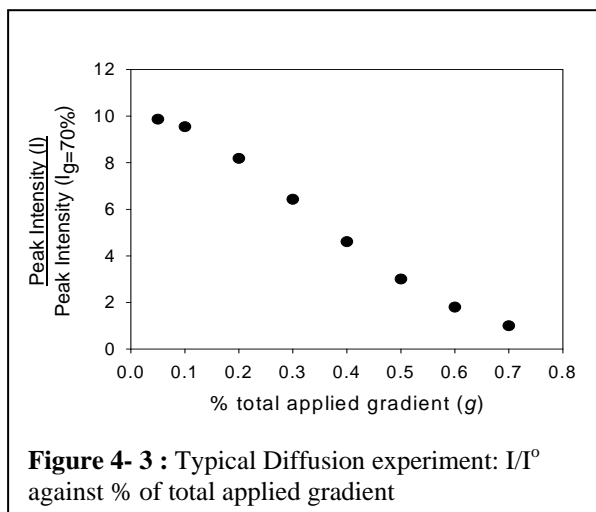


Before quantitative measurements can be made in determining diffusion coefficients the NMR's total applied gradient strength (g) has to first be calibrated. Therefore, as seen by Equation 4- 6 values for Δ , δ , τ , and D have to be known or determined through experimentation. Typically, the values for the time durations are $\Delta =$ milliseconds to seconds, $\delta =$ 0-10 milliseconds, and $\tau =$ two to three milliseconds.⁸ For slow diffusing molecules typically Δ is larger to allow for more diffusion time, while for faster diffusing molecules Δ is smaller. The value used for D has to be obtained using known diffusion coefficients at a given concentration and temperature. For the following study, two standards were used to calculate the gradient strength: ethanol in water at $x_{\text{EtOH}}=0.68$ ^{12, 13} ($D= 7.52 \times 10^{-10} \text{ m}^2/\text{sec}$) and benzene in acetonitrile at infinite dilution¹⁴ ($D= 3.81 \times 10^{-9} \text{ m}^2/\text{sec}$). The total applied gradient strength was calculated using non deuterated ethanol in non deuterated water and non deuterated benzene in deuterated acetonitrile. For the benzene/acetonitrile- d_3 system a 10 milliMolar (mM) solution of benzene was prepared to determine the diffusion coefficient. Two standards were used to check for consistency in determining the gradient strength, and in both cases the signal to noise ratio was greater than 100. Ethanol and water were used because the diffusion coefficients at different compositions of ethanol to water have been reported. The benzene in acetonitrile system was chosen as the second system because it more closely resembles the diffusing species in this study.

The following procedure was used to calculate the total applied gradient strength (g). The NMR was preheated to 25°C 30 minutes prior to calibration; to warm the probe and instrumentation. The mixture of known diffusion rate was accurately weighed on the balance. The sample was then mixed thoroughly and a 400 μ L sample was placed in a clean NMR tube. The height of the sample in the NMR tube was then checked with a standard ruler to ensure the sample was ≤ 3 centimeters (cm.). This is important for higher temperature diffusion experiments, because the heating coil on the NMR machine only heats the bottom 4 cm of the NMR tube uniformly. If the height of the sample in the NMR tube exceeds 4 cm. a temperature gradient in the z-direction may result, leading to the presence of convective mass transfer in the z-direction, which is typically much faster than molecular diffusion. Also, determining diffusion coefficients for highly volatile solvents at elevated temperatures may be a concern for convective mass transfer. As a volatile solvent evaporates it cools and collects near the top of the NMR tube. Eventually, enough of the cooled solvent collects and falls back to the liquid layer. This refluxing effect results in a temperature gradient in the z-direction.⁹

The NMR tube was then placed in the NMR and the temperature was allowed to equilibrate for 10 minutes prior to running the BPP-LED sequence. Following the advice from Kerssebaum⁹, the time constants: Δ , δ , and τ remained constant while the applied gradient strength is altered. To minimize possible damage to the gradient coil the maximum gradient strength used was $g=70\% \times g^{\max}$. For the calibrations: ethanol/water and benzene/acetonitrile- d_3 , the applied gradient strength was altered between $g=5\%$ to $g=70\%$ of the total applied gradient strength using 8 equal increments. To optimize the decay of peak intensities observe in Equation 4- 6 from $g=5\%$ to $g=70\%$ an order of magnitude difference between peak intensities observed at $g=5\%$ and $g=70\%$ must be obtained by selecting the right combinations for Δ and δ .⁹ Experimentally, it was determined that the optimal values for Δ and δ in the diffusion range for the calibrations was to maintain $\Delta=0.1$ seconds and changing δ . For the ethanol/water system the value for $\delta=1.7$ milliseconds, and for the

benzene/acetonitrile-d6 system $\delta=0.8$ milliseconds. A visual representation of the peak intensities related to the applied gradient for the optimized parameters used is illustrated in Figure 4- 3.



From the two calibrations the total applied gradient strength was experimentally determined by graphing the results obtain using Equation 4- 6 for both calibrations and taking the square root of the slope. Upon regressing both calibrations and minimizing the error between the reported values obtained by literature with experimentally determined diffusion coefficients the total applied gradient strength is 51.8 Gauss per meter (G/m), which is similar to the reported value of 53.5 G/m supplied by Bruker's instruction manual for similar probe types.⁹ The uncertainty of the diffusion coefficients are less than 5% from reported values. To validate the experimentally determined gradient strength the diffusion coefficient for aniline in acetone was analyzed at 25°C using a 15 mM solution of aniline in deuterated acetone. It has been reported that the diffusion coefficient for dilute aniline in acetone using a Taylor Dispersion method is $3.17e^{-9} \text{ m}^2/\text{sec}^{15}$, which is close to the experimentally determined value of $3.04e^{-9} \text{ m}^2/\text{sec}$.

All diffusion experiments were obtained following a similar procedure used in calibrating the applied gradient strength, however, instead of determining the total applied gradient strength in Equation 4- 6 the diffusion coefficient was determined. Experimentally, it has been determined that the applied field gradient strength is

affected by temperature, therefore calibration the applied field gradient must be conducted at every temperature for which diffusion coefficients are to be calculated. The following parameters were used to determine all diffusion coefficients at 25°C for which the applied field gradient has been calculated: $\Delta=0.1$ seconds, $\tau=0.2$ milliseconds, and δ was varied between 1 and 2.5 milliseconds. The value of δ is the parameter used to optimize the diffusion coefficient. The applied gradient strength was altered from $g=5\%$ (2.6 G/m) to $g=70\%$ (36.3 G/m) using 8 equal increments. The value of D was determined by the slope of the line when graphing Equation 4- 6.

4.3. Diffusion Results

Most likely the reaction between 1-methylimidazole and 1-bromohexane at the conditions specified are not resulting from mass transport limitations judging by the relative rates of reaction, which are tabulated in section 3.2. However, to confirm this assumption the binary diffusion coefficients for 1-methylimidazole, 1-bromohexane, and [HMIm][Br] in a number of solvents were measured. In addition, diffusion coefficients would provide fundamental data missing in the literature for ionic liquid diffusivity in mixtures; and aid the design of separation techniques beyond thermodynamic considerations. Table 4- 1 lists the results for a few solvents selected for diffusion coefficient calculations using the ^1H NMR technique described in section 4.2. The measurements for the diffusion coefficients were conducted near the infinitely-dilute regime in non-deuterated solvents with the ^1H NMR technique. Concentrations were chosen to provide an adequate NMR signal with a signal-to-noise ratio exceeding 200:1 as both, solute and solvent have magnetic moments as described in section 4.1. The signal resulting from the solvent is much greater than that observed for the solute when non-deuterated solvents are used examining infinitely dilute solute regime; consequently the resolution is limited by the intensity of the solvent peaks. This problem may be overcome by the use of a deuterated solvent, which is not detectable by the NMR, thus giving better resolution of the solute peak for determining the diffusion coefficient. However, deuterated solvents can often yield diffusion rates that are relatively different than their non-deuterated

equivalents. Goldammer and Hertz¹⁶ have demonstrated that the self diffusion rate of deuterated water must be multiplied by a factor of 1.23 to correspond to the self diffusion rate of non-deuterated water. Dimethyl sulfoxide (DMSO), acetonitrile, and acetone were chosen on the basis that they gave the highest rates of reactions, hence any effect resulting from diffusion limitations would be more apparent for these solvents. Methanol was the remaining solvent examined based on two observations: the rate of reaction methanol was the slowest of the solvents studied as seen in section 3.2; methanol is both polar and *protic* in nature. From Table 4- 1, it is seen that the diffusion rate of [HMim][Br] is much less than that of the reactants, which is expected since [HMim][Br] is much larger than the two reactants. Unfortunately at present, it is not clear whether [HMim][Br] exist as separate solvated cation and anion in solution. However, if they are separately solvated or even partially separately solvated columbic forces could also be affect the diffusion rates. Moreover, the solvation of the cation/anion may have large hydrodynamic radii resulting in the slow diffusion rates. From the NMR measurements at present only the cation's diffusion rate was determined since the anion contains no hydrogens which can be monitored using ¹H NMR diffusion. Also, examining Table 4- 1, it is observed that the diffusion coefficient decreases as the viscosity of the solvent increases and it seems that the 1-methylimidazole diffuses faster than 1-bromohexane for each solvent except for methanol. One possible explanation, as explained in section 3.2, may be a result of hydrogen bond formation between methanol and the lone pair of electrons with the nitrogen on the imidazole ring thus forming an intermolecular complex which would have a larger molecular and hydrodynamic diameter and thus slower diffusion.

Table 4- 1 : Diffusion Rate of reactants and product in a number of solvents at a temperature of 25°C and $x_{\text{solute}}=0.05$.

Solvent	viscosity ^a (mPa s) 25°C	$D_{12} \times 10^9$ (m ² /sec) 1-methylimidazole	$D_{12} \times 10^9$ (m ² /sec) 1-bromohexane	$D_{12} \times 10^9$ (m ² /sec) [HMIm][Br]
Acetone	0.306	2.85	2.76	0.74
Acetonitrile	0.369	2.74	2.44	0.89
Methanol	0.544	1.46	1.81	0.72
DMSO	1.987	0.61	0.59	0.20

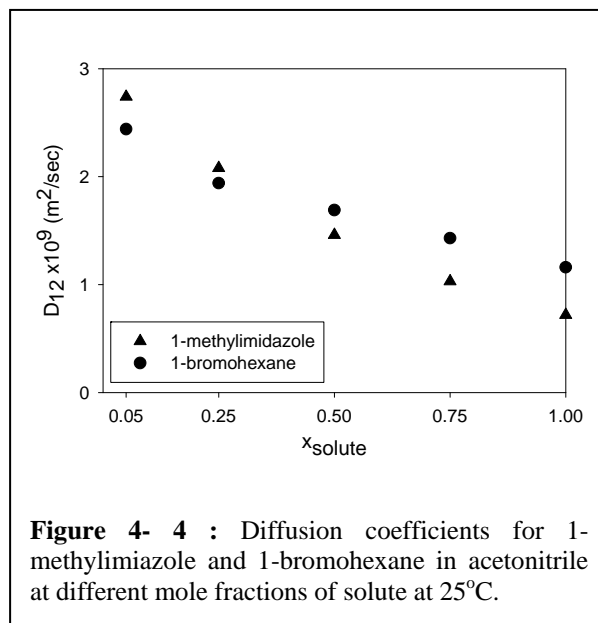
a.) Viscosities were taken from ref.¹

Table 4- 2 : Diffusion rate of 1-methylimidazole and 1-bromohexane in acetonitrile at different solute concentrations.

Solute (1)	$D_{12} \times 10^9$ m ² /sec at T=25°C					
	Solvent (2)	$x_1=0.05$	$x_1=0.25$	$x_1=0.50$	$x_1=0.75$	$x_1=1.00$
1-methylimidazole	Acetonitrile	2.74	2.08	1.46	1.03	0.72
1-bromohexane	Acetonitrile	2.44	1.94	1.69	1.43	1.16

A closer inspection of the diffusion coefficients for 1-methylimidazole and 1-bromohexane in acetonitrile, which was arbitrarily chosen, at different concentration indicates the diffusion rate can change dramatically depending on the concentration of the starting materials as presented in Table 4- 2 and Figure 4- 4. It is seen that the diffusion rate increases almost four fold when the mole fraction of 1-methylimidazole is changed from a mole fraction of 1 to a mole fraction of 0.05, and the diffusion coefficient for 1-bromohexane increases more than two fold under the same conditions.

One possible explanation for why the diffusion coefficient decreases for both: 1-bromohexane and 1-methylimidazole with increasing mole fraction of reactants may be due to the increasing number of reactant molecules in solution. 1-bromohexane and 1-methylimidazole have much larger hydrodynamic radii compared to acetonitrile. Therefore, as the number of reactant molecules increase in solution, the reactants must diffuse not only through the smaller solvent molecules, but also the larger reactant molecules. Thus, a decrease in the diffusion coefficient is observed. Comparing the change in diffusion coefficient between the 1-bromohexane and 1-methylimidazole as shown in Figure 4- 4 and Table 4- 2 it is seen that the change in the rate of diffusion is much greater for the 1-methylimidazole compared to the 1-bromohexane. This may result from pi stacking, or dimerization, between the aromatic imidazole rings. This has been observed by Karlstrom *et. al.*¹⁷ examining the interactions between multiple benzene rings. If pi stacking is occurring between multiple imidazole rings, it can be concluded that at higher concentrations of 1-methylimidazole the rate of diffusion would decrease resulting from the much larger dimer diffusing through the solution.



4.4. Diffusion controlled kinetic analysis

A detailed analysis for the reaction conducted in dimethyl sulfoxide (DMSO) will be described. DMSO was chosen as a solvent for the diffusion controlled analysis, because it had the fastest kinetic rate constant and the slowest diffusion rate of reactants in the solvent. Both of which are highly advantageous and is the best case scenario if the reaction is occurring in a diffusion limiting regime.

4.4.1. Analyzing Diffusion controlled kinetics; DMSO

The analysis for the diffusion-limited rate constant for a reaction in a homogeneous diffusion limiting regime is given by Equation 4- 7:¹⁸

$$k_d = 4\pi R^* D N_A \quad \text{Equation 4- 7}$$

where k_d is the diffusion-controlled rate constant, R^* is the distance at which the reaction occurs (assumed to be the average distance between the reactants hydrodynamic radius), D is the sum of the reactants diffusion coefficients at the concentration of the reaction, and N_A is Avogadro's constant. Using the Stokes-Einstein equation, which relates the diffusion coefficient to the hydrodynamic radius for each molecule can be calculated by¹⁸:

$$R_a = \frac{k_B T}{6\pi\eta D_a} \quad \text{and} \quad R_b = \frac{k_B T}{6\pi\eta D_b} \quad \text{Equation 4- 8}$$

where R_A and R_B are the hydrodynamic radii, k_B is the Boltzmann constant, T is the temperature in $^{\circ}\text{K}$, η is the viscosity of the media, and D_a and D_b are the diffusion coefficient for each species in the solvent media. Using Equation 4- 8 and the experimentally determined diffusion rates for 1-methylimidazole and 1-bromohexane given in Table 4- 1 the hydrodynamic radii for both reactants were calculated assuming a hard sphere model. The viscosity of the media used in calculating the hydrodynamic radii is assumed to be the viscosity of pure DMSO since the mole fraction for both reactants is less than 10 % of the total mole fraction in solution, and the diffusion coefficient taken at a mole fraction of 0.05 was sufficient in determining the hydrodynamic radius. The analysis is given in Table 4- 3.

Table 4-3: Calculating the k_d in DMSO for the reaction between 1-methylimidazole and 1-bromohexane

D_a (1-methylimidazole)	6.10×10^{-10}	m^2/sec
D_b (1-bromohexane)	5.90×10^{-10}	m^2/sec
$D=(D_a + D_b)$	1.20×10^{-9}	m^2/sec
viscosity DMSO ^a	1.987×10^{-3}	$\text{kg}/\text{m}\cdot\text{sec}$
R_a	1.80×10^{-10}	m
R_b	1.86×10^{-10}	m
$R^*=(R_a + R_b)/2$	1.83×10^{-10}	m
k_d	1.66×10^9	$\text{M}^{-1}\text{sec}^{-1}$
k (at 25°C) ^b	2.22×10^{-5}	$\text{M}^{-1}\text{sec}^{-1}$

Where D_a and D_b are the respected binary diffusion coefficients in DMSO at 25°C . a.) Taken from ref.¹ b.)Taken from section 3.2

It is seen in Table 4- 3 that the rate of reaction in DMSO is many orders-of-magnitude below that of a diffusion controlled regime. Consequently, the rate of reaction is dominated by the kinetics of the reaction and not by diffusion constraints, thus the kinetics rates reported here truly reflect the molecular interactions.

4.5. Summary of Results

As demonstrated, ^1H NMR is a powerful tool which can be utilized in determining diffusion coefficients. It was observed analyzing the diffusion rates for the reactants, 1-methylimidazole and 1-bromohexane, and the product, $[\text{HMIIm}][\text{Br}]$,

that the reactants diffused faster in all the solvents examined compared to [HMIm][Br]. This is expected since [HMIm][Br] is much larger in size compared to the reactants. Also demonstrated by analyzing the diffusion rates for both reactants in acetonitrile was the concentration of reactants greatly influenced the diffusion rates, with a 4 fold difference observed for 1-methylimidazole from a mole fraction of 1 to a mole fraction of 0.05, and a 2 fold difference observed for 1-bromohexane under the same conditions. While examining the diffusion rates for 1-methylimidazole and 1-bromohexane in DMSO, which has the fastest rates of reaction and the slowest diffusion rate out of the solvents examined, it was proven that the rates of reaction were primarily dominated by kinetic effects, and were not limited by diffusion mass transfer limitations.

References:

1. Lide, D., *CRC Handbook of Chemistry and Physics*. 88th ed.; CRC Press: 2007.
2. Wakai, C.; Nakahara, M., Attractive Potential Effect on the Self-Diffusion Coefficient of a Solitary Water Molecule in Organic Solvents. *J. Chem. Phys.* **1997**, 106, (18), 7512-7518.
3. Becker, C. R.; Schad, L. R.; Lorenz, W. J., Measurement of Diffusion Coefficients using a Quick Echo Split NMR Imaging Technique. *Magnetic Resonance Imaging* **1994**, 12, (8), 1167-1174.
4. Hayamizu, K.; Price, W. S., A new type of sample tube for reducing convection effects in PGSE-NMR measurements of self-diffusion coefficients of liquid samples. *J. Magn. Reson.* **2004**, 167, 328-333.
5. Nakahara, M.; Wakai, C.; Yoshimoto, Y.; Matubayasi, N., Dynamics of Hydrophobic Hydration of Benzene. *J. Phys. Chem.* **1996**, (100), 1345-1349.
6. Annat, G.; MacFarlane, D. R.; Forsyth, M., Transport Properties in Ionic Liquids and Ionic Liquid Mixtures: The Challenges of NMR Pulse Field Gradient Diffusion Measurements. *J. Phys. Chem. B* **2007**, 111, 9018-9024.
7. Price, W. S., Pulse-Field Gradient Nuclear Magnetic Resonance as a Tool for Studying Translational Diffusion: Part 1. Basic Theory. *Concepts Magn. Reson.* **1997**, 9, 299-336.
8. Price, W. S., Pulse-Field Gradient Nuclear Magnetic Resonance as a Tool for Studying Translational Diffusion: Part II. Experimental Aspects. *Concepts Magn. Reson.* **1998**, 10, (4), 197-237.
9. Kerssebaum, R., DOSY and Diffusion by NMR. In *Bruker Biospin manual - DOSY and Diffusion by NMR*, Rheinstetten, Germany, 2002; pp 3-23.
10. Tanner, J. E.; Stejskal, E. O., Spin Diffusion Measurements: Spin Echoes in the Presence of a Time-Dependent Field Gradient. *J. Chem. Phys.* **1965**, 42, (1), 288-292.
11. Wu, D.; Chen, A.; Johnson, C. S., An Improved Diffusion-Ordered Spectroscopy Experiment Incorporating-Gradient Pulses. *J. Magn. Reson.* **1995**, 115, 260-264.
12. Tyn, M. T.; Calus, W. F., Temperature and Concentration Dependence of Mutual Diffusion Coefficients of Some Binary Liquid Systems. *J. Chem. Eng. Data* **1975**, 20, (3), 310-316.
13. Ven-Lucassen, M. J. J. v. d.; Kieviet, F. G.; Kerkhof, P. J. A. M., Fast and Convient Implementation of the Taylor Dispersion Method. *J. Chem. Eng. Data* **1995**, (40), 407-411.
14. Eastal, A. J.; Woolf, L. A., Solute-Solvent Interaction Effects on Tracer Diffusion Coefficients. *J. Chem. Soc., Faraday Trans.* **1984**, 80, 1287-1295.
15. Chan, M. L.; Chan, T. C., Diffusion of Pseudoplanar Solutes: An investigation on the Effects of Hydrogen Bonding. *J. Phys. Chem.* **1995**, 99, 5765-5768.
16. Goldammer, E. V.; Hertz, H. G., Molecular Motion and Structure of Aqueous Mixtures with Nonelectrolytes As Studied by Nuclear Magnetic Relaxation Method. *J. Phys. Chem.* **1970**, 74, (21), 3734-3755.

17. Karlstrom, G.; Linse, P.; Wallqvist, A.; Jonsson, B., Intermolecular Potentials for the H₂O-C₆H₆ and the C₆H₆-C₆H₆ Systems Calculated in an ab initio SCF CI Approximation. *J. Amer. Chem. Soc.* **1983**, 105, 3777-3782.
18. Atkins, P., *Physical Chemistry 6th Edition*. W.H. Freeman and Company: 1998.

5. Reaction Engineering and Environmental Impact Analysis

There are many different ways that solvents can be classified as to their affect on humans and the environment. The United States Food and Drug Administration (FDA) typically uses three classes: Class 1, Class 2, Class 3; in addition to a Generally Regarded as Safe (GRAS) solvents.⁵⁻⁸ The United States Department of Health and Human Services have developed a risk assessment guideline for industry which recommends the acceptable amount of residual solvents to be used in pharmaceuticals and for safety of patients.^{5, 6} Under these guidelines any Class 1 solvent shall not be used in the production of pharmaceuticals as they are known or suspected human carcinogen; the list includes: Benzene, carbon tetrachloride, 1,2-dichloroethane, etc.^{5, 6} Class 2 solvents should be limited in the production of pharmaceuticals and have been deemed toxic; however, the toxicity resulting from exposure is reversible.^{5, 6} The amount of solvent acceptable under the classification of Class 2 is based on the inherent toxicity for a given solvent which is determined by the FDA's permitted daily exposure (PDE) limitations.^{5, 6} Class 3 solvents are accepted in the production of pharmaceuticals and have low toxicity.^{5, 6} PDE requirements for Class 3 solvents must be less or equivalent to 50mg/day.^{5, 6} GRAS solvents are preferred solvents which are accepted in the production of pharmaceuticals and have been deemed safe as food additives.^{7, 8} These guidelines are obviously based upon toxicity to humans, and in particular, ingestion or injection and do not necessarily address environmental issues.

For ILs to be truly a "green" solvent, it is important to examine the toxicology of solvents associated with the synthesis of ionic, which includes examining environmental exposure as well as human toxicities. Items such as aquatic toxicity, smog emissions, biodegradation potential, carcinogenicity, and global warming potential are important concerns which need to be addressed when choosing appropriate solvents. In addition, the weighting of these different measures of toxicity and environmental impact is also an important issue. In some ways, the weighting of different factors, i.e. highly weighed on environmental while neglecting

health concerns or vice versa, can bias the overall determination of the best solvent choice used in a particular application. None the less, examining a number of different solvent tables and weighting factors allows one to develop a system for determining the “greenest” solvent for a particular process.

5.1. Rowan Solvent Selection Table

One method which takes a large number of health and environmental concerns into consideration is the Rowan Solvent Selection Table (RSST).^{2, 10} Developed by Slater and Savelski at Rowan University in conjunction with Bristol-Myers Squibb, the (RSST) is a compilation of different toxicity and environmental impact factors. Each factor has its own unique units of measurements, but are normalized to a consistent scale, which are then combined in an overall index, called the *Pharmaceutical Index*, by weighting each normalized factor. The Pharmaceutical Index is the overall or global measure of the solvents impact on people and the environment. The follow components for the (RSST) are given in Table 5- 1.² The

following are the definitions for each factor which are defined by the (RSST) in determining the Pharmaceutical Index. Ingestion is the quantity of solvent (mg), which has been shown to be toxic per kg rats.² Inhalation is given by the threshold limiting value (TLV) which is the maximum concentration for a given solvent under repeated

Table 5- 1 : (RSST) 12 categories for solvent selection

Categories	Items Examined ^a
1	ingestion
2	inhalation
3	carcinogen potential
4	biodegradability
5	aquatic toxicity
6	half life
7	ozone depletion potential
8	global warming potential
9	smog formation
10	acidification
11	soil absorption coefficient
12	bio-concentration factor

a) Taken from ref.²

exposure without adverse health effects.² Carcinogenicity is a measure of the solvents known carcinogen level; in the (RSST) non carcinogens are given a value of 0 and known carcinogens are given a maximum value of 5.² Biodegradation is the ability for a solvent to be decomposed biologically using bacteria.² Aquatic toxicity

is the known amount of solvent (mg) per liter of water shown lethal to aquatic fish.² Half Life is the amount of time required for a solvent's concentration to reduce by half.² Ozone depletion is the change in the amount of ozone (O₃) in the stratosphere resulting from the release of a given solvent, and is related to the same amount released by trichlorofluoromethane's emission.² Global warming potential is the accumulation of infrared energy released by 1 kg of solvent relative to 1 kg CO₂.² Smog formation is the capacity for a given solvent to create smog formation agents.² Acidification is the number of moles of H⁺ per mole of solvent. Soil adsorption coefficient is the equilibrium mass absorption of a solvent per unit weight of organic carbon in the soil compared to that of the solvents concentration in the liquid phase.² Bio-concentration factor is the ratio of a chemicals concentration in the tissue of an aquatic organism compared to that in water.² Other factors which are not emphasized in the Pharmaceutical Index, but are also recorded in the (RSST) include Octanol/Water partitioning coefficient which is the measure of the equilibrium amount of a given solutes concentration in octanol compared to that of water, water solubility (given in mg/L), and the Henry's Law constant for a given solvent in an aqueous mixture.² In determining the Pharmaceutical Index, all solvents are compared to that of water which has a Pharmaceutical Index of zero.² Thus, the larger the value for the Pharmaceutical Index, the less "green" or sustainable the solvent is for a given application. Each category can be weighed differently in determining the Pharmaceutical Index, i.e. if aquatic toxicity and/or the soil absorbing potential are important considerations a large weighting factor can be placed on one or both of these categories in determining the Pharmaceutical Index. However, in general the Pharmaceutical Index weighting has slightly more emphasis on health factors: inhalation, ingestion, and the carcinogenic toxicity which is twice that of all the other environmental contributions and is used in determining the Pharmaceutical Index for this study.

Another feature built into (RSST) is the ability to compare the Pharmaceutical Index between two processes based on the amount of solvent necessary. If for

example, two different solvents were being compared for a given process and the Pharmaceutical Index between the two systems were very similar it would be hard to choose which process would result in a better selection. However, if one of the processes required twice the amount of solvent compared to the next it would be seen that the process which uses less solvent would be more beneficial, since there would be less waste, and/or environmental and health exposure; thus making the Pharmaceutical Index lower for the case in which less solvent was necessary.

Table 5- 3 is an abridged version of the (RSST) for the solvents selected in determining the kinetic rate constants.² For solvents which have not been examined using the (RSST), the closest related solvent was used and include: methyl formate for ethyl formate, methyl lactate for ethyl lactate, and cyclohexanone for cyclopentanone. Unfortunately, in the (RSST) table there was not a solvent which was closely related to chlorobenzene, thus was not used in the determination of a Pharmaceutical Index. The Pharmaceutical Index presented in the table is based on all health factors being weighed twice that of the environmental, and are based on the same mass used for each particular solvent. Table 5- 3 lists the solvents in order of decreasing rate of reaction of 1-bromohexane with 1-methylimidazole (DMSO is the fastest and methanol slowest). From Table 5- 3 it is seen out of all the solvents selected, using the specified weighting factor for the Pharmaceutical Index, DMSO seems the best solvent and chlorobenzene (o-Dichlorobenzene) would be the worst solvent choice based on how “green” each solvent is for the quaternization reaction.

5.2. GlaxoSmithKline’s(GSK) Pharmaceutical Solvent Selection Table

Another solvent selection guideline utilized for determining solvent toxicity was GlaxoSmithKline’s(GSK) pharmaceutical solvent selection table (GSK-SST) which is based on “International Conference on Harmonization of Technical Requirements for Registration of Pharmaceuticals for Human Use” guidelines, or (ICH guidelines).³ Within the (GSK-SST), solvent selection is examined based on 9 different categories for solvent toxicity and environmental impact. The 9 categories are presented in Table 5- 2, and are listed as: incineration of solvent, recyclability,

bio-treatment, volatile organic compounds (VOC) emissions, environmental impact on air, environmental impact on water, health hazards, exposure potential, and safety hazards for a given solvent.³ For each category a ranking of 1-10 is given, with 10 being the best and 1 being the worse.³ For a detailed explanation of how each category is calculated in determining an overall geometric means for a particular solvent the reader is referred to the (GSK-SST) software.³ Table 5- 4 is an abridged version for the (GSK-SST) analysis. Unfortunately, not all solvents used for determining the kinetics were listed in the (GSK-SST) nor were similar structured solvents for comparison. Thus, only a few solvents were analyzed using the (GSK-SST). Analyzing the solvents in Table 5- 4 it is shown that DMSO, acetone, and methanol would be the next best solvent choices, which is similar to the results obtained by the Rowan Solvent Selection Table in Table 5- 3 neglecting methyl lactate which was not calculated using the (GSK-SST). Thus, both tables although examining and weighting different factors in determining solvent toxicology and selection have concluded that the top three solvent choices are: **DMSO, acetone, and methanol.**

Table 5- 2 : (GSK-SST) 9 categories for solvent selection

Categories	Items Examined ^a
1	incineration
2	recyclability
3	bio-treatment
4	VOC emissions
5	environmental Impact on air
6	environmental Impact on water
7	health hazards
8	exposure potential
9	safety hazards

a.) taken from ref.³

Table 5- 3 : Results from the (RSST) for determining the Pharmaceutical Index with a examples of the various factors.

Solvent	Pharm. Index ^b	Inhalation TLV (ppm) ^b	Ingestion (mg/kg) rat ^b	Aquatic (mg/L) fish ^b	Soil Adsorption Coefficient ^b	Smog Formation ^b	Oct/Water partitioning coefficient ^b
Dimethyl Sulfoxide	0.42	1000	14500	66901.47	0.65	0.00	-1.35
Acetonitrile	3.21	40	3800	4111.44	0.65	0.00	-0.34
Cyclohexanone ^a	5.37	50	1800	754.47	1.18	0.53	0.81
Acetone	2.15	500	5800	6967.00	0.30	0.18	-0.24
2-Butanone	4.00	200	2737	3173.38	0.58	0.51	0.29
Dichloromethane	5.36	50	1600	428.49	1.38	0.03	1.34
Methyl Formate ^a	3.11	100	475	6260.44	0.33	0.00	0.03
Methyl Lactate ^a	1.57	1000	2000	29583.41	0.00	0.00	-0.67
Methanol	2.52	200	5628	8403.43	0.00	0.21	-0.77

a.) Similar to solvents used in the kinetic analysis b.) Values taken from ref.²

Table 5- 4 : (GSK-SST) results for solvent selection

Solvent	Geometric Mean ^a	Incineration ^a	Recyclability ^a	Bio-treatment ^a	VOC ^a
Dimethyl Sulfoxide	5.07	1.94	3.58	4.33	9.99
Acetonitrile	4	2.24	3.64	0.90	3.30
Acetone	4.73	3.21	5.43	1.59	1.30
2-butanone	4.61	3.82	2.25	2.90	3.17
Dichloromethane	3.58	1.00	9.85	3.63	0.97
Methanol	4.69	2.49	3.25	2.55	2.44
Solvent	Environmental Impact water ^a	Environmental Impact Air ^a	Health Hazard ^a	Exposure Potential ^a	Safety Hazard ^a
Dimethyl Sulfoxide	3.65	5.12	7	10.00	5.59
Acetonitrile	8.37	4.99	7	4.70	7.86
Acetone	10.00	8.91	10	6.75	5.42
2-butanone	6.88	5.82	10	6.09	4.92
Dichloromethane	3.04	8.91	4	2.61	10.00
Methanol	10.00	10.00	4	6.94	7.86

a.) taken from ref.³

5.3. Environmental Factor Analysis

Another important consideration in designing a “greener” synthesis for ILs is to examine the efficiency of the process. One particular measure of efficiency is the Environmental factor (E-factor) analysis.¹¹⁻¹³ The definition the E-factor is the kg of waste per kg of desired product obtained, where waste includes solvents, un-reacted material, catalyst, side reactions, etc.¹¹⁻¹³ It is worthy to note that the E-factor does not account for any recycled materials, such as solvent and catalyst, and therefore only relates the total amount of mass needed for a process to the desired mass. Thus, the more efficient a process is (less solvent, high conversion for desired product, etc.) the smaller the value of the E-factor. Table 5- 5 is a break down for E-factors based on different chemical industries.

Based on the E-factor analysis it is shown that oil refining has the least amount of waste, whereas, the pharmaceutical sector shows an extreme amount of waste per amount of desired product. The wide range of E-factors

Table 5- 5 : E-factor analysis for industry

Industry ^a	Product tonnage ^a	E-factor ^a
Oil Refining	10 ⁶ -10 ⁸	~0.1
Bulk Chemicals	10 ⁴ -10 ⁶	1-5
Fine Chemicals	10 ² -10 ⁴	5-50
Pharmaceuticals	10 ¹ -10 ³	50->50

a.) Taken from ref.¹²

presumably is a factor of both profitability of the product and number of years being optimized. Oil refining has low profit margins and has been researched for years. Whereas, pharmaceuticals have very high profit margins on small amounts of material, thus a lower incentive for process improvement.

Turning our attention to IL production, the E-factor can vary widely depending on the desired IL being produced. For quaternization reaction, similar to the reactions used to produce [HMIm][Br], Figure 5- 1, the E-factor is essentially ~0 if solvents were not used in the synthesis. As shown every mole of reactant is converted to the desired product, when stoichiometric amount of starting material are used.

the perfect solvent to produce [HMIm][Br]: the highest reaction rate and lowest toxicity/environmental impact. However, what is not considered within this analysis is the necessary separation of the solvent from the ionic liquid. If distillation/evaporation will be the method of separation, then consideration of the boiling point and heats of vaporization may yield an approximate energy analysis. In an actual distillation/evaporation, one would need to consider the phase equilibrium thermodynamics (activity coefficients, etc.) to design the separation train and energy requirements which are often more than simply the sensible and latent heat of vaporization.¹⁹ Table 5- 6 lists the boiling points, heats of vaporization, sensible heat, and the total energy for the solvents investigated. The sensible heats in Table 5- 6 are calculated based on the change in energy from the solvents boiling point to a temperature of 40°C, assuming the liquid C_p is constant throughout the range. The total energy required is the addition of the heats of vaporization at the boiling point in addition to the sensible heat. As seen in Table 5- 6, DMSO has the highest boiling point out of all the solvents listed in the table. Thus, shown in Table 5- 6 the total amount of energy needed to separate the DMSO solvent from the product, [HMIm][Br], would be quite high. This excess energy needed to remove the solvent would result in more pollution, which in turn would worsen its environmental impact. *Based on comparison of the reaction rate, the solvents' Pharmaceutical Index, and a simple look at energy requirements of separation, acetone appears to possess the optimal combination of properties for use, at least on the bench-scale, if not on an industrial scale. In addition, acetone is relatively inexpensive, can be purchased on a large scale, and can actually be produced by bio-renewable (fermentation) methods.*²⁰

Table 5- 6 : Boiling points, latent heats, sensible heats and total energy obtained for energy analysis

Solvent	MW (g/mol)	T_b^a (°C)	$\Delta H^{vap\ a}$ (KJ/mol)	C_p 25°C ^a (J/g-K)	Sensible heat to T_b (KJ/mol) ^b	Total Heat (KJ/mol)
Dimethyl Sulfoxide	78.13	189.0	43.1	1.958	22.79	65.89
Acetonitrile	41.05	81.7	29.75	2.229	3.84	33.59
Cyclopentanone	98.14	130.6	36.35	1.840	16.43	52.78
Acetone	58.08	56.1	29.1	2.175	2.06	31.16
2-Butanone	72.1	79.6	31.3	2.201	6.35	37.65
Dichloromethane	84.93	40.0	28.06	1.192	-0.02	28.04
Ethyl Formate	74.08	54.4	29.91	2.015	2.09	32.00
Chlorobenzene	147.01	131.7	35.19	1.334	17.85	53.04
Ethyl Lactate	118.13	154.5	N/A	2.150	28.70	28.70
Methanol	32.04	64.6	35.21	2.531	2.00	37.21

a.) taken from ref.¹ ; b.) Based on the temperature difference between the boiling point and a reaction conducted at 40°C, and assuming the C_p is constant throughout the entire temperature range

5.5. Reaction Engineering Analysis

Based on the globally determined solvent, acetone, a reactor engineering analysis is performed for the quaternization reaction between 1-methylimidazole and 1-bromohexane using an adiabatic and non-adiabatic process. For the adiabatic process, the goal is to determine the necessary amount of acetone needed in the feed for controlling the outlet temperature resulting from the exothermic reaction between 1-methylimidazole and 1-bromohexane at different extents of the reaction. Once a specified amount of acetone is obtained for a given extent of reaction, a non-adiabatic analysis will be performed. For the non-adiabatic process, the heat duty will be examined based on different amounts of acetone in the feed at the same outlet temperature and extent of conversion used in the adiabatic process. For an equal comparison between the two processes, the exiting temperature and extent of conversion will be used in the determination of the non-adiabatic process. Once the solvent and heat requirements (non-adiabatic process) have been determined, a comparison of reactor sizing and total heat duties will be examined based on energy removal from the reactor and the energy required for the subsequent separation of

solvent from the desired product. In determining the heat duty analysis for the separation step, only the latent and sensible heats will be analyzed.

Since limited data is available for the 1-methylimidazole and 1-bromohexane system, only an approximate quantitative analysis could be performed. The assumptions made in both processes are:

- All heat capacities (C_p) presented are independent of temperature, thus no excess heat capacities are used in the calculations.
- The heat of reaction (ΔH^{rxn}) is equivalent to -96 KJ/mol, which is the reported value for a similar reaction between 1-methylimidazole and 1-bromobutane.⁹
- The mixture volumes, needed for determining molar concentrations, are calculated by dividing the moles entering the reactor by their respective densities taken at 25°C, which are then summed.
- The volume change associated with conversion is negligible, thus, the reaction is maintained at constant volume.

At present the heat capacity (C_p) for 1-methylimidazole could not be found in the literature. Therefore, it is also assumed that

- 1-methylimidazole's C_p is comparable to pyridine's, which is very similar in structure and size, C_p taken at 25°C.¹

Table 5- 7 shows all of the physical properties used in the adiabatic and non-adiabatic calculations.

Table 5- 7 : Properties needed for calculating an adiabatic / non-adiabatic process				
Component	C_p (J/mol-K)	density (g/cm ³) ^d	Arrhenius Parameters ^e	
			k_o (M ⁻¹ sec ⁻¹)	E_a (KJ/mol-K)
1-methylimidazole	132.7 ^a	1.0325	2.20x10 ⁶	67.261
1-bromohexane	204 ^b	1.1744		
acetone	126.3 ^b	0.7845	Heats of Reaction ^f	
[HMIIm][Br]	344 ^c		ΔH^{rxn} (J/mol) = -96000	

a.) Based on the C_p of pyridine at 25°C; taken from ref.¹ b.) Taken from ref.¹ at 25°C c.) Taken from ref.⁴ at 25°C d.) Taken from ref.¹ e.) experimentally determined in section 3.2 f.) Taken from ref.⁹

The general mass/energy balance used for calculating the temperature rise associated with a steady state adiabatic and non-adiabatic process can be given by Equation 5- 1.²¹

$$\frac{dE}{dt} = 0 = Q + \sum_{i=1}^I (H_i)_{out} - \sum_{i=1}^I (H_i)_{in} + \Delta H^{rxn} X_i \quad \text{Equation 5- 1}$$

where, Q is the total heat added/removed from the system, H_i is the molar enthalpic energy of reactants, solvent, and product entering/leaving the reactor, ΔH^{rxn} is the heat of reaction per mole of reactant entering the reactor, and X_i is the extent of the chemical reaction (conversion).²¹ Under adiabatic operation Equation 5- 1 can further be simplified since the heat added/removed from the system is assumed zero. In both the adiabatic and non-adiabatic processes it is assumed stoichiometric amounts of both: 1-methylimidazole (liquid) and 1-bromohexane (liquid), are entering the reactor. It is also assumed that the solution acts ideally and the heat capacities as well as the heat of reaction are independent of temperature. Making these assumptions we can directly use the molar heat capacities given in Table 5- 7 in determining the molar enthalpic terms in Equation 5- 1 using Equation 5- 2 and Equation 5- 3.²¹

$$\sum_{i=1}^I (H_i)_{in} = \sum_{i=1}^I C_{pin} (T_{in} - T_{ref}) \quad \text{Equation 5- 2}$$

where C_{pin} are the molar heat capacities for the unreacted reactants and solvent (acetone) entering the reactor, T_{in} is the temperature of the feed stream entering the reactor, and T_{ref} is a reference temperature. Using a suggestion given by Levenspiel,²¹ it is assumed that $T_{in}=T_{ref}$, thus Equation 5- 2 is equal to zero. For the molar enthalpies leaving the reactor:

$$\sum_{i=1}^I (H_i)_{out} = \sum_{i=1}^I [C_{pout} (T_{out} - T_{in})(1 - X_i)]_{react} + [C_{pout} (T_{out} - T_{in})(X_i)]_{product} + [C_{pout} (T_{out} - T_{in})]_{solvent} \quad \text{Equation 5- 3}$$

where, $[C_{pout}]_{react}$ are the molar heat capacities for the reactants, based on the number of unreacted moles entering the reactor, $[C_{pout}]_{product}$ is the molar heat capacity for the product, based on the number of moles obtained at total extent of the reaction,

$[C_{pout}]_{solvent}$ is the heat capacity of the solvent, based on the total moles of acetone entering the reactor, and T_{out} is the temperature of the product stream.²¹ By substituting Equation 5- 2 and Equation 5- 3 into Equation 5- 1 the general mass/energy balance relationship is made, which can be used for both: the adiabatic and non-adiabatic calculations.

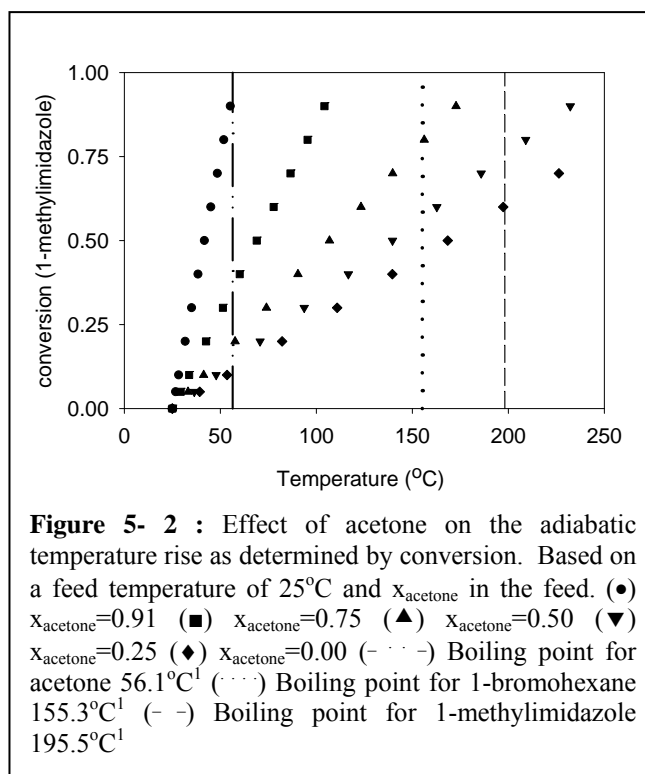
5.5.1. Adiabatic Temperature Rise

The first item considered for the adiabatic reactor analysis was to examine how varying the amount of solvent (inert component) in the feed affects the overall temperature generated during an exothermic adiabatic reaction at different conversions. By rearranging the general energy balance, given in Equation 5- 1, and using all assumptions previously stated, the adiabatic temperature rise can be examined using Equation 5- 4 where Q is assumed zero under adiabatic conditions.

$$T_{out} = \frac{\left[\sum_{i=1}^I n_i^o C_{pi} (1 - X_{sm}) + n_j C_{pj} X_{sm} + n_s^o C_{ps} \right] [T_{in}] - n_j \Delta H^{rxn} X_{sm}}{\left[\sum_{i=1}^I n_i^o C_{pi} (1 - X_{sm}) + n_j C_{pj} X_{sm} + n_s^o C_{ps} \right]} \quad \text{Equation 5- 4}$$

where n_i^o are the moles of reactants entering the reactor (equal mole ratio of reactants), C_{pi} are the molar heat capacities for the reactants, n_j are the moles of product, [HMIm][Br], based on total conversion of either starting material, C_{pj} is the molar heat capacity for [HMIm][Br], n_s^o are the initial moles of solvent (acetone) entering the reactor, C_{ps} is the molar heat capacity for acetone, and X_{sm} is the conversion for either starting material.

As shown by Equation 5- 4 the temperature rise resulting from the exothermic reaction is being managed solely by the C_p 's for the reactants, solvent, and product. By changing the moles of acetone in the feed as well as the extent of the reaction an outlet temperature can be computed. Using a feed temperature of 25°C the results for the adiabatic temperature rise are displayed against different conversions in Figure 5- 2, along with the boiling points for acetone and the reactants.



From Figure 5- 2 it is observed that an increase in solvent concentration (acetone) in the feed stream reduced the temperature rise in an adiabatic reaction at different extents of reaction, which is as expected. When additional acetone is added the concentration of the reactant is reduced, thus the amount of heat absorbed during the exothermic reaction can be handled much more efficiently by the moles and C_p of acetone. For a real process, it would be desired that high rates of conversion be achieved. However, examining the figure more closely it is observed that the mole fraction of acetone in the feed must be equal or greater than 91 mole % for this to occur, without exceeding the boiling point of acetone. In the *solvent-free* case, where acetone's boiling point is not a concern, it is shown that approximately only 45% conversion would be achievable before the boiling point of 1-bromohexane was reached. By exceeding the boiling points for either case: 1-bromohexane for the neat reaction or acetone for all other reactions, the resulting temperatures would lead to unsafe pressures in the reactor. To achieve a conversion greater than 90%, a solvent concentration of 91 mole % does not seem practical on an industrial scale; this will be

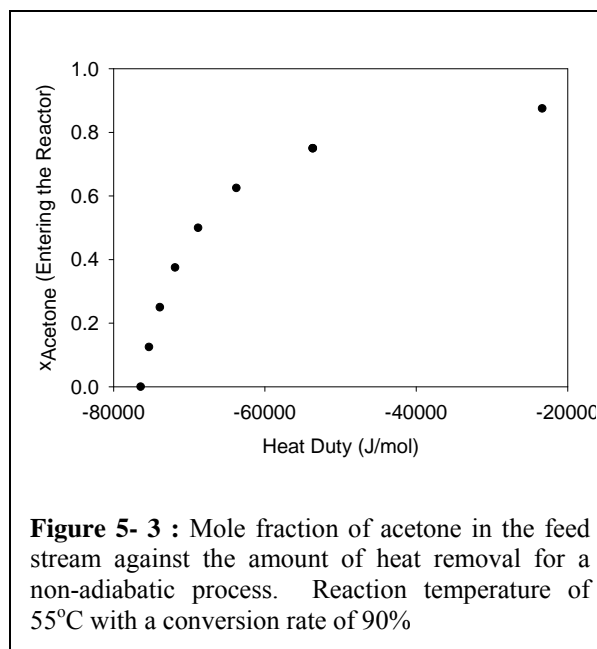
shown in section 5.5.3 for the reactor sizing. Thus for practical use, some amount of heat removal must be included.

5.5.2. Non-Adiabatic Reactor

From the adiabatic reactor analysis it was determined that a 91 mole % of acetone was needed in the feed to manage the heat evolved by the exothermic reaction between 1-methylimidazole and 1-bromohexane, based entirely on the C_p 's for reactants, solvent and product. Based on this adiabatic analysis, a non-adiabatic reactor study was conducted under the same reaction conditions: 25°C inlet temperature and 55°C for an exiting temperature at 90 % conversion. In solving the non-adiabatic process, the ΔH^{rxn} is used to heat the reactor, and any excess heat is removed from the reactor using a heat duty (Q). Based on varying the amount of moles in the feed, the heat duty requirements are examined using Equation 5- 5, which is derived based on the general energy balance as well as all assumptions made in section 5.5.

$$Q = \left[\sum n_i^o C_{pi} (1 - X_{sm}) + n_j C_{pj} X_{sm} + n_s^o C_{ps} \right] [T_{out} - T_{in}] + \Delta H^{rxn} X_{sm} \quad \text{Equation 5- 5}$$

where, X_{sm} is assumed 90 % conversion, T_{out} is 55°C, and T_{in} is 25°C. The results for the non-adiabatic analysis are given in Figure 5- 3. Low concentration of acetone in the feed stream results in a considerable amount of excess energy, which must be removed from the reactor to maintain the operating temperature specified (see Figure 5- 2). Examining Figure 5- 3 shows that the amount of heat removed from the reaction drops significantly as more acetone is added to the initial feed. Thus, under non-adiabatic conditions, a balance must be made between the



desired energy cost for heat removal from the reactor with the relative amounts of acetone.

5.5.3. Reactor Sizing / Energy Cost for Adiabatic and Non-Adiabatic Process

For calculating the reactor size and the total energy requirements for both, the adiabatic and non adiabatic process, a basis of 500 kg/week of desired product, [HMIm][Br], will be used based on 24 hours a day / 7 days a week operation. For a side-by-side comparison between the adiabatic and non-adiabatic process it will be assumed that both processes will be operating at a temperature of 55°C with a 90% conversion. Since, the ΔH^{rxn} is very large (assumed -96 KJ/mol from section 5.5 for the reaction between 1-methylimidazole and 1-bromohexane) the analysis will be performed entirely on a steady state continuous mixed flow reactor operating at constant volume with *equal mole ratios of reactants entering the reactor*. Using 2nd order kinetics the performance equation for the steady state continuous mixed flow reactor can be represented by Equation 5- 6.

$$\frac{kV}{F_{sm}^o} = \frac{X_{sm}}{[C_{sm}^o (1 - X_{sm})]^2} \quad \text{Equation 5- 6}$$

where V is the reactor volume (Liters), C_{sm}^o is the initial concentration (mol/Liter) of reactants (1-methylimidazole or 1-bromohexane) entering the reactor, F_{sm}^o is the molar feed rate (moles/second) of reactants (1-methylimidazole or 1-bromohexane) entering the reactor, and k is the kinetic rate constant (Liter/moles-seconds). For this qualitative analysis, constant volume is assumed and the temperature dependency for the rate constant can be expressed in terms of the Arrhenius equation as shown in Equation 5- 7.

$$k = k_o \exp\left(-\frac{E_a}{RT}\right) \quad \text{Equation 5- 7}$$

where k_o is the pre-exponential term, E_a is the activation energy, R is the gas constant and T is the temperature. It is assumed that the outlet temperature leaving the reactor is the same temperature as the reactor, thus the mass/energy balances solved for the

adiabatic and non-adiabatic study in section 5.5.1 and 5.5.2 can be utilized in solving the temperature in Equation 5- 7. Furthermore, the values E_a and k_o for acetone have been calculated previously (section 3.2) and are given in Table 5- 7.

In determining the total energy cost for each process, the required energy removal for the reactor (non-adiabatic process) and the energy needed for separating the solvent from the product post reaction will be analyzed. For the separation energy, it is assumed that the energy requirements for solvent removal from product can be expressed using the sensible heats as given by Equation 5- 8 and the latent heats of vaporization for acetone.

$$SensibleHeat = \dot{n}_{Tot} \left(\sum_{i=1}^I x_i C_{pi} \right) (T_{bp} - T_{reactor}) \quad \text{Equation 5- 8}$$

where, \dot{n}_{Tot} is the total number of moles leaving the reactor, x_i and C_{pi} are the mole fractions and molar heat capacities for each component leaving the reactor, which are assumed independent of temperature and are given in Table 5- 7, T_{bp} is the boiling point for acetone (56.1°C), and $T_{reactor}$ is the reactor temperature (55°C). The results for the reactor sizing and total energy requirements between the two processes are given in Table 5- 8.

From Table 5- 8 it is seen that the reactor volumes at different concentrations of solvent in the feed (non-adiabatic operation) are well below that needed for the adiabatic process. Examining the non-adiabatic process in which a mole fraction of 0.125 mole % of acetone is in the feed, it is shown that the reactor is 50 times smaller than that observed for the adiabatic process. This is primarily attributed to the lower amount of the inert (solvent) required for the reaction, as shown by the non-adiabatic process with increasing mole fractions of acetone in the feed. Also, interesting to note in Table 5- 8 is the relative total energy requirements between the two processes. Again, examining the non-adiabatic process conducted at 0.125 mole % of acetone in the feed, compared to the adiabatic process, it is seen that the total energy cost is almost 8 times less using the non-adiabatic process. Clearly, a large majority of the energy cost resides in the separation step. Examining the sensible heats for both

processes, in Table 5- 8, the amount of sensible heat change is relatively small resulting from a temperature rise from a reactor temperature (55°C) to the boiling point of acetone (56.1°C), see Equation 5- 8. Sensible heat rises with the addition of acetone, which is as expected since the total throughput for the reactor is increased to maintain the desired flow rate of product (500kg/week). Examining the latent heats, the same trend is observed with an increase in energy cost resulting from a larger amount of solvent removal from product. Based on the reactor sizing and this simple energy analysis it can be concluded that the non-adiabatic process is far more effective than an adiabatic process. By removing heat from the reactor the total amount of solvent necessary for the reaction is greatly reduced.

Based on the analysis given above, the question most commonly asked is: Why is solvent necessary? Examining the reactor volume and energy requirements in the absence of acetone, shown in Table 5- 8, the total energy cost as well as reactor sizing are minimized. Pure [HMIm][Br] is highly viscous, thus any pumping cost associated with product removal would be relatively high compared with product extraction using a solvent/product combination. Under the neat reaction, maintaining uniform mixing could be a concern, which would lead to a drop in the total conversion rate leaving the reactor. Based on the energy requirements, it may be possible for a runaway reaction to occur if the reactors surface area to volume ratio is small. If a runaway reaction were to occur the reactor may over pressurize if the boiling point is exceeded for either of the reactants.

Table 5-8 : Reactor sizing and energy requirements for an adiabatic and non adiabatic process operating at 55°C with 90% conversion.

Adiabatic						
Reactor		Separation			Total Energy ^c	
$X_{\text{Acetone in feed}}$	Q^a (J/sec)	Reactor Volume (L)	Sensible Heat ^b (J/sec)	Latent Heat ^b (J/sec)	Total Energy ^c (Separation) (J/sec)	Total Energy ^d (J/sec)
0.909	0	22606.6	11.77	2172.10	2183.88	2183.88
Non Adiabatic Process						
Reactor		Separation			Total Energy ^e	
$X_{\text{Acetone in feed}}$	Q^a (J/sec)	Reactor Volume (L)	Sensible Heat ^b (J/sec)	Latent Heat ^b (J/sec)	Total Energy ^e (Separation) (J/sec)	Total Energy ^d (J/sec)
0.000	-282.82	375.7	1.40	0.00	1.40	284.22
0.125	-278.80	451.4	1.55	30.90	32.45	311.25
0.250	-273.43	563.2	1.75	72.10	73.84	347.28
0.375	-265.92	740.3	2.02	129.77	131.80	397.72
0.500	-254.66	1051.4	2.44	216.29	218.73	473.39
0.625	-235.88	1690.9	3.12	360.49	363.61	599.49
0.750	-198.33	3423.3	4.50	648.87	653.38	851.71

a.) based on 500 kg/week of product [HMIm][Br] (equivalent to 3.34×10^{-3} mol/sec) b.) Values tabulated based on information given in Table 5- 6 and Table 5- 7 for acetone. c.) The sum of the sensible heat (to raise the temperature to 56.1°C) as well as latent heat d.) The sum of the separation energy and reactor energy

Using a solvent free design may not be adequate based on the nature of the final product. For example, the reaction between 1-methylimidazole (liquid) and 1-ethylbromide (liquid), forms a solid product which has a melting point of 76.3°C.¹⁸ If the reaction is occurring at a temperature lower than the melting point of the product, uniform mixing within the reactor and the reaction volume may be reduced, which would lead to reactor clogging and a decrease in total conversion. Moreover, the product lines leaving the reactor would have to be heated to prevent the product from solidifying in the lines resulting in an increased energy consumption.

5.6. Summary of Results

When selecting a solvent for a given process a large number of health and environmental concerns must be considered. Two solvent selection guides which were utilized in determining the best “environmentally friendly” solvent for the production of [HMIm][Br] were the (RSST) and the (GSK-SST). Although both selection tables weighed and analyzed different aspects of solvent toxicity and environmental impact, both tables concluded to the same three solvent choices: DMSO, acetone, and methanol. Based on the combined kinetic analysis and the environmental analysis it was concluded, out of the solvents analyzed, that DMSO and acetone were the two best solvent candidates for producing imidazolium based ILs. Using a simple energy analysis it was shown that the relatively high boiling point of DMSO would result in higher separation cost and subsequently increased pollution for solvent removal. Therefore, based on all three criteria: high rate of reaction, low environmental impact, and the low energy requirements necessary for separation, acetone was chosen as the preferred solvent for the production of imidazolium based ILs.

Using the globally determined solvent, acetone, a continuous-flow stirred reactor was design based on an adiabatic and non-adiabatic analysis. The size as well as the total energy required for both process were compared based on a specified conversion rate and outlet temperature. Between the two processes the non-adiabatic

process was shown to be superior to the adiabatic process as determined by smaller reactor volumes and lower total energy costs for the non-adiabatic reactor.

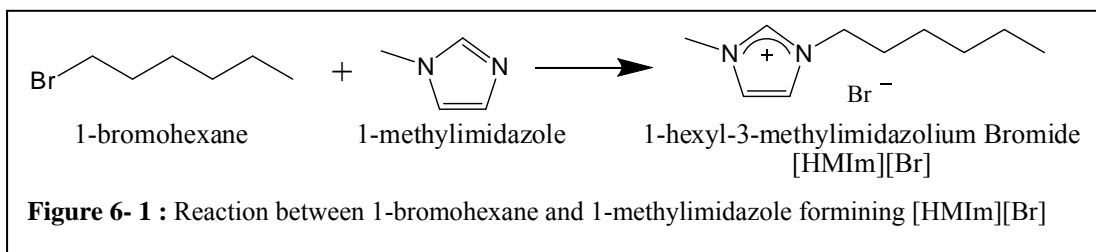
References:

1. Lide, D., *CRC Handbook of Chemistry and Physics*. 88th ed.; CRC Press: 2007.
2. Rowan University, Rowan Solvent Selection Table. In <http://www.rowan.edu/greenengineering>, Accessed: April 08, 2007.
3. GlaxoSmithKline(GSK) pharmaceuticals *Corporate Environment and Safety PRODUCT STEWARDSHIP GUIDE: SOLVENT SELECTION GUIDELINES*, Guide v3; 2003.
4. Crosthwaite, J. M.; Muldoon, M. J.; Dixon, J. K.; Anderson, J. L.; Brennecke, J. F., Phase transition and decomposition temperatures, heat capacities and viscosities of pyridinium ionic liquids. *J. Chem. Thermodyn.* **2005**, 37, 559-568.
5. U.S.FDA, Guidance for Industry Q3C Impurities: Residual Solvents. <http://www.fda.gov/cber/gdlns/q3cresolvent.pdf> **1997**.
6. U.S.FDA, Guidance for Industry Q3C Tables and List. <http://www.fda.gov/cber/gdlns/ichq3ctablist.pdf> **2003**.
7. U.S.FDA, FDA/Center for Food Safety & Applied Nutrition: Food Additive List. In CFSAN/Office of Food Additive Safety: <http://www.cfsan.fda.gov/~dms/opa-appa.html#ftnE>: 2006.
8. U.S.FDA, EAFUS: A Food Additive Database. <http://vm.cfsan.fda.gov/~dms/eafus.html> **2007**.
9. Waterkamp, D. A.; Heiland, M.; Schluter, M.; Sauvageau, J. C.; Beyersdorff, T.; Thoming, J., Synthesis of ionic liquids in micro-reactors-a process intensification study. *Green Chem.* **2007**, 9, 1084-1090.
10. Slater, C. S.; Savelski, M. J., A Method to Characterize the Greenness of Solvents used in Pharmaceutical Manufacture. *J. Environ. Sci. Health., Part A* **2007**, 42, (11), 1595-1605.
11. Sheldon, R. A., Selective catalytic synthesis of fine chemicals: opportunities and trends. *J. Mol. Catal. A: Chem.* **1996**, 107, 75-83.
12. Sheldon, R. A., Catalysis: The Key to Waste Minimization. *J. Chem. Tech. Biotechnol.* **1997**, 68, 381-388.
13. Sheldon, R. A., Roger A Sheldon. *Green Chem.* **2004**, 6, G55-G56.
14. Tokuda, H.; Hayamizu, K.; Ishii, K.; Susan, M. A. B. H.; Watanabe, M., Physicochemical Properties and Structures of Room Temperature Ionic Liquids. 1. Variation of Anionic Species. *J. Phys. Chem. B* **2004**, 108, 16593-16600.
15. Tokuda, H.; Hayamizu, K.; Ishii, K.; Susan, M. A. B. H.; Watanabe, M., Physicochemical Properties and Structures of Room Temperature Ionic Liquids. 2. Variation of Alkyl Chain Length in Imidazolium Cation. *J. Phys. Chem. B* **2005**, 109, 6103-6110.
16. Tokuda, H.; Ishii, K.; Susan, M. A. B. H.; Tsuzuki, S.; Hayamizu, K.; Watanabe, M., Physicochemical Properties and Structures of Room Temperature Ionic Liquids. 3. Variation of Cationic Structure. *J. Phys. Chem. B* **2006**, 110, 2833-2839.

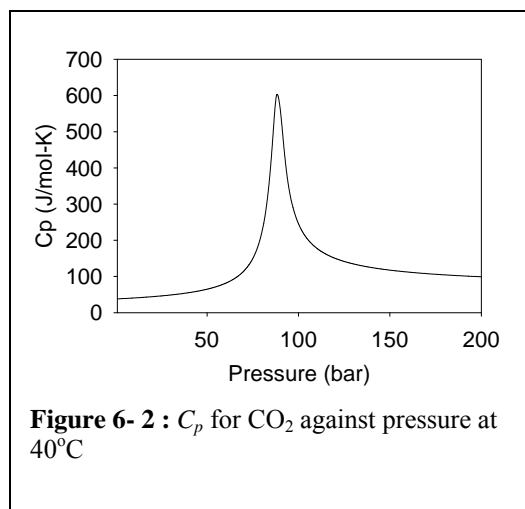
17. Hunt, P. A., Why Does a Reduction in Hydrogen Bonding Lead to an Increase in Viscosity for the 1-Butyl-2,3-dimethyl-imidazolium-Based Ionic Liquids? *J. Phys. Chem. B* **2007**, 111, 4844-4853.
18. Turner, E. A.; Pye, C. C.; Singer, R. D., Use of ab Initio Calculations toward the Rational Design of Room Temperature Ionic Liquids. *J. Phys. Chem. A* **2003**, 107, 2277-2288.
19. McCabe, W. L.; Smith, J. C.; Harriott, P., *Unit operations of chemical engineering*. 7th ed.; McGraw-Hill: 2005.
20. Zverlov, V. V.; Berezina, O.; Velikodvotskaya, G. A.; Schwarz, W. H., Bacterial acetone and butanol production by industrial fermentation in the Soviet Union: use of hydrolyzed agricultural waste for biorefinery. *Appl. Microbiol. Biotechnol* **2006**, 71, 587-597.
21. Levenspiel, O., *Chemical Reaction Engineering*. 3rd. ed.; John Wiley & Sons. Inc: 1999.

6. Ionic Liquid Synthesis and Phase Equilibrium in Carbon Dioxide

Producing imidazolium based ionic liquids using compressed carbon dioxide CO₂ as a solvent has many advantageous qualities over using traditional solvents. CO₂ is gaseous at atmospheric conditions making separation of compressed CO₂ from products easily attainable by releasing pressure on a system. This is unlike traditional solvents which require more steps for separation, such as distillation. CO₂ is also seen described as being benign due to its low toxicity and is considered a “green” more environmentally friendly solvent.³ While CO₂ is considered a “green house” gas, its use here is envisioned from non-sequestered sources.



For exothermic reactions, like the presently studied synthesis of ILs, the heat capacity (C_p) of CO₂ may provide an engineering advantage over conventional solvents. It has been reported that a similar reaction between 1-methylimidazole and 1-bromobutane has a heat of reaction (ΔH^{rxn})=-96 KJ/mol.⁶ Such a large heat of reaction is often handled with a large amount of solvent, with organic solvents with high heat capacities, and/or by the use of heat exchangers (chillers, etc.). An interesting physical property CO₂ possesses is a large variance in the C_p with pressure. The C_p for CO₂ at 40°C, as shown Figure 6- 2, was calculated for a wide range of pressures using an ultra-accurate equation of state for CO₂ in the database REFPROP.⁹ REFPROP is a software package supplied by the National Institute of Standards and Technologies (NIST) which uses the Span-Wagner



Equation of State to calculate the C_p values for pure CO₂. In Figure 6- 2 it is clearly seen that the C_p for CO₂ increases dramatically near the critical pressure, therefore a large majority of energy released during an exothermic reaction can be absorbed much greater by the CO₂ in the near critical pressure. This trend has also been observed at elevated temperatures and pressures for the binary systems: n-pentane/acetone and methanol/acetone.¹⁰

When comparing the C_p 's for CO₂ against the C_p 's for a few organic solvents taken at ambient pressure, displayed in Table 6- 1, it is seen that the C_p 's for the organic solvents are two to three times greater than those represented by CO₂ at 30 bar. However, at pressure greater than 60 bar, the C_p of CO₂ is comparable if not greater than those of organic solvents. Moreover, near the critical pressure of CO₂ the C_p is seen to be over six times greater than

Table 6- 1 : Table of C_p for organic solvents and CO₂ at 40°C

Solvent	C_p (J/mol-K) T=40°C
Dimethyl Sulfoxide ^b	149.40 ^a
Acetonitrile ^c	92.04 ^a
Methanol ^d	84.03
CO ₂ at 30.0 bar ^e	48.73
CO ₂ at 60.0 bar ^e	80.69
CO ₂ at 88.6 bar ^f	594.31
CO ₂ at 90.0 bar ^e	564.78
CO ₂ at 140.0 bar ^e	124.93

a.) Extrapolated from data b.) Taken from ref.²
c.) Taken from ref.⁵ d.) Taken from ref.⁸ e.)
Taken from REFPROP⁹ f.) Highest approximate
value for C_p as determined by REFPROP⁹ at
40°C

methanol and nearly four times greater than DMSO, making CO₂ in this regime a much better solvent choice for absorbing the heat generated from an exothermic reaction. While CO₂ has only a finite solubility in the liquid phase below the mixture critical point, the CO₂-rich phase could also be used to moderate temperatures.

Other important considerations which have to be addressed when running reactions using CO₂ include: reactivity of starting materials with CO₂, solubility studies of CO₂, and phase equilibrium between reactants/products with CO₂. Studies have shown that primary amines as well as secondary amines react with CO₂ in a reversible reaction forming carbamic acids.¹¹⁻¹⁴ The starting material, 1-methylimidazole which is a tertiary amine, was inspected for carbamic acid formation by bubbling CO₂ through a closed vial containing 1-methylimidazole for three days.

After three days the bubbled 1-methylimidazole was analyzed using NMR and no formation of carbamic acid was detected.

In concurrent studies to these, Han *et. al.*¹⁵ demonstrated that imidazolium ionic liquids can be produced in CO₂ in high yields for the reaction between 1-methylimidazole with 1-bromobutane. However, they made no correlation to the phase behavior involved in the reaction, as well as publishing a kinetic rate. The focus of the following study will be used to examine the phase behavior for the reaction between 1-methylimidazole with 1-bromohexane using sub-critical and super critical CO₂ as a solvent media and to examine how pressure affects the overall rate of reaction at the isotherm 40°C.

Another interesting feature with producing ILs using compressed CO₂ is the allowable concentration of IL in the CO₂ phase. Blanchard *et al.*^{16, 17} have demonstrated analyzing the phase behavior between CO₂ and 1-butyl-3-methylimidazolium hexafluorophosphate [BMIm][PF₆] that the solubility of the IL in the gas phase was immeasurably low with the mole fraction of [BMIm][PF₆] in the CO₂ phase below the limit of detection of 10⁻⁵ mole fraction even at pressure up to 40 Mega Pascals (MPa). This is contrary to observations seen with organic compounds, such as the reactants, with CO₂ pressure,¹⁸⁻²⁰ where there is some or total miscibility of the organic component in the vapor (CO₂) phase. From a reactor standpoint, having a low solubility of IL in the CO₂ phase is highly beneficial since the product IL can be extracted in only one phase. Moreover, because organic components are more soluble in the vapor phase compared to that of the IL, the organic reactants which have not reacted can be extracted with the use of CO₂ pressure.

6.1. Phase Behavior

6.1.1. Six Types of Phase Behavior

Depending on the chemical interactions between two components in a binary system a number of different phase behaviors can exist at elevated pressures. In general, however, most binary high-pressure systems can be qualitatively represented using six different phase types. Figure 6- 3 (Illustration adapted from Prausnitz *et.*

al.²¹) is a visual representation of the six types of common phase behavior present in binary systems. Out of the six types of phase behaviors presented Van Konynenburg and Scott,²² five can be qualitatively determined using Van Der Waals equation of state and mixing rules. For a more detailed analysis on the different phase behavior types, The reader is referred to Van Konynenburg²² as well as Rowlinson and Swinton.²² The following is an overview of the six phase behavior types.

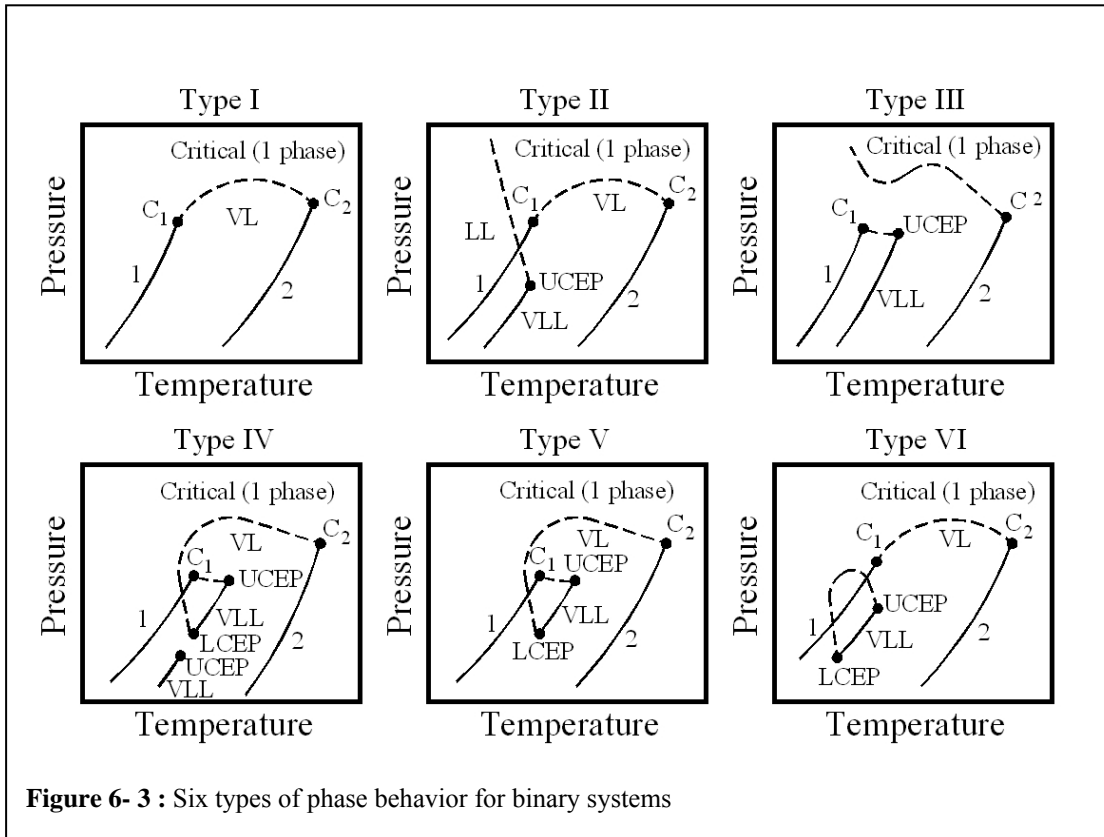


Figure 6-3 : Six types of phase behavior for binary systems

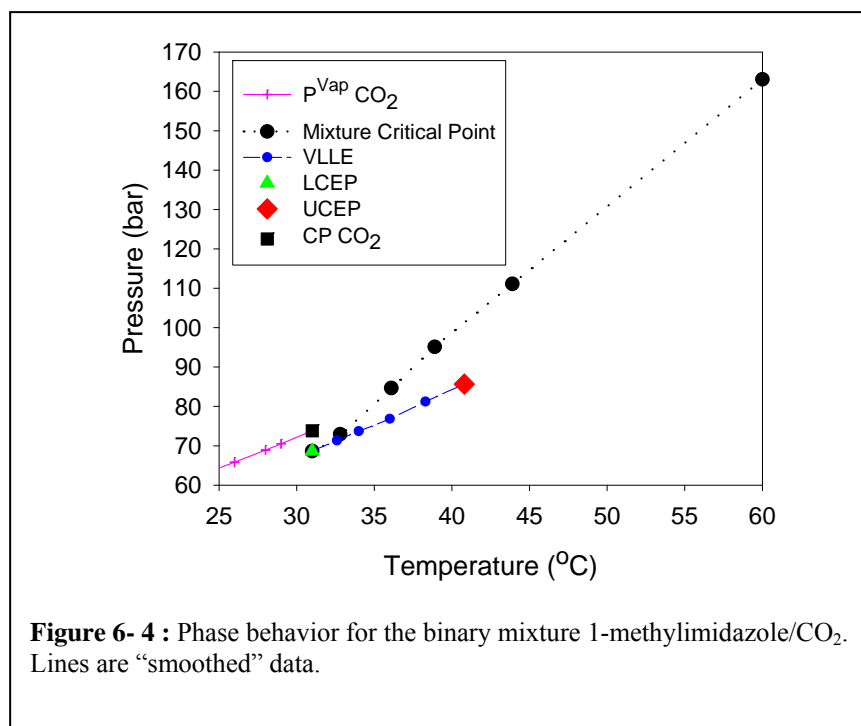
Phase behavior between two components can change dramatically at different temperature and pressure. Type I phase behavior is characterized by mixture critical points that begin and end at the pure components critical points; for instance examining Type I phase behavior in Figure 6- 3, the critical point for component 1, the more volatile of the two components, is connected to the critical point for component 2 through a critical locus. When operating below the critical locus it is seen that both components are miscible in all proportions, and vapor liquid equilibrium (VLE) is present. For conditions at or above the mixture locus the

mixture is critical, then only one phase is present. Typically, components which have similar chemical properties exhibit a Type I phase behavior. When components which are not chemically similar are mixed there are regions in which immiscibility exists resulting in Types II-VI phase behavior. Examining Type II phase behavior it is seen that the phase behavior is very similar to that of Type I, however, at lower temperatures, liquid immiscibility exists in liquid-liquid (LLE) equilibrium and vapor-liquid-liquid equilibrium (VLLE). Also, shown in a Type II phase behavior is the existence of an upper critical end point (UCEP), which is a point when the two liquid layers become miscible with each other resulting in VLE. To the left of this line and above the vapor pressure line of component 1 the mixture is in liquid-liquid equilibrium (LLE), as shown in Figure 6- 3. Type III phase behavior shows two separate critical loci; one joining the critical point of component 1 to the UCEP, and the second, which is connected to component 2 (less volatile component) and rises with pressure. Type IV and V phase behavior are quite similar to each other. Both Type IV and V have a critical locus which spans between the critical point of component one to a UCEP, as well as a second locus which connects the pure critical point for component two with a lower critical endpoint (LCEP). The LCEP is similar to that of an UCEP in which the two liquid phases become miscible with each other resulting in VLE. What makes a Type IV slightly more complex than a Type V phase behavior is that below the LCEP exists another region of immiscibility with a corresponding UCEP. In some ways it can be seen that a Type IV phase behavior is similar to a combined Type II and Type V phase behavior. Type VI phase behavior unlike all the other phase behaviors has a second critical mixture locus which connects the UCEP and LCEP. When operating above the vapor pressure line of the pure component 1, but under the mixture critical locus there is a region by which LLE is present.

6.1.2. Phase Behavior for 1-methylimidazole/CO₂; 1-bromohexane/CO₂

Initially examining the 1-methylimidazole/CO₂ system at 40°C it was determined experimentally that a multi-phase vapor-liquid-liquid equilibrium (VLLE)

exists in a certain temperature/pressure region. This was not observed examining the vapor liquid equilibrium (VLE) using the VLE apparatus for the CO₂/1-bromohexane system, as CO₂ and 1-bromohexane are miscible at and above the vapor pressure of CO₂ ($T < T_c$). In determining which phase type was present between 1-methylimidazole and CO₂ the phase behavior was further investigated. The experimental phase behavior of 1-methylimidazole and CO₂ was measured between 2°C and 60°C and 1 to 160 bar. A pressure-temperature (*PT*) study was conducted using the autoclave outlined in section 2.1.2. Figure 6- 4 is an expanded pressure-temperature (*PT*) view for the global phase behavior for 1-methylimidazole/CO₂ system. As depicted in Figure 6- 4, vapor-liquid-liquid (VLLE) was present well beyond the critical point of pure CO₂ as shown by Figure 6- 3. Also, the existence of two critical endpoints: a LCEP at 30.9°C and 68.5 bar and an UCEP at 40.8°C and 80.6 bar, was experimentally determined. As the mixture critical point connects the LCEP to the critical point of 1-methylimidazole (theoretically), it can be concluded that 1-methylimidazole/CO₂ exhibit a type IV or V phase behavior. To distinguish between the two types of phase behaviors, Type IV or V phase behavior, a search for a low temperature VLLE region was performed down to 2°C. However, it was determined that VLLE was not present for the 1-methylimidazole/CO₂ system concluding that most likely a Type V phase behavior exists. However, cryogenic measurements should be investigated to lower temperature to completely confirm this behavior. Other CO₂ systems which have similar phase behavior as 1-methylimidazole/CO₂ include: o-Nitrophenol/CO₂²³ and nitrobenzene/CO₂.²⁴



To explain Figure 6- 4 let us first take the isotherm 40°C. Initially, while pressurizing with CO₂ there first exhibits VLE until a pressure of 84.2 bar is reach; at which point there is a phase transition to VLLE. Once pressurized above 84.2 bar, the system converts to VLE/LLE (or more precisely: fluid-liquid equilibrium) until the mixture critical point is reached at 98.6 bar. If however, we were at a temperature greater than 40.8°C, above the UCEP point, or below 30.9°C, below the LCEP point, the immiscibility gab observed between 1-methylimidazole/CO₂ would not be observed throughout an entire pressure range.

6.2. Phase Equilibrium

Understanding phase equilibrium is crucial in determining kinetic rate constants using compressed carbon dioxide. Knowing mixture critical points (when the reactants and CO₂ become completely miscible) as well as the solubility of carbon dioxide in reactions at various temperature and pressures gives valuable insight to reaction molarities which are required when calculating kinetic rates of reactions.

6.2.1. Mixture Critical Points

Mixture critical points were measured using the autoclave apparatus, outlined in section 2.1.2, for the binary mixtures: 1-methylimidazole/CO₂ and 1-bromohexane/CO₂, and for the ternary system: 1-methylimidazole/1-bromohexane/CO₂ at equal mole ratios of 1-methylimidazole and 1-bromohexane at 40°C. For the 1-bromohexane/CO₂ system, the mixture critical point is 83.3 bar, 1-methylimidazole/CO₂ mixture's critical point is 98.6 bar, and the ternary mixture's critical point for the 1-methylimidazole/1-bromohexane/CO₂ at equal mole ratio of reactants is 84.1 bar. Table 6- 2 is a summary of the results.

Table 6- 2 : Experimentally acquired mixture critical points for reactants in CO₂ taken at 40°C

System	Critical Pressure (bar)
1-bromohexane / CO ₂	83.3
1-methylimidazole / CO ₂	98.6
1-methylimidazole / 1-bromohexane / CO ₂ ^a	84.1

a) Taken at a 1:1 mole ratio of reactants 1-methylimidazole:1-bromohexane

6.2.2. Phase Equilibrium Below the Mixture Critical Point

Examining the reaction between 1-methylimidazole and 1-bromohexane at elevated pressures it is important to know the concentration of the reactants in determining the rate constants. When operating above the ternary mixture critical point (complete miscibility), the molar concentration of reactants is easily obtained by knowing the reactant loading as well as the total volume of the autoclave. However, when operating below the mixture critical point any addition of CO₂ will affect the concentration of reactants in the liquid phase resulting from gas-expansion, or in our case CO₂-expansion of the liquid.^{25, 26} The volume of the liquid increases with increased pressure, because the vapor, in our case CO₂, becomes more soluble in the liquid phase as the pressure increases. This is an important observation which needs to be accounted when calculating the rate of reaction, because the initial molarity or concentration in the liquid phase is different depending on the initial loading of reactants as well as CO₂ pressure/composition. Using the apparatus described in

section 2.3, volume expansion and mole fractions of CO₂ in the liquid phase were measured for the binary systems: 1-methylimidazole/CO₂ (up to the point where VLLE exists), 1-Bromohexane/CO₂, [HMIm][Br]/CO₂, and the ternary system 1-methylimidazole/1-bromohexane/CO₂ at 40°C and are presented in Figure 6- 5 and Figure 6- 6.

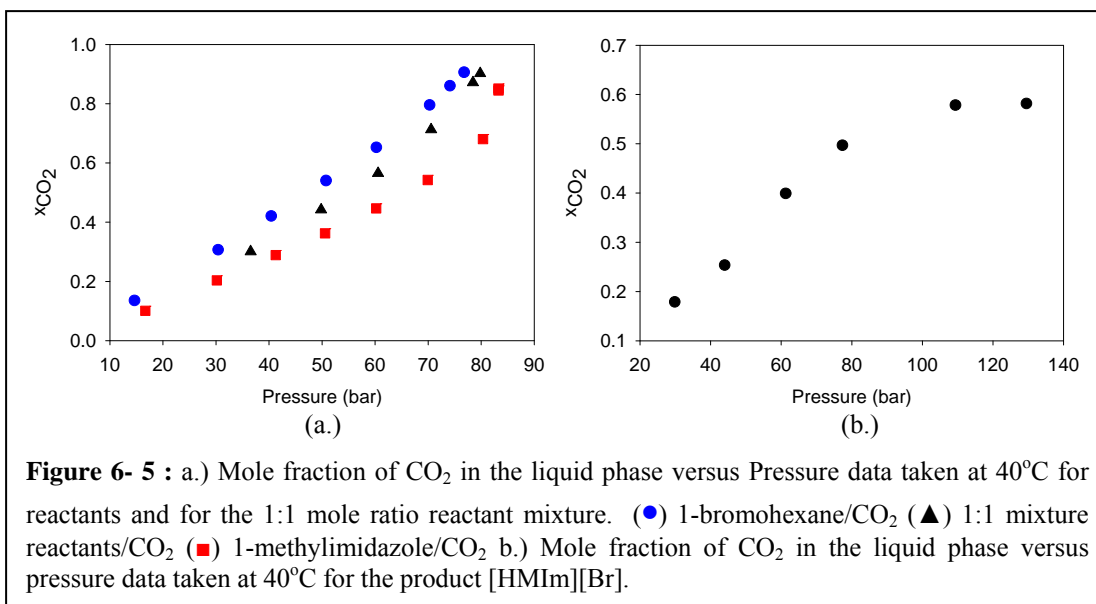


Figure 6- 5 : a.) Mole fraction of CO₂ in the liquid phase versus Pressure data taken at 40°C for reactants and for the 1:1 mole ratio reactant mixture. (●) 1-bromohexane/CO₂ (▲) 1:1 mixture reactants/CO₂ (■) 1-methylimidazole/CO₂ b.) Mole fraction of CO₂ in the liquid phase versus pressure data taken at 40°C for the product [HMIm][Br].

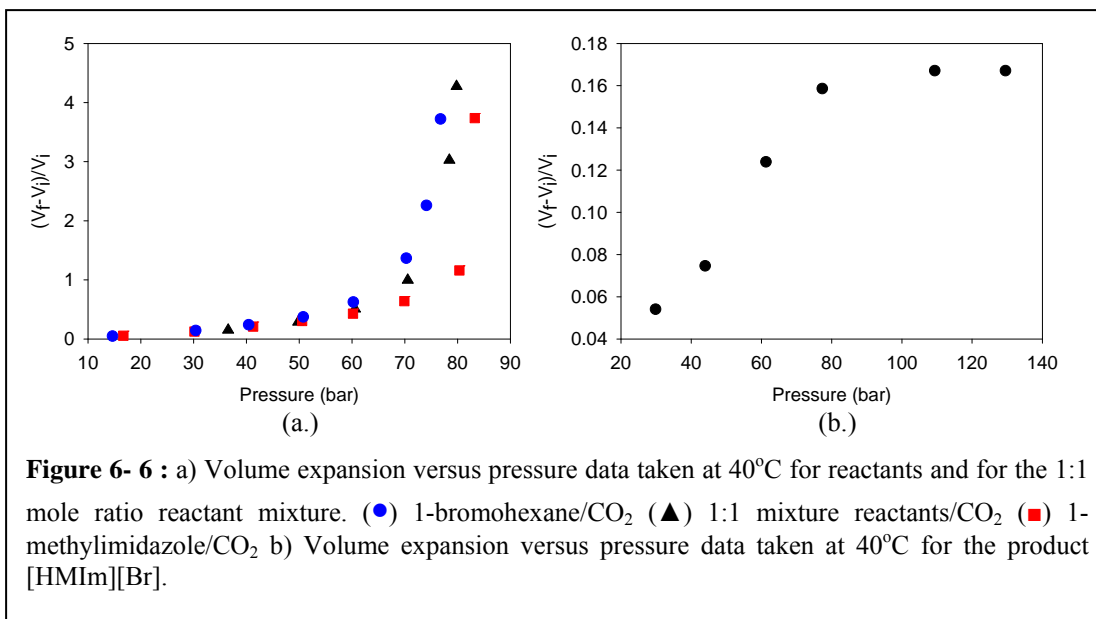


Figure 6- 6 : a) Volume expansion versus pressure data taken at 40°C for reactants and for the 1:1 mole ratio reactant mixture. (●) 1-bromohexane/CO₂ (▲) 1:1 mixture reactants/CO₂ (■) 1-methylimidazole/CO₂ b) Volume expansion versus pressure data taken at 40°C for the product [HMIm][Br].

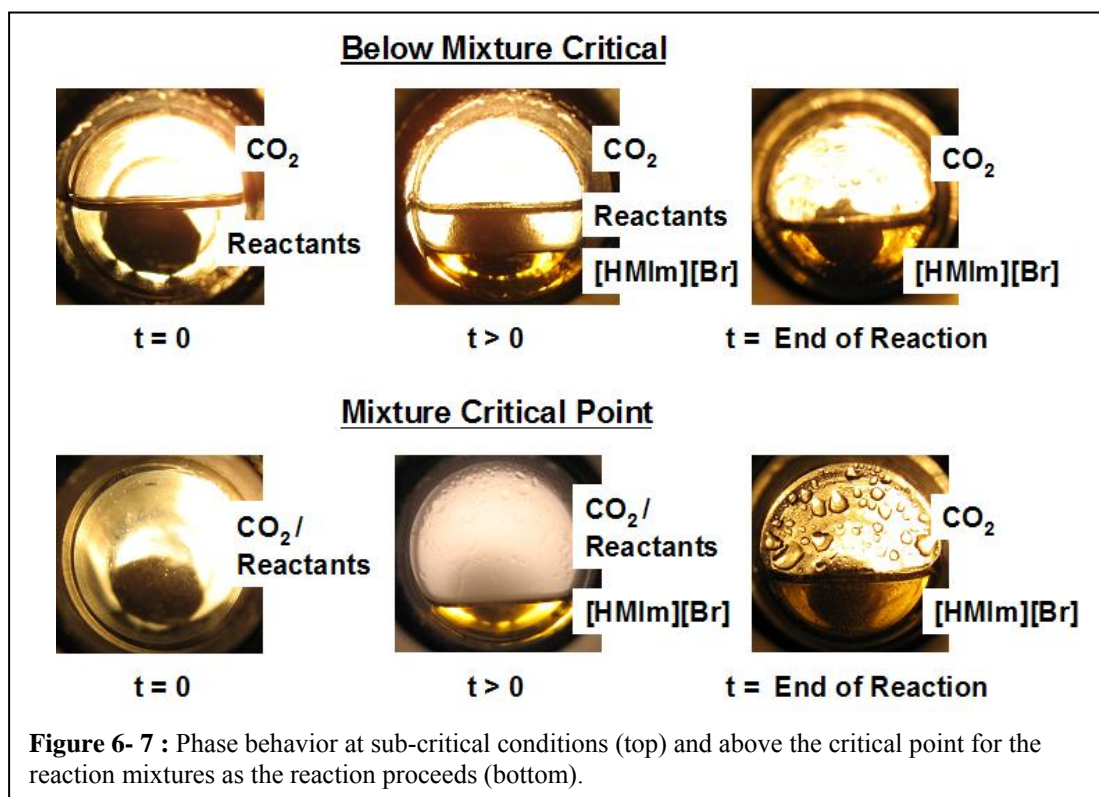
Examining Figure 6- 5 a and b reveals the mole fraction of CO₂ in the liquid phase for all reactants, reactant mixture, and product (IL) increase with pressure. However, examining Figure 6- 5b more closely it is observed that above 110 bar the amount of CO₂ in the [HMIm][Br] phase plateaus resulting from the smaller marginal solubility of CO₂ in the IL [HMIm][Br]. Aki *et. al.*²⁷ have shown similar trends examining CO₂ solubility in a number of ILs. The volume expansion data, as given by Figure 6- 6a and b, reveals that the volume expansion of the liquid associated with CO₂ increases exponentially as the pressure is increased for both the reactants and the reactant mixtures, resulting from the mixture converging on the critical point of the mixture. However, examining the product, [HMIm][Br] in Figure 6- 6b, which does not contain a mixture critical point, only a moderate expansion is observed with the dissolved CO₂: 17% volume expansion at the highest measured solubility of CO₂ in the liquid phase. Since the volume expansion data for the 1-methylimidazole/1-bromohexane/CO₂ system have been measured, the concentrations for each sub-critical reaction can be obtained in the determination of kinetic rate constants.

6.3. Kinetics

Kinetic measurements of the model IL synthesis in CO₂ at 40°C were conducted in the autoclave outlined in section 2.1.2 with an initial loading of 0.744 g of 1-methylimidazole and 1.496 g of 1-bromohexane giving a 1:1 mole ratio of reactants, at two sub-critical mixture pressures: 30 and 60 bar and two super critical mixture pressures: 90 and 140 bar using CO₂ pressure loading. All rate constants presented using CO₂ were analyzed using Equation 2.1 in section 2.1 assuming 2nd order kinetics at constant volume. The values for the kinetic rate constants are based on overall kinetics observed.

From the phase behavior it is seen that the concentration of the reactants in the liquid phase are highly dependent on the pressure and can alter significantly when operating near the mixture's critical point. What is not shown by the phase behavior

is the mutual miscibility of the reactants with products in CO₂; See Figure 6- 7 (bottom).



Initially, when the reaction begins the two reactants and CO₂ are totally miscible in each other (Figure 6- 7 bottom left), however, as the reaction proceeds an ionic liquid rich phase, [HMIm][Br], separates from solution; the CO₂-rich phase is cloudy due to precipitating ionic liquid droplets. The synthesis reaction can also occur in this newly formed IL phase. Thus, as shown from Figure 6- 7 the reaction can occur in as many as three phases, when operating below the mixture's critical pressure. Since the partitioning of reactants in each phase is different the subsequent kinetic rates in each phase may be different. Moreover, it has been experimentally observed that the pressure of the autoclave slightly increases as the reaction proceeds. The increase in pressure can be explained using Figure 6- 8b, which plots the solubility of CO₂ in the liquid phase for both the reactant mixture and [HMIm][Br] resulting from CO₂ pressure. It is observed that the solubility of CO₂, given by

Figure 6- 8b, is greater in the reaction mixture compared to the product [HMIm][Br] for a given pressure, therefore, as the product ionic liquid is being formed CO₂ is released and increases the pressure in the fixed-volume autoclave. Thus, under batch operation, the amount of reactants as well as CO₂ pressure must be carefully monitored so that the reactor is not inadvertently over-pressurized. The much lower solubility of CO₂ in the product IL-phase over the reactant mixture may be advantageous in a continuous flow process. Ultimately, when the IL product is removed from the reactor, it does not bring much CO₂ with it to be lost upon decompression. A large amount of CO₂ loss would incur larger compression/re-compression costs, which is not the case for this system.

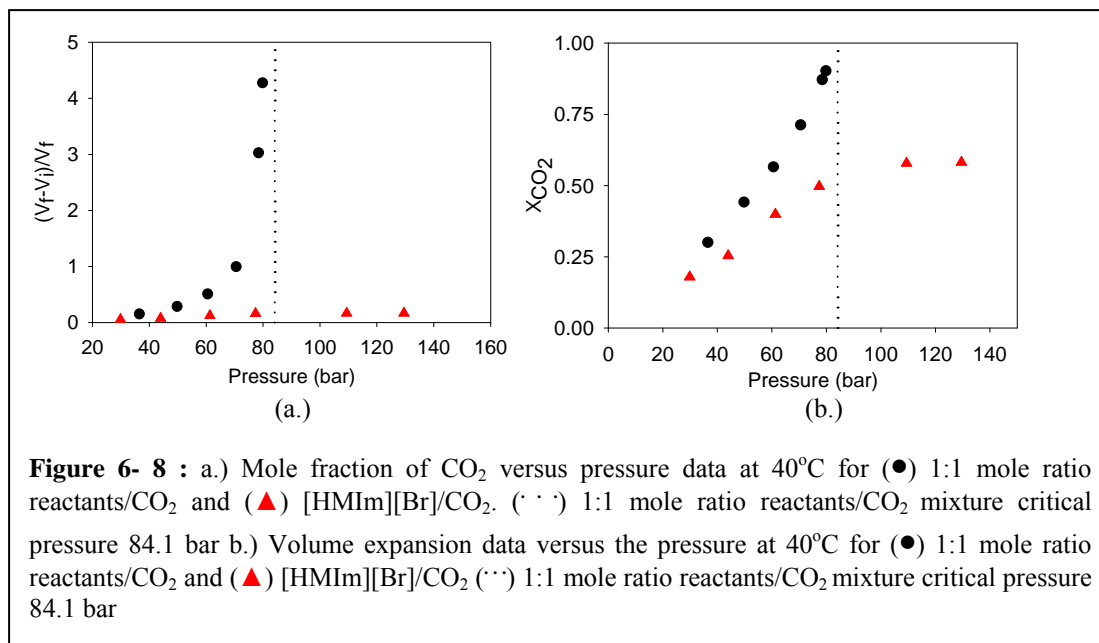


Table 6- 3 lists the overall kinetic rate constants at different CO₂ pressure loadings as well as the phase transition observed throughout the reaction. As demonstrated in Table 6- 3, the overall rate of reaction changes considerably with altering pressures induced by CO₂, and the addition of more CO₂ decreases the overall rate of reaction to some extent. One possible explanation for the wide range of overall rate constants observed in Table 6- 3 may be a consequence of the partitioning of the reactant in each phase as the reaction proceeds at a given pressure.

When operating above the reactant's mixture critical pressure, the reaction starts as a one phase reaction, but phase splits to a vapor and liquid phase (VLE): one layer rich in CO₂ / reactants and the other rich in ionic liquid product. When operating below the mixture's critical point the reaction begins as VLE: an expanded liquid and a CO₂ rich phase, but proceeds to VLLE: CO₂-rich phase, reactant-rich phase, and an ionic liquid-rich phase. Multiphase phenomena are problematic when determining rates of reactions since individual kinetic rate constants are needed for each phase for proper reaction engineering. Moreover, typically in multi-phase liquid systems, interphase mass transfer may result in an overall reduction in the kinetic rate. However, for CO₂, it has been reported that mass transport and transfer properties are enhanced by addition of CO₂, since the viscosity of liquids are decreased with CO₂ addition resulting in an increase in diffusivity as well as enhanced inter-phase mass transfer.^{28,}
²⁹ Thus, multi-phase phenomena may not be the only factor which can be used to explain the wide range of overall rate constants presented in Table 6- 3.

Phase Transition	Pressure (bar)	k x10 ⁶ (M ⁻¹ sec ⁻¹)
2→3→2 phases	30	14.85 ± 0.49
2→3→2 phases	60	8.24 ± 0.75
1→2 phases	90	7.97 ± 0.20
1→2 phases	140	5.91 ± 0.11

Another factor that may be influencing the overall rates of reaction is the polarity change; specifically the change in the KT parameters resulting from CO₂ addition in the reaction mixture. It has been reported that the KT values for CO₂ are dependent on temperature as well as pressure.^{4, 30-32} Sigma *et. al.*⁴ have published KT values for CO₂⁴ showing π^* ranging from -0.01-(-0.90) from a pressures of 222.6-88.8 bar at ~40°C, and β varying between -0.09-(-0.14) under the same conditions using the solvatochromic probe set specified in section 2.2.1.⁴ Also, shown in the literature is α ranging from 0.000-0.195 from a pressure range of 96.2-81.1 bar at 45°C¹. By increasing the pressure induced by CO₂, the solubility of CO₂ in the liquid

phase increases, thereby changing the KT values as well as the polarity of the liquid phase. This trend has been observed in studies performed on CO₂/n-alcohol mixtures³³ as well as in Diels-Alder type reactions using CO₂.³⁴⁻³⁶ Table 6- 4 is a list of KT parameters for CO₂ at the specified condition states above, as well as the KT parameters for both starting materials and product [HMIm][Br] taken at ambient pressure at 25°C.

Table 6- 4 : KT parameters for CO₂, reactants, and product

Component	α	β	π^*
CO ₂	0.000-0.195 ^a	(-0.09) – (-0.14) ^b	(-0.01) – (-0.90) ^b
1-Methylimidazole	0.232 ± 0.012	0.712 ± 0.016	0.961 ± 0.014
1-Bromohexane	N/A ^c	(-0.009) ± 0.011	0.500 ± 0.001
[HMIm][Br] ^d	N/A ^d	0.90 ^e	1.09 - 0.96 ^f

a.) taken from ref.¹ for a pressure range of 96.2-81.1 bar b.) taken from ref.⁴ for a pressure range 222.6-88.8 bar c.) solubility issues with solvatochromic dye and could not be determined d.) was not found in literature e.) taken from ref.⁷ f.) taken from ref.⁷ using 2 separate equation in determining π^*

Looking back at the regression made with the organic solvent analysis, section 3.2, the LSER regression concluded that solvents containing small α and large β and π^* were desired in maintain high rate of reaction. This was assuming a 1:1:20 mole ratio (1-methylimidazole:1-bromohexane:solvent) in the regression. Unfortunately, for the case of CO₂ this is not possible at all the pressures analyzed in Table 6- 3 because the solubility of CO₂ in the liquid phase is constrained by the phase behavior present at a given pressure. Therefore, examining the reactions conducted at the sub-critical pressures 30 bar and 60 bar the 1:1:20 mole ratio was not achievable.⁹ However, what has been shown is the solubility of CO₂ at 60 bar is greater than at 30 bar as shown in Figure 6- 8b. Thus, the excess CO₂ in the liquid phase at 60 bar compared to 30 bar must be lowering the KT parameters, β and π^* to such an extent as to have an affect on the overall rate of reaction. The same KT parameter argument can be made at pressures exceeding the mixture critical point. However, another factor leading to the decrease in the overall rates of reaction, *specifically at pressures above the mixture critical point*, is the molarity of CO₂ in the autoclave compared to the molarity of reactants. When operating above the mixture critical point, the

molarity of the reactants are constrained by the reactor volume. Consequently, while molarity doesn't change with respect to the reactants, the mole fraction of the CO₂ (solvent) increases which as shown from Table 6- 4 would decrease the α , β and π^* and, thus, the overall rate constant would decrease. Because the overall rates of reaction can be controlled primarily by CO₂ pressurization, it has been demonstrated that CO₂ can be utilized as a “tunable” solvent for achieving desired rates of reaction.³⁷

Comparing the rates of reaction using CO₂ with the organic solvents as depicted in Table 6- 5, it is seen that the rate values using CO₂ are found in the middle of the list. At the lower pressures, it is comparable to using cyclopentanone, while at high pressures, above the mixture's critical pressure, the rate of reaction are relative to that observed by ethyl formate. Moreover, because the product is not totally miscible using CO₂, the reaction and separation can take place simultaneously in a reactor. Also, utilizing the high C_p for CO₂ the exothermic reaction

Table 6- 5 : Comparison of rates of reactions for CO₂ with those obtained in organic solvents

Solvent	$k \times 10^6 \text{ (M}^{-1} \text{ sec}^{-1}\text{)}$ 40°C
Dimethyl Sulfoxide	77.89 ± 1.72
Acetonitrile	21.56 ± 0.21
Neat Reaction 1→2	17.63 ± 0.06
Cyclopentanone	15.11 ± 0.11
Acetone	12.67 ± 0.06
2-Butanone	11.56 ± 0.08
CO ₂ 30 bar	14.85 ± 0.49
CO ₂ 60 bar	8.24 ± 0.75
CO ₂ 90 bar	7.97 ± 0.20
CO ₂ 140 bar	5.91 ± 0.11
Dichloromethane	8.47 ± 0.11
Ethyl Formate	7.97 ± 0.14
Chlorobenzene	3.64 ± 0.11
Ethyl Lactate	2.86 ± 0.06
Methanol	2.03 ± 0.08

between 1-methylimidazole and 1-bromohexane can be managed much greater by the use of CO₂ compared to traditionally used organic solvents, which may require a large amount of solvent (or additional cooling) to maintain an isothermal temperature. All these benefits make CO₂ a possible choice for producing [HMIIm][Br] in a benign way.

6.4. Summary of Results

To conclude, CO₂ has many characteristics that make it advantageous for producing [HMIm][Br]. By controlling the pressure loading of CO₂ a desired rate of reaction can be maintained and in certain instances be as attractive as using organic solvent. Another attractive feature using CO₂ is that it is non-toxic and environmentally-benign compared with organic solvents, making CO₂ a more “green” solvent choice for producing ionic liquids. It has also been demonstrated that although the rate of reaction slightly decreases with increasing CO₂ pressure for imidazolium based ionic liquids, the heat capacity of CO₂ can far exceed traditional solvents when operating near the critical pressure for CO₂. Also, it has been demonstrated that phase equilibrium as well as the solubility of CO₂ play a significant role in understanding kinetics by decoupling the various effects of compressed CO₂.

References:

1. Ikushima, Y.; Saito, N.; Arai, M.; Arai, K., Solvent Polarity Parameters of Supercritical Carbon Dioxide as Measured by Infrared Spectroscopy. *Bull. Chem. Soc. Jpn.* **1991**, 64, 2224-2229.
2. Comelli, F.; Francesconi, R.; Bigi, A.; Rubini, K., Excess Molar Enthalpies, Molar Heat Capacities, Densities, Viscosities, and Refractive Indices of Dimethyl Sulfoxide + Esters of Carbonic Acid at 308.15 K and Atmospheric Pressures. *J. Chem. Eng. Data* **2006**, 51, 665-670.
3. Poliakov, M.; Fitzpatrick, J. M.; Farren, T. R.; Anastas, P. T., Green Chemistry: Science and Politics of Change. *Science* **2002**, 297, 807-810.
4. Sigma, M. E.; Linley, S. M.; Leffler, J. E., Supercritical Carbon Dioxide: Behavior of pie* and beta Solvatochromic Indicators in Media of Different Densities. *J. Amer. Chem. Soc.* **1985**, 107, 1471-1472.
5. Checoni, R. F.; Francesconi, A. Z., Measurements of the Molar Heat Capacities and Excess Molar Heat Capacities of Acetonitrile + Diethylamine or sec-Butylamine Mixtures at Various Temperatures and Atmospheric Pressure. *J. Solution Chem.* **2007**, 36, 913-922.
6. Waterkamp, D. A.; Heiland, M.; Schluter, M.; Sauvageau, J. C.; Beyersdorff, T.; Thoming, J., Synthesis of ionic liquids in micro-reactors-a process intensification study. *Green Chem.* **2007**, 9, 1084-1090.
7. Oehlke, A.; Hofmann, K.; Spange, S., New aspects on polarity of 1-alkyl-3-methylimidazolium salts as measured by solvatochromic probes. *New. J. Chem* **2006**, 30, 533-536.
8. Sun, T.; Biswas, S. N.; Trappeniers, N. J.; Seldam, C. A. T., Acoustic and Thermodynamic Properties of Methanol from 273 to 333 K and at Pressures to 280 MPa. *J. Chem. Eng. Data* **1988**, 33, 395-398.
9. Lemmon, E. W.; Huber, M. L.; McLinden, M. O. *REFPROP Reference Fluid Thermodynamic and Transport Properties*, 8.0; 2007.
10. Mulia, K.; Yesavage, V. F., Isobaric heat capacity measurements for n-pentane-acetone and the methanol-acetone mixtures at elevated temperatures and pressures. *Fluid Phase Equilib.* **1999**, 158-160, 1001-1010.
11. Dijkstra, Z. J.; Doornbos, A. R.; Weyten, H.; Ernsting, J. M.; Elsevier, C. J.; Keurentjes, J. T. F., Formation of carbamic acid in organic solvents and in supercritical carbon dioxide. *J. Supercrit. Fluids* **2007**, 41, 109-114.
12. Hampe, E. M.; Rudkevich, D. M., Exploring reversible reactions between CO₂ and amines. *Tetrahedron* **2003**, 59, 9619-9625.
13. Omae, I., Aspects of Carbon Dioxide Utilization. *Catal. Today* **2006**, 115, 33-52.
14. Schaefer, W. H., Reaction of Primary and Secondary amines to form Carbamic Acid Glucuronides. *Current Drug Metabolism* **2006**, 7, (8), 873-881.
15. Wu, W.; Li, W.; Han, B.; Zhang, Z.; Jiang, T.; Liu, Z., A green and effective method to synthesize ionic liquids: supercritical CO₂ route. *Green Chem.* **2005**, 7, 701-704.

16. Blanchard, L. A.; Gu, Z.; Brennecke, J. F., High-Pressure Phase Behavior of Ionic Liquid/CO₂ Systems. *J. Phys. Chem. B* **2001**, 105, (44), 2437-2444.
17. Blanchard, L. A.; Hancu, D.; Beckman, E. J.; Brennecke, F. F., Green processing using ionic liquids and CO₂. *Nature* **1999**, (399), 28.
18. Dohrn, R.; Brunner, G., High-pressure fluid-phase equilibria: experimental methods and systems investigated (1988-1993). *Fluid Phase Equilib.* **1995**, 106, (1-2), 213-282.
19. Kraska, T.; Leonhard, K. O.; Turna, D.; Schneider, G. M., Correlation of the solubility of low-volatile organic compounds in near- and supercritical fluids. Part I: applications to adamantane and beta-carotene. *J. Supercrit. Fluids* **2002**, 23, 209-224.
20. Miller, D. J.; Hawthorne, S. B., Determination of Solubilities of Organic Solutes in Supercritical CO₂ by On-Line Flame Ionization Detection. *Anal. Chem.* **1995**, 67, 273-279.
21. Prausnitz, J. M.; Lichtenthaler, R. N.; de_Azevedo, E. G., *Molecular Thermodynamics of Fluid-Phase Equilibria*. 3 ed.; Prentice Hall PTR: 1999; p 860.
22. Van-Konyenburg, P. H.; Scott, R. L., Critical lines and phase equilibriums in binary Van der Waals mixtures. *Philos. Trans. R. Soc.* **1980**, 298, (1442), 495-540.
23. Scheffer, F. E. C.; Smittenberg, J., Binary Systems II. *Recueil des Travaux Chimiques des Pays-Bas et de la Belgique* **1933**, 52, 1-8.
24. Kohnstamm, P.; Reeders, J. C., Phenomena of Condensation in Mixtures of Carbonic Acid and Nitrobenzene in Connection with Double Retrograde Condensation. *Proc. Acad. Wetenschappen* **1913**, 14, 270-280.
25. Hallett, J. P.; Kitchens, C. L.; Hernandez, R.; Liotta, C. L.; Eckert, C. A., Probing the Cybotactic Region in Gas-Expanded Liquids (GXLs). *Acc. Chem. Res.* **2006**, 39, 531-538.
26. Jin, H.; Subramaniam, B., Homogeneous catalytic hydroformylation of 1-octene in CO₂-expanded solvent media. *Chem. Eng. Sci.* **2004**, 59, 4887-4893.
27. Aki, S. N. V. K.; Mellein, B. R.; Saurer, E. M.; Brennecke, J. F., High-Pressure Behavior of Carbon Dioxide with Imidazolium-Based Ionic Liquids. *J. Phys. Chem. B* **2004**, 108, 20355-20365.
28. Ahosseini, A.; Ren, W.; Scurto, A. M., Homogeneous catalysis in biphasic ionic liquid/CO₂ systems. *Supplement to Chimica Oggi/Chemistry Today* **2007**, 25, (2), 40-42.
29. Sih, R.; Dehghani, F.; Foster, N. R., Viscosity measurements on gas expanded liquid systems-Methanol and carbon dioxide. *J. Supercrit. Fluids* **2007**, 41, 148-157.
30. Hyatt, J. A., Liquid and Supercritical Carbon Dioxide as Organic Solvents. *J. Org. Chem.* **1984**, 49, 5097-5101.
31. Maiwald, M.; Schneider, G. M., Solvatochromism in Supercritical Fluids. *Ber. Bunsen-Ges. Phys. Chem.* **1998**, 102, (7), 960-964.
32. Abbott, A. P.; Eardley, C. A.; Scheirer, J. E., Analysis of dipolarity/polarizability parameter, π^* , for a range of supercritical fluids. *Phys. Chem. Chem. Phys.* **2001**, 2001, 3722-3726.
33. Bulgarevich, D. S.; Sako, T.; Sugeta, T.; Otake, K.; Takebayashi, Y.; Kamizawa, C.; Horikawa, Y.; Kato, M., The Role of General and Hydrogen-Bonding

Interactions in the Solvation Process of Organic Compounds by Supercritical CO₂/n-alcohol Mixtures. *Ind. Eng. Chem. Res.* **2002**, 41, 2047-2081.

34. Chapuis, C.; Kucharska, A.; Rzepecki, P.; Jurczak, J., Influence of the Solvent Polarity on the Stereoselectivity of the Uncatalyzed [4+2] Cycloaddition of Cyclopentadiene to N,N'-Fumaroyldi[(2R)-borane-10,2-sultam]. *Helv. Chim. Acta* **1998**, 81, 2314-2325.

35. Ford, J. W.; Lu, J.; Liotta, C. L.; Eckert, C. A., Solvent Effects on the Kinetics of a Diels-Alder Reaction in Gas-Expanded Liquids. *Ind. Eng. Chem. Res.* **2007**.

36. Ikushima, Y.; Saito, N.; Arai, M., Supercritical Carbon Dioxide as Reaction Medium: Examination of It's Solvent Effects in the Near-Critical Region. *J. Phys. Chem.* **1992**, 96, 2293-2297.

37. Leitner, W., Supercritical Carbon Dioxide as a Green Reaction Medium for Catalysis. *Acc. Chem. Res.* **2002**, 35, 746-756.

7. Conclusion/Future Work

7.1. Conclusion

It has been determined that imidazolium based ILs can be synthesized in more environmentally friendly solvents, or by using compressed CO₂ which is considered an environmentally benign reaction media. Using a number of organic solvents it has been demonstrated that the quaternization reaction is highly dependent on the solvent media. Examining a number of polar protic as well as polar aprotic solvents it was shown that polar aprotic solvents were desired over polar protic solvents, as DMSO had the largest rate of reaction out of the 10 solvents. Using solvent specific Kamlet Taft parameters a method was developed for estimating the rates of reaction in a number of solvents using a Linear Solvation Energy Relationship (LSER) regression. Thus, quick solvent screening can now be performed for a wide range of environmentally friendly solvents in estimating the rates of reaction without the need for drawn out experimental procedures.

In a number of sub-studies, it was shown that leaving group contributions, branching, alkyl halide chain length, and different concentrations of starting materials also affect the rates of reaction. Depending on the halogenated leaving group, an order of magnitude difference in the experimentally determined rate constants was observed with 1-iodohexane being the fastest and 1-chlorohexane being the slowest. With the alkyl chain length study it was proven that the rates of reactions only slightly decreased with longer bromo-alkane reactants (C₄-C₁₀), however, at very short chain lengths (C₂, 1-bromoethane), the rate constant was much faster in comparison. Examining a number of different bromopentane isomers revealed branching near the site of nucleophilic attack for 1-methylimidazole tremendously decreased the rates of reaction, and based on this observation it was also confirmed that a S_N2 type reaction mechanism was present.

Using a diffusion mass transport study, the kinetic rate constants obtained in the various solvents were examined for diffusion controlled kinetics. Using the diffusion coefficients determined for 1-methylimidazole and 1-bromoethane in

DMSO, which has the fastest rate of reaction but slowest diffusion rate out of all the solvents examined, it was determined that the kinetic rate constants were several orders of magnitude less than the calculated diffusion limiting kinetic rate constants. Based on this observation it was concluded that the reaction is dominated extensively by the kinetics of the reaction and not by mass transport limitations.

In synthesizing ILs concerns other than the relative rates of reaction must be considered if ILs are to be synthesized in a more environmentally beneficial way. A number of health and environmental concerns must also be factored when making a solvent selection. Two such solvent guides which were used in this study which examined a number of health and environmental issues were the Rowan Solvent Selection Table (RSST) and the GlaxoSmithKline's pharmaceutical Solvent Selection Table (GSK-SST). Of all the organic solvents analyzed in this study it was determined that the top three solvent choices were: DMSO, acetone, and methanol. However, based on energy cost and relative rates of reaction it was systematically determined that the best globally acceptable solvent choice (out of the solvents studied) for producing ILs was acetone, which has a high rate of reaction, low environmental impact, and low energy requirements necessary for separation.

Compressed CO₂ was investigated as a potential alternative solvent for synthesizing ILs. The phase equilibrium as well as the solubility of CO₂ in the liquid phase play a significant role in decoupling the various kinetic effects involved with using compressed CO₂. By controlling the pressure loading of CO₂ a desired rate of reaction was maintained and in certain instances was just as attractive as using an organic solvent. Although the rate of reaction slightly decreases with increasing CO₂ pressure for imidazolium based ILs, the heat capacity of CO₂ far exceeds traditional solvents when operating near the critical pressure for CO₂. This is very beneficial in the synthesis since the quaternization reaction has been reportedly highly exothermic. Another advantageous quality with using CO₂ as a solvent media is the natural separation of reactants and product. Because, the reactants and [HMIm][Br] are relatively insoluble within each other, both the reaction and separation can be

conducted in a single step. Moreover, since the solubility of CO₂ is low in the desired product, [HMIm][Br], the re-compression needed for CO₂ make-up in a reactor is minimal under a continuous flow process.

In conclusion, solvents that are environmentally friendly or benign (compressed CO₂) are highly advantageous in producing ILs on a bench scale if not an industrial scale. From the solvent analysis it was seen that some of the more environmentally friendly solvents, i.e. DMSO and acetone, (of the solvents analyzed) were the top solvents selected based on high rates of reaction and being the most environmentally friendly. Therefore, slow reaction rates can not be a justification for not using an environmentally friendly solvent. From the CO₂ analysis it was determined that the phase equilibrium as well as the high heat capacities for CO₂ especially near the critical pressures for CO₂ make it an innovative contender for producing ILs.

7.2. Future Work

More research is needed to optimize the synthesis of ILs in both organic solvents and in CO₂. By using organic solvents to synthesize ILs, proper activity coefficients need to be obtained between the IL and the organic solvents in determining the true energy requirements for removal of solvent from the IL in the subsequent separation steps. Also, the amount of solvent truly necessary for the synthesis has to be optimized. At low solvent concentrations, the pumping cost for product removal from the reactor would be high resulting from the viscosity of the product. However, when high solvent concentrations are used the amount of energy required for solvent removal becomes a concern. Thus both factors have to be weighed accordingly in determining the correct amount of solvent. For a true reactor design analysis to be conducted the heat capacities and the heat of reaction need to be measured for 1-methylimidazole and 1-bromohexane at different temperatures. Another consideration which may be beneficial for IL synthesis is to examine solvents which yield high rates of reaction and low health/environmental concerns, but are highly immiscible with the IL product.

The production of imidazolium based ILs prefer small α 's, and large β 's and π^* 's. Subsequent studies could be performed on other classes of ILs which include: pyridinium, phosphonium, and ammonium to determine if similar trends exist between different IL classes. The quaternization reaction is also a precursor for many anion exchanging mechanisms in which the halide anion is replaced by bulkier anions. The kinetics for these anion exchange reactions should be addressed. Moreover, it could be optimally beneficial if the quaternization reaction and the ionic exchange step could take place simultaneously in a "one pot" synthesis with easy removal of the desired product since it usually takes copious amounts of solvent at present in a two pot synthesis.

CO₂ has proven to be an innovative way of synthesizing imidazolium based ILs. The phase behavior is quite complex and thus only overall rates of reactions are presented. More research should be conducted in obtaining individual partitioning coefficients for each reactant based on temperature and pressure effects. Rates of reactions are highly dependent on different aspects of solvent polarities, specifically the KT parameters. The reaction mixture's polarity using CO₂ at elevated pressures and temperatures must be determined to evaluate the polarity effects for the reaction. The pumping cost and CO₂ recycle are concerns which need to be addressed if CO₂ is to be used as a solvent media. During a continuous flow process some CO₂ will be evacuated from the reactor as it is entrained with the product. During depressurization the CO₂ will be separated from the product, however, there has to be a mechanism by which the CO₂ can be recompressed and added back to the reactor. Finally, a side-by-side Life-Cycle analysis as well as a cost analysis must be made for both the organic solvent synthesis and using compressed CO₂, weighing a number of factors such as reaction rates, material cost, separations, recyclability of solvent/reactants, reactor sizing, energy requirements, toxicity and environmental issues in determining the best sustainable production for synthesizing ILs.

Appendix I: Data for Figures

Table A- 1 : 1-methylimidazole against alkylbromide

Bromoalkane	$k \times 10^6 \text{ M}^{-1} \text{ sec}^{-1}$
1-bromoethane	45.96 ± 0.51
1-bromopropane	23.73 ± 0.70
1-bromopentane	22.35 ± 0.40
1-bromohexane	21.56 ± 0.21
1-bromodecane	19.75 ± 0.60

Data for Figure 3-8. Concentration for both reactants is 0.76 M. The reactions were conducted at 40°C in acetonitrile

Table A- 2 : Phase behavior for the binary mixture 1-methylimidazole/CO₂

Determining VLLE;UCEP;LCEP

Temperature (°C)	Pressure (bar)	# of Phases
30.9	68.5	LCEP
32.6	71.3	3
34.0	73.6	3
36.0	76.8	3
38.3	81.0	3
40.8	85.6	UCEP

Mixture Critical Point

Temperature (°C)	Pressure (bar)
32.9	72.9
36.1	84.6
38.9	95.1
43.9	111.1
60.0	163.3

Vapor Pressure CO₂

Temperature (°C) ^a	Pressure (bar) ^a
29.0	70.5
28.0	68.9
26.0	65.8
24.0	62.9
22.0	60.0

Critical Point CO₂

Temperature (°C) ^a	Pressure (bar) ^a
30.98	73.77

Data for Figure 4-4 a) was calculated using REFPROP

Table A- 3 : Mole fraction of CO₂ in the liquid phase and volume expansion data for different pressures at 40°C as determined by the VLE apparatus (section 2.3)

1-methylimidazole / CO ₂			1-bromohexane / CO ₂		
Pressure (bar)	x_{CO_2}	$\frac{(V_f - V_i)}{V_i}$	Pressure (bar)	x_{CO_2}	$\frac{(V_f - V_i)}{V_i}$
16.68	0.1008	0.0543	14.64	0.1355	0.0487
30.15	0.2035	0.1268	30.41	0.3067	0.1434
41.27	0.2887	0.2100	40.43	0.4206	0.2411
50.56	0.3621	0.3035	50.76	0.5405	0.3741
60.2	0.4464	0.4281	60.24	0.6527	0.6253
69.92	0.5424	0.6406	70.30	0.7957	1.3656
80.34	0.6804	1.1605	74.12	0.8607	2.2587
83.27	0.8446	3.7360	76.79	0.9062	3.7216
1:1 mole ratio reactants / CO ₂			[HMIm][Br] / CO ₂		
Pressure (bar)	x_{CO_2}	$\frac{(V_f - V_i)}{V_i}$	Pressure (bar)	x_{CO_2}	$\frac{(V_f - V_i)}{V_i}$
36.54	0.3006	0.1515	29.86	0.1789	0.0541
49.81	0.4420	0.2860	43.99	0.2536	0.0746
60.57	0.5654	0.5097	61.30	0.3991	0.1239
70.56	0.7128	0.9946	77.35	0.4970	0.1586
78.46	0.8715	3.0259	109.39	0.5783	0.1671
79.82	0.9024	4.2755	129.51	0.5816	0.1671

Data used in Figures 4-5 and Figure 4-6

Appendix II: Sigmaplot Regression Equation/Constraints

2nd Order Kinetics

The following was used in the regression for determining the kinetics when equal mole ratios of starting material were used.

Equation:

$$C=1/(1/y_0+k*t)$$

fit C to y

Variables:

t = col(1) ' {{prevmin: 0.000000}} {{prevmax: 5.000000}}

y = col(2)

y0= col(3)

'Automatic Initial Parameter Estimate Functions

F(q)=ape(t,y,1,0,1)

Initial Parameters:

k = F(0)[1] "Auto {{previous: 0.0130703}}

Options:

Iterations: 100

Step Size: 100

Tolerance: 0.000000001

The following was used in the regression for determining the kinetics when different mole ratios of starting material were used.

Equation:

$$f=C_b/(M*\exp(Ca_0*(M-1)*t*k))$$

fit f to Ca

Variables:

t = col(1) ' {{prevmin: 0.000000}} {{prevmax: 10.000000}}

Ca = col(2)

Cb = col(5)

M = col(4)

Ca0 = col(3)

'Automatic Initial Parameter Estimate Functions

F(q)=ape(t,ln(Ca),1,0,1)

Initial Parameters:

k = F(0)[2] "Auto {{previous: 2.50917e-005}}

Constraints:

k>0

Options:

Iterations: 10000

Step Size: 0.001

Tolerance: 0.0000001

LSEr regression

The following was used for regressing the coefficients A, B, and C in the LSEr using KT parameters neglecting the polarizability correction term.

Equation:

$$f=y_0+a*x+b*y+c*w$$

fit f to z

Variables:

x = col(3) ' {{prevmin: 0.000000}} {{prevmax: 10.000000}}

y = col(4) ' {{prevmin: 0.000000}} {{prevmax: 5.000000}}

w = col(5) ' {{prevmin: 0.000000}} {{prevmax: 5.000000}}

z = col(2)

'Automatic Initial Parameter Estimates

F(q,r)=ape(q,r,1,0,1)

Initial Parameters:

y0 = F(x,z)[1] "Auto {{previous: -15.3719}}

a = F(x,z)[2] "Auto {{previous: -2.21021}}

b = F(y,z)[2] "Auto {{previous: 1.38058}}

c = F(w,z)[2] "Auto {{previous: 4.92296}}

Options:

Iterations: 1000

Step Size: 1

Tolerance: 0.00001

The following was used for regressing the coefficients A, B, C, and D in the LSER using KT parameters including the polarizability correction term.

Equation:

$$f=y_0+a*x+b*y+c*(w+d*v)$$

fit f to z

Variables:

x = col(3) ' {{prevmin: 0.000000}} {{prevmax: 10.000000}}

y = col(4) ' {{prevmin: 0.000000}} {{prevmax: 5.000000}}

w = col(5) ' {{prevmin: 0.000000}} {{prevmax: 5.000000}}

v = col(6) ' {{prevmin: 0.000000}} {{prevmax: 5.000000}}

z = col(2)

'Automatic Initial Parameter Estimates

F(q,r)=ape(q,r,1,0,1)

Initial Parameters:

y0 = F(x,z)[1] "Auto {{previous: -14.6918}}

a = F(x,z)[2] "Auto {{previous: -2.17153}}

b = F(y,z)[2] "Auto {{previous: 0.065398}}

c = F(w,z)[2] "Auto {{previous: 5.02108}}

d = F(v,z)[2] "Auto {{previous: -0.223278}}

Options:

Iterations: 100

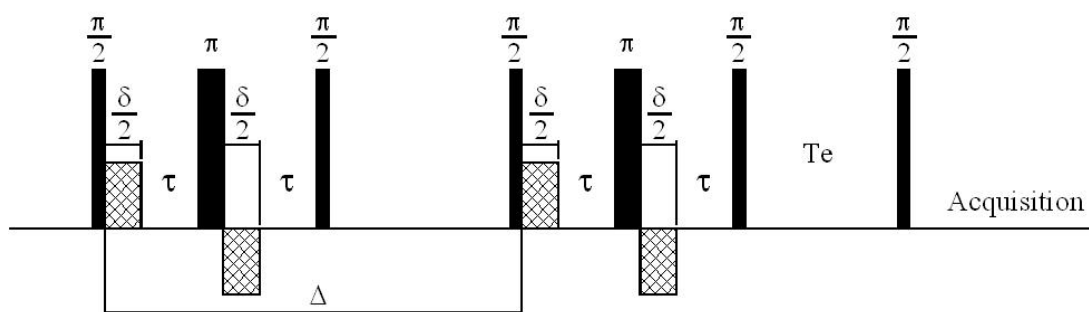
Step Size: 1

Tolerance: 0.0001

Appendix III: Procedure for NMR Diffusion

Pulse Sequence/Equation

A Bruker 400 MHz ^1H NMR was used to measure the translational diffusion using a bipolar longitudinal eddy decay (BPP-LED) sequence. The software supplied with the NMR machine was Topspin version 1.3. The following is a representation of the BPP-LED sequence and the equation used for determining translational diffusion with NMR.



$$I = I^o e^{-(\gamma\delta g)^2 D \left(\Delta - \frac{\delta}{3} - \frac{\tau}{2} \right)}$$

where,

I =Intensity of the NMR Peak

I^o =Intensity of NMR Peak initial

γ =gyromagnetic ratio. Equal to $26750 \text{ Gauss}^{-1} \text{ sec}^{-1}$ for ^1H NMR.

g = gradient strength [related to gpz6 using $g=g*(gpz6/100)$] where g^* is the total gradient strength

δ = length of gradient (p30= $\delta*0.5$)

Δ = Diffusion time (d20)

τ =dephasing and rephrasing parameter for bipolar gradients (p31)

D = Diffusion coefficient

Note: items in parenthesis are the parameters used for each symbol in the pulse sequence.

Procedure for Calibration/Determining Diffusion Coefficients

The following procedure is intended for use by our laboratory at the University of Kansas for the 400 MHz NMR.

Note: for all commands the under bar () is representative of a space, and not an actual underbar.

`cp_r /opt/topspin/data/jcschlei/nmr/1difftemp /opt/topspin/data/(your user name here)/nmr/1difftemp`

press enter. This will copy the diffusion template saved under my account and place it under your user name with the title 1difftemp. Within the diffusion template there

will be a number of files, with the first being a standard ^1H NMR pulse program (PULPROG) **zg30** and files 3-10 being the BPP-LED sequence (PULPROG) **ledbpgp2s1d**. **Note:** the second file is not used, however, was set-up by Dr. Vander Velde.

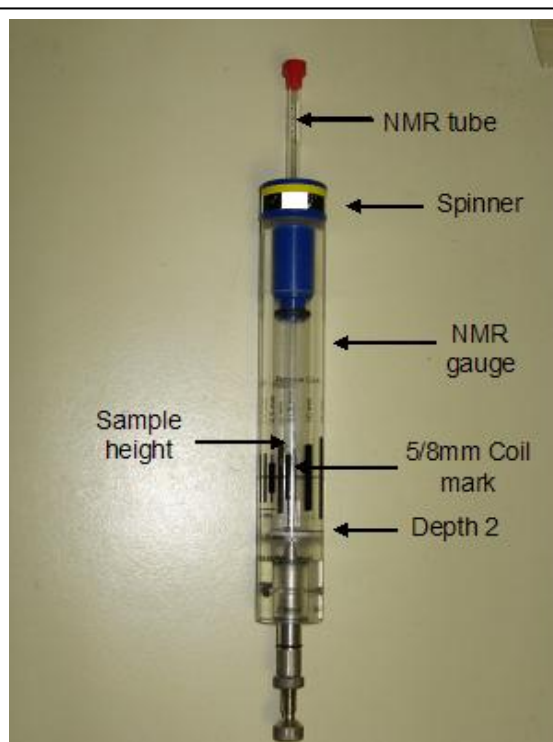
Before determining diffusion coefficients, the NMR must first be calibrated by determining the total applied gradient (g) for the probe supplied with the NMR at each temperature for which diffusion measurements are to be made. **Note:** all diffusion measurements made with the Bruker 400 MHz NMR using a high resolution Z-gradient probe. The following are a step wise procedure for calibrating the total applied gradient (g).

1. Before beginning calibrations, accurate diffusion coefficient must be obtained from literature at a specified temperature and concentration or mole fraction. **Note:** make sure the diffusion coefficient obtained is at the same temperature, which is to be used for determining unknown diffusion coefficients later.
2. Make a sample with the known concentrations/mole fraction for which the diffusion coefficient is known.
3. Using a clean NMR tube fill the NMR tube to a height of 3 cm. **Note:** The heating element for the NMR is restricted to only the bottom 3.5 cm of the NMR tube. Any excess sample in the NMR tube could result in a temperature gradient in the NMR tube resulting in convective mass transfer which is undesirable when determining translational diffusion since convective mass transfer is typically much faster than translational mass transfer.
4. Log into the NMR machine and open a shell. Type **shmrn** press enter, then type **topspin** press enter. After the software is loaded type **edte** on the command line and press enter. A box will come up with the temperature and flow rate of the NMR. Specify a temperature and turn the temperature controller on. Change the flowrate to 535 L/min. At this point you should see the temperature rise slowly. Close the edte box. Let the NMR warm to the desired temperature for at least 20 minutes before placing the sample in the NMR. At this time you can close the topspin software and lock the session or stay logged on while the NMR thermally equilibrates. To lock the session click on the red hat and click on the lock session tab. ***NOTE: If you are planning to run high temperature diffusion experiments make sure you do not exceed the boiling point and/or a pressure of 4 bar within the NMR tube at the desired temperature for which diffusion coefficients will be obtained. FURTHERMORE: NEVER exceed a temperature of 50°C without first obtaining a special spinner which has a melting point exceeding 50°C.***
5. Once preheated for a minimum of 20 minutes place the NMR tube in a spinner, then place both in the NMR gauge. Make sure the bottom of the gauge is set to 2 and place the NMR tube in the gauge. If less than 3 cm of sample was added to the NMR tube check the height of the sample by using the side of the NMR gauge. There is a black line on the NMR gauge which says 5/8"; this is the probe width for the 400 MHz NMR machine. If the sample is lower than the 5/8 marker pull the NMR tube out of the spinner

slightly so that approximately 1/2 a cm is above the 5/8" mark. **Note:** If you have to pull the NMR tube up some make sure there is enough sample in the NMR tube to fill in the entire black section where the 5/8" line is. I.e. the sample should be above and below the 5/8" mark.



Sample height in NMR tube



NMR gauge

6. Place the NMR tube in the carousel just left of the opening for the NMR. On the control panel (the box next to the printer) press the on/off button (top left most button on the control panel). The carousel will spin one notch drop the

- NMR tube right above the NMR. Press the on/off button again and the air flow will decrease, thus loading the NMR tube into the NMR.
7. If you are in the topspin software close the software. In a shell type the following:
 8. **cd /opt/topspin/data/(your user name here)/nmr** then press enter. Next type **ls** then press enter.
 9. Type **cp -r 1difftemp /opt/topspin/data/(your user name)/nmr/(file name here)** press enter. This will make a copy of the 1difftemp file and names it what ever you type for the (File Name Here). If you do not have the 1difftemp file you cannot proceed past this part. Type **shmrn** press enter then type **topspin** press enter.
 10. After topspin loads look under your user name for the file you typed in for (file name here). When you open this file you will notice there are 10 files. The first file is a typical proton pulse sequence the second file is not used and the 3-10 are the actual diffusion files which will be used. **Open the first file** and type **getprosol** press enter, **rsh** press enter, a box will appear, click on BBO click OK. If you are using a deuterated solvent lock the solvent as you would normally and go to step 9. If you are using a non deuterated solvent click the sweep button on the control panel so the light turns off for the sweep button. Type **gradshim** and press enter then click on Start gradshim. Let the gradshim run through two iterations. After it is done close the iteration box, the gradshim box, and the spectrum box which generated a straight horizontal line with a little zigzag in the middle.
 11. Type **rga** press enter. When it is done type **zg** then press enter. There will only be one scan which is taken. When zg has finished type **ef** press enter, **apk** press enter, **abs** press enter. Find one of the peaks associated with the diffusion component of interest (preferably a singlet, however, any multiplicity peak can be used). Zoom in around that particular peak and place the cursor at the highest point on the peak. Type **olp** press enter. A dialog box will appear; type the number next to the ppm which is displayed at the top left of the spectrum screen then press enter. This will center the spectrum around the particular peak selected. *Note: The remaining steps have to be based on the peak selected when specifying the olp. If another peak is to be selected you must repeat the olp as well as the remaining steps for the new peak specified.* Next click on the tab that says *Aqupars* and change the PULPROG from **zg30** to **zg**. Click on the *Spectrum* tab and type **p1** press enter when a box appears type 30 press enter. **Note:** This step is a beginning step used for accurately determining a 90° pulse which is necessary for the BPP-LED sequence. Type **zg** press enter. After it is done type **ef** press enter, then **abs** press enter **DO NOT TYPE apk then enter this will autophase your spectrum.** The spectrum will look weird. Find the highest intensity for this peak and write down the value. The highest intensity is determined by moving the cursor over the peak and looking at the top left of the spectrum screen until you find the largest intensity value. Next type **p1** press enter and

- change it to 31. Repeat the process: **zg** enter once finished type **ef** enter, **apk** enter, and **abs** enter and write down the lowest intensity value. Do this same procedure for **p1** equal to 32, 40, 39, and 38. You will notice that for 40, 39, and 38 that the peak went negative. Write down the largest negative values at each specified p1 values. Next, in excel plot p1 values 30, 31, 32, 40, 39, and 38 (in the x-axis) versus their maximum intensity (y-axis). graphed, it should be a straight line which passes through the x-axis. Accurately, determine the x-intercept point and record the value. This is the exact p1 value necessary for a 360° pulse. In the BPP-LED sequence a 90° pulse is required, thus dividing the p1 value recorded, the x-axis intercept, by 4 will grant you the necessary p1 value which will be used for the BPP-LED sequence.
12. Once done in excel, in topspin type **rg** press enter and record the number, followed by typing **olp** and recording the value. Everything up to this point has been in file 1, next we are going to examine the remaining files 3-10.
 13. Open up file number 3. Type **rg**, press enter and write down the value you obtained in step 12. Type **olp**, press enter and type the value recorded in step 12. Type **p1**, press enter and type the value determined for the 90° pulse here (it should be around ~8 to ~9). **Do this for the remaining files: 4-10.**
 14. Open file 3 and type **p30** press enter. Change the value to 500. Do the same for file 4. While you are in file 4 type **gpz6** press enter. Change this value to 70. This initial change in file 4 will look at the maximum value that the pulse gradient will go through. *Note: gpz6 is the gradient strength it is different for each diffusion experiment number. (File 3 gpz6=5, File 4 gpz6=10, File 5 gpz6=20, File 6 gpz6=30.....)The maximum value for gpz6 is 70. The gpz6 value should never exceed 70 to prevent damage to the coil. Also, noteworthy is the gradient strength is typically linearly proportional to the Amperage through the coil. i.e. gpz6=100 is equivalent to 10A, gpz6=5 is equivalent to 5A. See Bruker's manual for more details.*
 15. Open file 3 and type **multizg** press enter a dialog box will come up press 2 enter. This will run through two cycles beginning with file 3 and finishing with file 4. When the message "multizg complete" appears press okay and open file 3. Type **ef** press enter, **apk** press enter, **abs** press enter, and then **multiefp** press enter. When the dialog box appears type 3 press enter then type 2 press enter. Multiefp analyzes both and generates both files using the same parameters. While in file 3 zoom in on the specified peak determined in step 11. Find the maximum intensity and write the number down. Do the same for file 4. Divide the Intensity from file 3 by the intensity of 4. If the ratio is 10 ± 0.5 you can move on to next step. If however it is not 10 ± 0.5 repeat steps 14 and 15 using a different value for p30. **NOTE: If the ratio is less than 10 increase the value of p30 for both files 3 and 4. If the value is greater than 10 decrease the value for p30 for both files 3 and 4. However, make sure that for both files 3 and 4 the same value for p30 is used. Keep iterating p30 until the ratio is 10 ± 0.5 . It is very important to get this ratio as close as possible to 10.**

16. Once an appropriate p30 value is obtained open file 4 and change the **gpz6** setting back to 10. Next change all p30 values from files 3-10 to the determined p30 value. **Note: At this point all the files: 3-10 should have the same rg, p1, p30, o1p, and d20 values, and the only difference between the files should be the values for gpz6.** Next, open file 3 and type **multizg** press enter. This time type 8. This will run through all 8 diffusion files. Once it is completed open file 3 and type **ef** press enter, **apk** press enter, **abs** press enter, then type **multiefp**. When the dialog box opens, type 3 press enter then 8 press enter. For each file, 3-10, record the maximum peak intensity as well as the gpz6 value for each file. **Note: from earlier to determine the gpz6 value for each file type gpz6 then press enter.** At this point all the information needed has been recorded.
17. Type **edte** press enter. Turn the temperature controller off and set the flow rate back to 200L/min. Make sure you allow enough time at the end of your NMR session to allow the NMR to adequately cool before the next scheduled time.
18. In excel plot the natural logarithm of I/I^0 versus $-[(\gamma\delta(gpz6/100))^2 D(\Delta-\delta/3-\tau/2)]$ which will be a linear line with a slope equal to g^2 . Where $(gpz6/100)$ is a fraction of the total applied gradient. By taking the square root of the slope the total applied gradient (g) is determined. The total applied gradient must be calibrated at different temperatures. Currently, a (g) value has only been calculated for 25°C. **Note: Be careful of the units placed in the excel sheet for each parameter in step 18: d20= Δ (0.1 seconds, however can be altered), p30= δ *0.5 (microseconds), D16= τ (200 milliseconds, but can be altered), D=(m²/second or cm²/second), and γ =(26750 Gauss⁻¹sec⁻¹)**
19. Once a total applied gradient (g) is determined at a specified temperature, unknown diffusion coefficients may be determined using the same procedure: from step 2-18. The only difference is in step 18, where the natural logarithm of I/I^0 must be graphed against $-[(\gamma\delta g(gpz6/100))^2(\Delta-\delta/3-\tau/2)]$. Where the slope is D .

Appendix IV: Autoclave Schematic

